Combining Statistical Methods with Dynamical Insight to Improve Nonlinear Estimation

LSE

Hailiang Du

Department of Statistics

London School of Economics and Political Science

A thesis submitted for the degree of

Doctor of Philosophy

April 2009

Statement of Authenticity

I confirm that this Thesis is all my own work and does not include any

work completed by anyone other than myself. I have completed this docu-

ment in accordance with the Department of Statistics instructions and with

in the limits set by the School and the University of London.

Signature:　　　　　　　　　　　　　　　　Date:　2009 − 06 − 08

Abstract

Physical processes such as the weather are usually modelled using nonlinear dynamical systems. Statistical methods are found to be difficult to draw the dynamical information from the observations of nonlinear dynamics. This thesis is focusing on combining statistical methods with dynamical insight to improve the nonlinear estimate of the initial states, parameters and future states.

In the perfect model scenario (PMS), method based on the Indistinguishable States theory is introduced to produce initial conditions that are consistent with both observations and model dynamics. Our methods are demonstrated to outperform the variational method, Four-dimensional Variational Assimilation, and the sequential method, Ensemble Kalman Filter.

Problem of parameter estimation of deterministic nonlinear models is considered within the perfect model scenario where the mathematical structure of the model equations are correct, but the true parameter values are unknown. Traditional methods like least squares are known to be not optimal as it base on the wrong assumption that the distribution of forecast error is Gaussian IID. We introduce two approaches to address the shortcomings of traditional methods. The first approach forms the cost function based on probabilistic forecasting; the second approach focuses on the geometric properties of trajectories in short term while noting the global behaviour of the model in the long term. Both methods are tested on a variety of nonlinear models, the true parameter values are well identified.

Outside perfect model scenario, to estimate the current state of the model one need to account the uncertainty from both observational

noise and model inadequacy. Methods assuming the model is perfect are either inapplicable or unable to produce the optimal results. It is almost certain that no trajectory of the model is consistent with an infinite series of observations. There are pseudo-orbits, however, that are consistent with observations and these can be used to estimate the model states. Applying the Indistinguishable States Gradient Descent algorithm with certain stopping criteria is introduced to find relevant pseudo-orbits. The difference between Weakly Constraint Four-dimensional Variational Assimilation (WC4DVAR) method and Indistinguishable States Gradient Descent method is discussed. By testing on two system-model pairs, our method is shown to produce more consistent results than the WC4DVAR method. Ensemble formed from the pseudo-orbit generated by Indistinguishable States Gradient Descent method is shown to outperform the Inverse Noise ensemble in estimating the current states.

Outside perfect model scenario, we demonstrate that forecast with relevant adjustment can produce better forecast than ignoring the existence of model error and using the model directly to make forecasts. Measurement based on probabilistic forecast skill is suggested to measure the predictability outside PMS.

Contents

Chapter 1

Introduction

Nonlinear dynamical systems are frequently used to model physical processes such as the dynamics of breeding population, the electronic circuit and weather. The ultimate goal we have in mind is forecasting the future states of the system. Of course there are many operational details involved, but the mathematical principle is simple, first estimate the state of the model of the dynamical system, then integrate this initial condition forward to obtain a forecast. When the equations of motion that describe the system are known, which is the perfect model scenario case, the key to the problem is the accurate estimation of state given observations. But given a perfect model of a chaotic system and a set of noisy observations of arbitrary duration, it is not possible to determine the state of this system precisely. Traditional approaches to statistical estimation are rarely optimal when applied to nonlinear models. Even in the perfect model class scenario, likelihood methods have difficulty in estimating either the initial condition or the model parameters. The question is besides getting information from the observations, how much the information we can draw from the nonlinear system itself (that is, information implicit in the equations). Our aim is to enhance the

balance between the information contained in the dynamic equations and the information in the observations themselves. Outside perfect model scenario, things become more difficult. The uncertainty of the initial conditions comes from both observational noise and model inadequacy. To estimate the future states of the model by interacting the initial condition forward will eventually fail to shadow the observations no matter what initial condition is used. To produce more consistent estimate of the current or future states, information from the model error need to be extracted. This chapter provides an overview of the thesis. Some terms undoubtly are new to the reader, all terms are defined in the later chapters when they are first used.

Outline of the thesis: In Chapter 2. Some terminologies of dynamical system are introduced and general properties of nonlinear dynamical systems are illustrated. An overview of the systems and models used in the thesis is presented. Other than details on the system-model pairs, nothing new is presented in this chapter.

In Chapter 3. we consider the nowcasting problem in the perfect model scenario. We illustrate a new ensemble filter approach within the context of indistinguishable states (48), using Gradient Descent to find a model trajectory from which an ensemble is formed. An introduction of traditional variational method, Four-dimensional Variational Assimilation (4DVAR), is presented. The difference between our method and 4DVAR is discussed. Results presented show that 4DVAR is only applicable to short assimilation windows while our method does not have such shortcoming. The popular sequential method, Ensemble Kalman Filter, is also applied to solve the nowcasting problem. For the first time we demonstrate that the indistinguishable states approach systematically outper-

forms the Ensemble Kalman Filter in both low dimension Ikeda Map and higher dimension Lorenz96 system.

In Chapter 4. we provide new results to solve the problem of parameter estimation of deterministic nonlinear models within the perfect model scenario where the mathematical structure of the model equations are correct, but the true parameter values are unknown. Traditional parameter estimation methods like least squares often base on the assumption that the forecast error is Gaussian distributed. Unlike linear models, when one put a Gaussian uncertainty through the nonlinear model, one will get non-Gaussian forecast error. Results show that the least squares estimates may even reject the true parameter value of the system in preference for incorrect parameter values (64). Two new approaches are introduced to address the shortcomings of traditional methods. The first approach forms the cost function based on probabilistic forecasting; the second approach focuses on the geometric properties of trajectories in short term while noting the global behaviour of the model in the long term. Both methods are tested on a variety of nonlinear models, the true parameter values are well identified.

In Chapter 5. we consider the nowcasting problem outside the perfect model scenario. Outside perfect model scenario, to estimate the current state of the model one need to account the uncertainty from both observational noise and model inadequacy. Methods assuming the model is perfect are shown to be either inapplicable or unable to produce the optimal results. It is almost certain that no trajectory of the model is consistent with an infinite series of observations. There are pseudo-orbits (50), however, that are consistent with observations and these can be used to estimate the model states. Applying the Indistinguishable States Gradient Descent algorithm with a stopping criteria is found to be able

3.

to produce more consistent pseudo-orbit and estimates of the model error than the Indistinguishable States approach introduced in the PMS and the approach introduced in Judd and Smith 2004. An introduction of Weak Constraint 4DVAR is presented. Although the Weak Constraint 4DVAR method accounts the model inadequacy by introducing the model error term in the cost function, like 4DVAR method it still suffers from the increasing density of local minimums. Our new method is shown to produce more consistent results than the WC4DVAR method. Ensemble formed from the pseudo-orbit generated by Indistinguishable States Gradient Descent method is shown to outperform the Inverse Noise ensemble in estimating the current states.

In Chapter 6. we consider the problem of estimating the future states outside the perfect model scenario. We demonstrate that forecast with relevant adjustment can produce better forecast than ignoring the existence of model error and using the model directly to make forecasts. The adjustment can be obtained from the estimates of the model error using Indistinguishable States Gradient Descent with a stopping criteria. Methods of interpreting predictability are discussed. We suggest using the probability forecast skill to measure the predictability outside PMS. Traditional ways of evaluating the predictability of one model, e.g. Lyapunov exponents and doubling time, are discussed. Measurement based on probabilistic forecast skill is suggested to measure the predictability outside PMS.

A bullet point list of new results is on Page 157.

Chapter 2

Background

In this chapter we will first introduce some terminology of dynamical system and the properties of nonlinear dynamical systems. Details of the systems used in this thesis are then provided. In the end, some relevant nonlinear dynamics modelling methods are described.

2.1 Dynamical system

A *Dynamical system* is a system that evolves in time. The set of rules that determine the evolution of the state of the system in time are called *Dynamics*. For example we write $x_t = F^t(x_0)$ where F represents the dynamics, x represents the *state* of the system, $x \in \mathbb{S}$ where $\mathbb{S}$ denotes the *state space*, which is the collection of all possible states (typically $\mathbb{S} \equiv \mathbb{R}^m$) and t is the time evolution. The starting state x_0 is called the *initial condition*.

Mathematically dynamical system can be categorised into two types, deterministic and stochastic. The evolution of a *stochastic dynamical system* is irre-

ducibly random. A *deterministic dynamical system*, on the other hand, is one for which the dynamics and initial condition define the future state unambiguously. In this thesis, we will only study the case where the system is deterministic and especially *nonlinear*. The evolution of a nonlinear system involves nonlinear dynamics and the observed behaviour of system can be irregular.

2.2 Flow and Map

Dynamical systems may evolve either continuously or discretely in time. The continuous dynamical system, called *flow*, is usually represented as a set of first order ordinary differential equations of the form

$$\frac{d\mathbf{x}(t)}{dt} = F(\mathbf{x}) \tag{2.1}$$

where the state $\mathbf{x}$ and the dynamics F are defined for all real values of time $t \in \mathbb{R}$ and $\{\mathbf{x}_t\}_{t=0}^{T}$ forms an unbroken trajectory in the system state space.

The evolution of a discrete dynamical system, called *map*, takes place at regular time intervals. The mathematical form of a map is defined by

$$\mathbf{x}_{t+1} = F(\mathbf{x}_t) \tag{2.2}$$

where time $t \in \mathbb{Z}$.

For continuous dynamical systems, solving the ordinary differential equations analytically may prove difficult, or even impossible. One can, however, study the flow by numerical procedures. In this thesis, continuous dynamical systems are simulated by 4th-order Runge-Kutta approximation and we define the numerical

realization to be the *system*.

2.3 Chaos

Given the state space $\mathbb{S}$ of a deterministic dynamical system, A subset $\mathbb{A} \subseteq \mathbb{S}$ is an invariant set [1] for the dynamics F if $F^t(\mathbf{x}) \in \mathbb{A}$ for $\mathbf{x} \in \mathbb{A}$ and all t. A closed invariant set $\mathbb{A} \subseteq \mathbb{S}$ is called an attracting set if there is some neighbourhood $\mathbb{U}$ of $\mathbb{A}$ such that $F^t(\mathbf{x}) \in \mathbb{U}$ for $t \geq 0$ when $F^t(\mathbf{x}) \to \mathbb{A}$ as $t \to \infty$, for all $\mathbf{x} \in \mathbb{U}$ (35). The attracting set, also called *on attractor* or *invariant measure* of the dynamical system, describe the long term behaviour of the dynamical system. The probability distribution of states in the set of invariant measure is called unconditional probability distribution, which can be treated as prior distribution of the states before any state information is available. The invariant measure is, however, rarely known analytically, but can be approximated by evolving the system forwards over a long period of time if the system dynamics are known. We define the observed invariant measure to be *climatology*. Without knowing the dynamics of the system, the distribution of all previously observed states, termed *sample climatology*, is usually treated as the estimate the unconditional probability distribution.

Given a nonlinear system whose long term dynamics converges to the attracting set $\mathbb{A}$, *chaos* is often observed from the phenomena, *sensitive dependence on initial conditions*, where points that are initially close are separated on length scales commensurate with the range of the dynamics over relatively short lead times. Mathematically, for every initial condition $\mathbf{x}_0 \in \mathbb{A}$, and any $|\epsilon| > 0$, there

---

[1] We assume that $\mathbb{A}$ can not be decomposed into smaller invariant sets

7

exists $\delta > 0$ such that for some $t > 0$, $\parallel F^t(\mathbf{x}_0 + \epsilon) - F^t(\mathbf{x}_0) \parallel > \delta$. Another property of chaotic system is *recurrent* but not periodic. A system is recurrent if the state of the system returns to itself, i.e. for any initial condition $\mathbf{x}_0 \in \mathbb{A}$, we require that $\parallel \mathbf{x}_0 - F^t(\mathbf{x}_0) \parallel < \epsilon$ for any $\epsilon > 0$ (Note t could be very large).

2.4 Analytical systems

In order to demonstrate that our results is rather general than restricted in a particular system, methods will be applied to a variety of systems with different properties. In this section, we define those analytical systems that will be used to illustrate the questions to be addressed and discuss the difference among different methods.

2.4.1 Logistic map

The logistic map is a one dimensional map first introduced by Hutchinson (44) in order to investigate the role of explicit delays in ecological models. It is then applied in modelling the dynamics of breeding population to capture the effect that the growth rate of the population varies according to the size of the population (60). The mathematical form of the logistic map is defined by

$$x_{i+1} = ax_i(1 - x_i), \tag{2.3}$$

where x_i represents the population at year i. Logistic map is a non-invertible map as each state x_n has two preimages. The invariant measure of the logistic map strongly depends on the parameter value of a. Figure 2.1 shows how the

8 .

system behaviour changes corresponding to the value of a. For $a=4$, a change of
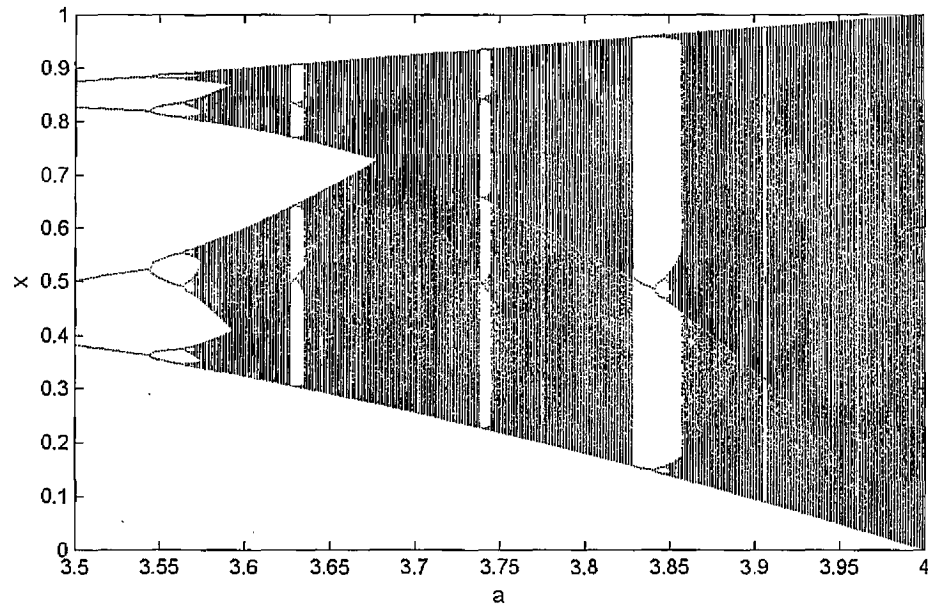
Figure 2.1: The bifurcation diagram of logistic map

variables (substitute x with $sin^2(\frac{\pi y}{2})$) transforms the logistic map into the tent map, which is proven to be chaotic (69).

The logistic map was also used as a computer random number generator by Ulam and Neumann (1947) who studied the logistic map in its equivalent form

$$x_{n+1} = 1 - ax_n^2. \tag{2.4}$$

2.4.2 Henon map

Henon Map was introduced by Henon (40) as a simplified model of Lorenz63 model (61). The two dimensional Henon map is defined by

$$X_{n+1} = 1 - aX_n^2 + Y_n \qquad (2.5)$$

$$Y_{n+1} = bX_n. \qquad (2.6)$$

The parameter values used in Henon (1976) were $a = 1.4$ and $b = 0.3$ in order to produce chaotic behaviour. Figure 2.2 shows the attractor of Henon Map in the state space.
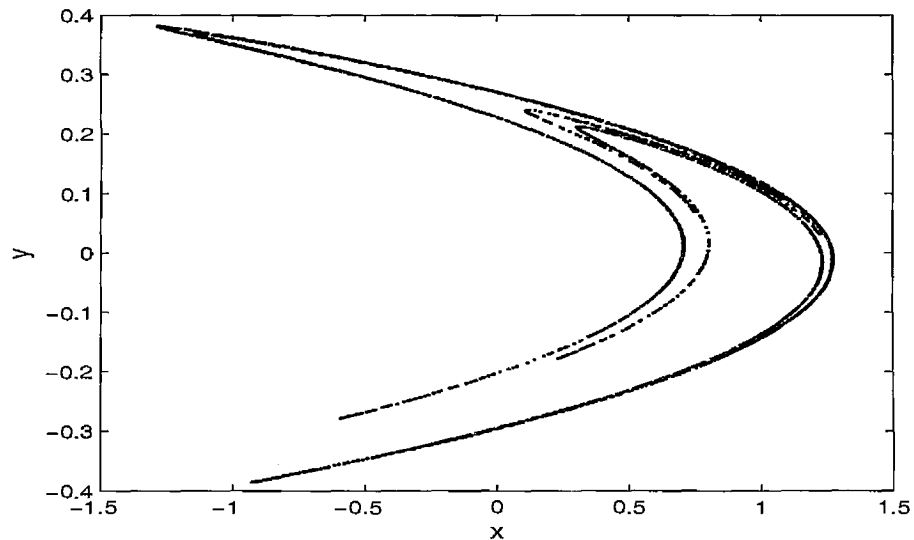
Figure 2.2: The attractor of Henon Map

10

2.4.3 Ikeda map

Ikeda Map was introduced by Ikeda (45) as a model of laser pulses in an optical cavity. With real variables it has the form

$$X_{n+1} = \gamma + u(X_n \cos \phi - Y_n \sin \phi) \tag{2.7}$$

$$Y_{n+1} = u(X_n \sin \phi + Y_n \cos \phi), \tag{2.8}$$

where $\phi = \beta - \alpha/(1 + X_n^2 + Y_n^2)$.

With the parameter $\alpha = 6, \beta = 0.4, \gamma = 1, u = 0.83$, the system is believed to be chaotic. Figure 2.3 shows the attractor of Ikeda Map in the state space. An imperfect model of Ikeda Map is obtained by replacing the trigonometric
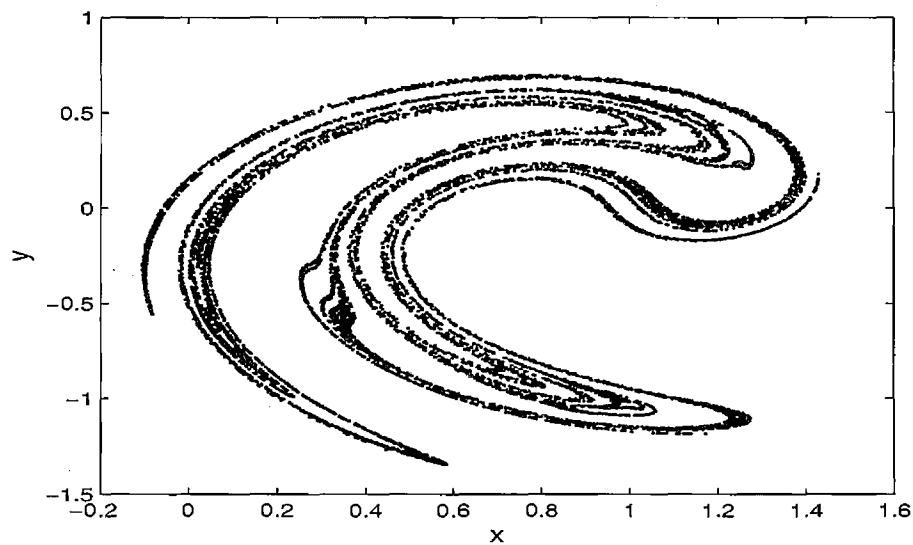
Figure 2.3: The attractor of Ikeda Map

functions in Equation 2.7 with truncated power series (50). The truncations used

in the experiments of the thesis are

$$\cos\theta = \cos(\omega + \pi) \mapsto -\omega + \omega^3/6 - \omega^5/120 \tag{2.9}$$

$$\sin\theta = \sin(\omega + \pi) \mapsto -1 + \omega^2/2 - \omega^4/24 \tag{2.10}$$

where the change of variable to ω was suggested by Judd and Smith (2004) since θ has the approximate range -1 to -5.5, and $-\pi$ is conveniently near the middle of this range. We call this model truncated Ikeda model.

2.4.4 Moore-Spiegel system

The Moore-Spiegel Flow was introduced by Moore and Spiegel (66) as a model of the nonlinear oscillator dynamics. The flow is defined by:

$$dx/dy = y \tag{2.11}$$

$$dy/dt = z \tag{2.12}$$

$$dz/dt = -z - (T - R + Rx^2)y - Tx. \tag{2.13}$$

We use the forth order Runge-Kutta scheme to simulate the differential equations. The simulation time step is 0.01 time unit. Figure 2.4 shows an attractor of Moore-Spiegel system for $T = 36$ and $R = 100$ in the state space.

2.4.5 Lorenz96 system

A system of nonlinear ODEs was introduced by Lorenz (63) in 1995. The variables involved in the system are analogous to some atmospheric variables regionally distributed around the earth. For the system containing m variables $x_1, ..., x_m$
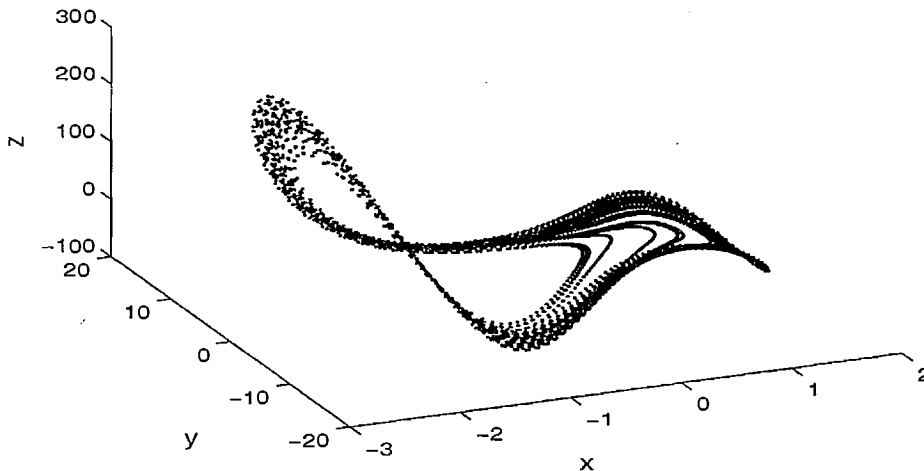
Figure 2.4: The attractor of Moore-Spiegel system for $T = 36$ and $R = 100$.

with cyclic boundary conditions (where $x_{m+1} = x_1$), The equations are

$$\frac{d\tilde{x}_i}{dt} = -\tilde{x}_{i-2}\tilde{x}_{i-1} + \tilde{x}_{i-1}\tilde{x}_{i+1} - \tilde{x}_i + F, \tag{2.14}$$

where following (83) and (67) the parameter F is set to be 10 in all of our experiments. We call the ODEs of equation 2.14 as Lorenz96 Model I. As a simulation to the weather model, Lorenz (63) assume the time unit of the Lorenz96 Model I equal to 5 days as the doubling time of the Lorenz96 Model I is roughly equal that of the current state of the art weather model. In the thesis, we will use the same scaling in all the experiments related to Lorenz96 model.

In addition to equation 2.14 Lorenz also introduced another set of ODEs. The second set of ODEs consists of $m \times n$ "fast" small scale variables in addition to the m "slow" variables. The time scale of those variables are shorter than the

variable x_i in Model I. The equations of the two sets of ODEs are

$$\frac{d\tilde{x}_i}{dt} = -\tilde{x}_{i-2}\tilde{x}_{i-1} + \tilde{x}_{i-1}\tilde{x}_{i+1} - \tilde{x}_i + F - \frac{h_{\tilde{x}}c}{b}\sum_{j=1}^{n}\tilde{y}_{j,i} \qquad (2.15)$$

$$\frac{d\tilde{y}_{j,i}}{dt} = cb\tilde{y}_{j+1,i}(\tilde{y}_{j-1,i} - \tilde{y}_{j+2,i}) - c\tilde{y}_{j,i} + -\frac{h_{\tilde{y}}c}{b}\tilde{x}_i \qquad (2.16)$$

Let us call the ODEs of equation 2.15 and 2.16 to be Lorenz96 Model II. The small-scale variables $y_{j,i}$ have the cyclic boundary conditions as well (that is $y_{n+j,i} = y_{j,i+1}$). A set of n small-scale variables are coupled to every large scale variable. The constants b and c are set to be 10, in that case the dynamics, represented by the small scale variables, is 10 times as fast and 1/10 as large as that represented by the large scale variables. In the thesis the coupling coefficients $h_{\tilde{x}}$ and $h_{\tilde{y}}$ are set to be 1. The design of Lorenz96 Model I and II is to simulate the reality that the model is built on the m dimensional (slow dynamics) space while the underlying system is also contain $m \times n$ fast dynamics variables which one can not observe. In this thesis, both Lorenz96 Model I and II are simulated by the forth order Runge-Kutta scheme with simulation time step 0.001 time unit.

2.5 Nonlinear dynamics modelling

2.5.1 Delay reconstruction

In reality, the state of the unknown dynamical system is observed in the observation space $\mathbb{O}$. It is often the case that the observation space is not sufficient to express the dynamics of the system unambiguously, for example, only one com-

ponent of the system state may be measured. Rather than model in observation space $\mathbb{O}$, it is therefore usual to reconstruct the dynamics of the system in a further space: the model state space $\mathbb{M}$. How can we construct a higher dimensional model state space given the observation is scalar? Takens' Theorem (89) tells us that we do not have to measure all the state space variables of the system. We can reconstruct an equivalent dynamical system using delays of the observed component, such method is called delay reconstruction (79; 81). Given a time series of scalar observations, $s_t, t = 1, ..., n$, recorded with uniform sampling time, a trajectory of model state $\mathbf{x}_t$ can be reconstructed in M dimensions from the single observable s_t, by delay reconstructions. This yields a series of vectors

$$\mathbf{x}_t = \left(s_t, s_{t-\tau_d}, , s_{t-(M-1)\tau_d}\right), \tag{2.17}$$

where τ_d is called the delay time. To predict a fixed period in the future, we consider a third time scale, τ_p, the prediction time. Each state $\mathbf{x}_t$ on the trajectory has a scalar image $s_{t+\tau_p}$ and we wish to construct a predictor to determine this image for any $\mathbf{x}$.

2.5.2 Analogue models

Analogue modelling is a popular and straightforward method which is effective to systems whose trajectories are recurrent in state space. Extracting the spatial information of the system dynamics requires sufficient historical data to form a learning set from which neighbours of the preimage of the state to be predicted are defined. In this thesis the nearest neighbour is determined by the distance between the current state and its neighbour.

- Local analogue

  For local analogue, we firstly find the nearest neighbour in the model space. We then report the nearest neighbour's image as the prediction.

- Local Random Analogue

  We are not always lucky enough to determine whether or not the data from a stochastic process or deterministic process. Paparella et al. (70) introduced a hybrid approach, Random Analogue Prediction(RAP), which exploits the deterministic nature of the process while incorporating variations in the local probability distribution function, thereby adhering to the stochastic nature of each observed trajectory. To produce the Local Random Analogue prediction we firstly define a local neighbourhood in the model state space, usually with a fixed radius or fixed number of k nearest neighbours. We then select a near neighbour randomly from the k nearest neighbours and report its image as the prediction. The probability of selecting a particular neighbour can be based on the distance between the preimage of the state to be predicted and that neighbour or treat the k neighbours equally.

2.5.3 Radial Basis Functions

Analogue models, when considered as a kind of local models, require constructing a new local predictor for each initial condition by searching the learning set. As a result, a large amount of computational resources are needed. Global models can cover the entire domain once the model is constructed. In this section we illustrate the Radial Basis Functions as an example of global model.

The Radial Basis Functions are a global interpolation technique. They con-

struct a predictor (map), $F(\mathbf{x}) : \mathbb{R}^m \to \mathbb{R}^1$ which estimates the scalar observation s for any $\mathbf{x}$ based on n_c centres, denoted as $\mathbf{c}_j, j = 1, ..., n_c$ where $\mathbf{c}_j \in \mathbb{R}^m$. The predictor $F(\mathbf{x})$ is defined by

$$F(\mathbf{x}) = \sum_{j=1}^{n_c} \lambda_j \phi(\| \mathbf{x} - \mathbf{c}_j \|), \qquad (2.18)$$

where $\phi(\cdot)$ are radial basis functions (14; 15; 79), $\| \cdot \|$ is the Euclidean norm. Typical choices of radial bases functions include $\phi(r) = r, r^3$, and $e^{-r^2/\sigma}$ where the constant σ reflects the average spacing of the centres $\mathbf{c}_j$. In the simplest case the centres are chosen to cover the region of state space. To determine the value of λ_j, we assume

$$F(\mathbf{x}) \approx s_i. \qquad (2.19)$$

The λ_j are then determined by solving a linear minimisation problem, i.e.

$$\mathbf{b} = \mathbf{A}\lambda. \qquad (2.20)$$

where $\lambda = [\lambda_1, ..., \lambda_{n_c}]$, $\mathbf{A}$ is defined by $A_{ij} = \phi(\| \mathbf{x}_i - \mathbf{c}_j \|)$ and $\mathbf{b} = [s_1, ..., s_{n_l}]$ where n_l is the size of the learning set based on which the model is constructed (14; 15; 79).

2.5.4 Summary

In this chapter, some terminologies of dynamical system and its properties are defined; details of the systems used in this thesis are then provided and some

relevant nonlinear dynamics modelling methods are described. Although nothing new is presented in this chapter, the content of this chapter provide the background knowledge of the thesis.

Chapter 3

Nowcasting in PMS

The quality of forecasts from dynamical nonlinear models depends both on the model and on the quality of the initial conditions. This chapter is concerned with the identification of the current state of a nonlinear chaotic system given both previous and current observations in the Perfect Model Scenario (PMS). It has been shown that even under the ideal conditions of a perfect model of a deterministic nonlinear system and infinite past observations, uncertainty in the observations makes identification of the exact state impossible (48). Such limitations mean that.a single "best guess" prediction is not an ideal solution to the problem of accurate estimation of the initial state. Instead an ensemble of initial conditions better accounts for uncertainty in the observations. Here we define the problem of state estimation of the current state conditioned on the past as a *nowcasting* problem. In the PMS, there are states that are consistent with model's dynamics and those states that are not. Those consistent states lie on the model's attractor. States off the model's attractor are pulled towards the attractor. For nonlinear chaotic systems, this collapse onto the attractor dom-

inates the model's dynamics. Intuitively, it make sense in state estimation to identify those states that are not only consistent with observations but also consistent with the model's dynamics. The perfect model scenario is firstly defined in Section 3.1. The theory of Indistinguishable States (IS) is then described in Section 3.2. In Section 3.3, we introduce our methodology to address the problem of nowcasting in PMS by first producing a reference trajectory by the method called Indistinguishable States Gradient Descent (ISGD) and then an ensemble of initial conditions being formed by Indistinguishable States Importance Sampler (ISIS). Other state estimation methods including Four-dimensional Variational Assimilation (4DVAR), Ensemble Kalman Filter (EnKF) and Perfect ensemble are described in Section 3.4, 3.5 and 3.6 respectively. Comparison are made in Section 3.7 i) between ISGD method and 4DVAR method relative to the reference trajectory (defined in Section 3.3) they produce; ii) between the initial condition ensemble generated by ISIS and that produced by EnKF; iii) between the initial condition ensemble generated by ISIS and that of a perfect ensemble. It is the first time that IS theory is applied to produce analysis and initial condition ensemble and contrast with 4DVAR method and Ensemble Kalman Filter method.

3.1 Perfect Model Scenario

Let $\tilde{x}_t \in \mathbb{R}^{\tilde{m}}$ to be the state of a deterministic dynamical system at time $t \in \mathbb{Z}$. The evolution of the system is given by $\tilde{F}(\tilde{x}_t, \tilde{a}) : \mathbb{R}^{\tilde{m}} \to \mathbb{R}^{\tilde{m}}$ and $\tilde{x}_{t+1} = \tilde{F}(\tilde{x}_t, \tilde{a})$, where $\tilde{F}$ donates the system dynamics that evolves the state forward in time in the system space $\mathbb{R}^{\tilde{m}}$ and the system's parameters are contained in the vector $\tilde{a} \in \mathbb{R}^{\tilde{l}}$.

Define $x_t \in \mathbb{R}^m$ to be the state of the deterministic dynamical model at time $t \in \mathbb{Z}$. The model is defined by $F(x_t, a) : \mathbb{R}^m \to \mathbb{R}^m$ and $x_{t+1} = F(x_t, a)$, where F donates the model dynamics that evolves state forward in time in the model space $\mathbb{R}^m$ and $a) \in \mathbb{R}^l$ donates the model parameters.

We define the observation at time t to be $s_t = h(\tilde{x}_t) + \eta_t$, where $\tilde{x}$ is the true state of the system. $h(\cdot)$ is the observation operator which projects the state in the model space into observational space. For simplicity, we take $h(\cdot)$ to be the identity. Unless otherwise stated, it is assumed that all components of $\tilde{x}_t$ are observed, i.e. $s_t \in \mathbb{R}^{\tilde{m}}$. The $\eta_t \in \mathbb{R}^{\tilde{m}}$ represent observational noise (or *measurement error*); otherwise stated the η_t are taken to be independent and identically distributed.

In the *Perfect Model Scenario(PMS)*, we assume i) the system state and model states evolve according to the same structure of the dynamics, i.e. $\tilde{F} \equiv F$. Note that it does not require the system parameters $\tilde{a}$ and the model parameters a having the same values. In this chapter, however, we focus on the case that not only the model class F but also the model parameters a are identical to those of the system. ii) the system state $\tilde{x}$ and the model state x share the same state space, i.e. $\tilde{m} = m$. iii) model state and system state correspond exactly and iv) the noise model is independent and identically-distributed and the statistical characteristics of the observational noise are known exactly.

The problem of nowcasting in the PMS will be interpreted as how to form an ensemble to estimate the current state $\tilde{x}_0$ given the history of observations $s_t, t = -N + 1, ..., 0$, a perfect model class with perfect parameter values and the parameters of the observational noise model.

3.2 Indistinguishable States

Given a perfect model, an ideal point forecast is possible if we initialise the model with the true state of the system. For periodical system, the state can be identified uniquely when $t \to -\infty$. For chaotic systems, noisy observations prevent us from identifying the true state of the system precisely, nonetheless one can find a set of states that are *indistinguishable* from the true state given the perfect model and the noise model (48). In this section we describe the background knowledge of Indistinguishable States Theory following the work of Judd and Smith in (48). Figure 3.1 (reproduced from Figure 1 in (48)) shows
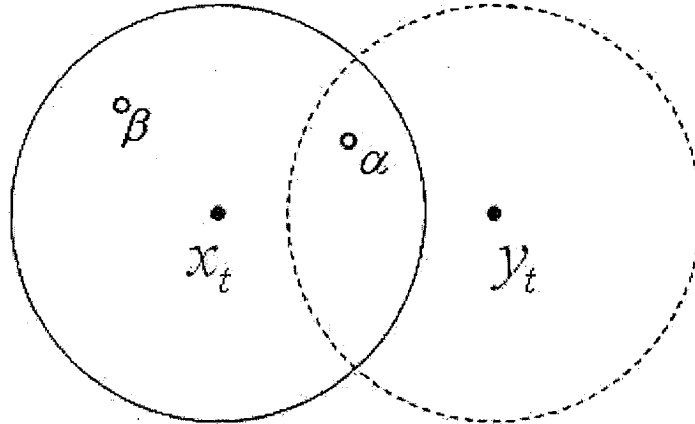
Figure 3.1: Following Judd and Smith (2001), Suppose x_t is the true state of the system and y_t some other state where x_t and $y_t \in \mathbb{R}^2$. The circles centred on x_t and y_t represent the bounded measurement error. When an observation falls in the overlap of the two circles (e.g., at α), then the states x_t and y_t are indistinguishable given this single observation. If the observation falls in the region about x_t, but outside the overlap region (e.g., at β), then on the basis of this observation one can reject y_t being the true state, i.e., x_t and y_t are distinguishable given the observation.

that based on one single observation s_t of state $\mathbf{x}_t$, there exist many states $\mathbf{y}_t$ each of which is indistinguishable from $\mathbf{x}_t$ because of the observational uncertainty if the overlap region in Figure 3.1 covers the observation s_t. Notice that given the bounded noise model, $\mathbf{x}_t$ and $\mathbf{y}_t$ are indistinguishable as there exist the overlap region in Figure 3.1. However, a particular realization of observation, e.g. β in Figure 3.1, could distinguish $\mathbf{x}_t$ from $\mathbf{y}_t$.

We describe the statistical background of Indistinguishable State Theory in the following. For the convenience of explanation, x_t, y_t and s_t are scalars. Let the probability density function of the observational noise be $\rho(\cdot)$, the joint probability density of x_t and y_t being indistinguishable is then defined by

$$\int \rho(s_t - x_t)\rho(s_t - y_t)ds_t. \tag{3.1}$$

This joint density function depends only on the difference between x_t and y_t and the distribution of the measurement error $s_t - x_t$, since

$$\int \rho(s_t - x_t)\rho(s_t - y_t)ds_t \equiv \int \rho(s_t - x_t)\rho(s_t - x_t + x_t - y_t)d(s_t - x_t), \tag{3.2}$$

The *indistinguishability* of two states x_t and y_t can be quantified by the normalised density function

$$q(x_t - y_t) = \frac{\int \rho(s_t - x_t)\rho(s_t - x_t + x_t - y_t)d(s_t - x_t)}{\int \rho(s_t - x_t)\rho(s_t - x_t)d(s_t - x_t)}. \tag{3.3}$$

This function is called *q density*. The normalisation implies the constraint that when $x_t = y_t$, the density function reaches its maximum value of 1: in no case that x_t is distinguishable from itself. If $q(x_t - y_t) = 0$, then the states x_t and y_t are distinguishable with probability one, any particular realization of observation will only be consistent with either x_t or y_t but not both. A value $q(x_t - y_t) > 0$ indicates that x_t and y_t are indistinguishable given the noise model. One should notice that there might be some particular observations that can distinguish x_t from y_t for example, in the bounded noise case, if β in Figure 3.1 is observed $\mathbf{x}_t$ and $\mathbf{y}_t$ are distinguishable. Therefore particular realizations will give extra information to distinguish x_t and y_t besides the q density.

Such q density can be generalised to a sequence of observations. Any system state x_0 defines a trajectory (we will often drop the subscript for x_0 afterwards), that goes infinite past and terminates at x. Given a time series of observations $s_t, t = 0, -1, -2, ...$, it follows from the independence of the measurement error that by considering all the states on the trajectory, the indistinguishability of two state x and y is then given by the product

$$Q(x, y) = \prod_{t \leq 0} q(x_t - y_t), \qquad (3.4)$$

Similar to the single observation case, If $Q(x, y) > 0$, then the trajectory ending at x and the trajectory ending at y are not distinguishable, given the noise model. Therefore the set of indistinguishable states of x is defined as

$$\mathbb{H}(x) = \{y \in \mathbb{R} : Q(x, y) > 0\}. \qquad (3.5)$$

As showed in (48), for three typical measurement error densities $\rho(\cdot)$ (Gaussian error density, Uniform error and non-uniform bounded error), $\mathbb{H}(x)$ is non-trivial and is a subset of the unstable set of x. In practice, only finite observations are available. The Q density used in the later application is calculated within a finite time interval. This requires a reference trajectory as discussed in Section 3.3.1.

3.3 Nowcasting using indistinguishable states

In this section we introduce a new methodology to address the problem of nowcasting in the perfect model scenario by applying the Indistinguishable States (IS) theory. An illustration of this methodology is depicted in the schematic flowchart of Figure 3.2.

Given a sequence of observations, we firstly identify a trajectory of the model, here termed a *reference trajectory*[1] in order to apply the IS theory to form an ensemble of initial conditions. The reference trajectory is discussed in detail in Section 3.3.1. The Indistinguishable States Gradient Descent (ISGD) (48) method is suggested to find the reference trajectory. Based on the reference trajectory, we introduce a method called Indistinguishable States Importance Sampler (ISIS) to form an N^{ens} member ensemble of initial conditions (details are discussed in Section 3.3.3). The ISIS method includes two procedures, i) draw N^{ens} candidate trajectories from the set of indistinguishable states of the reference trajectory according to Q density; ii) use the end point of each candidate trajectories as the ensemble member of the estimation of current state and weight them according to the likelihood of the observations.

---

[1] In practice particular model trajectory chosen to be the reference trajectory will depend on the details of algorithm.
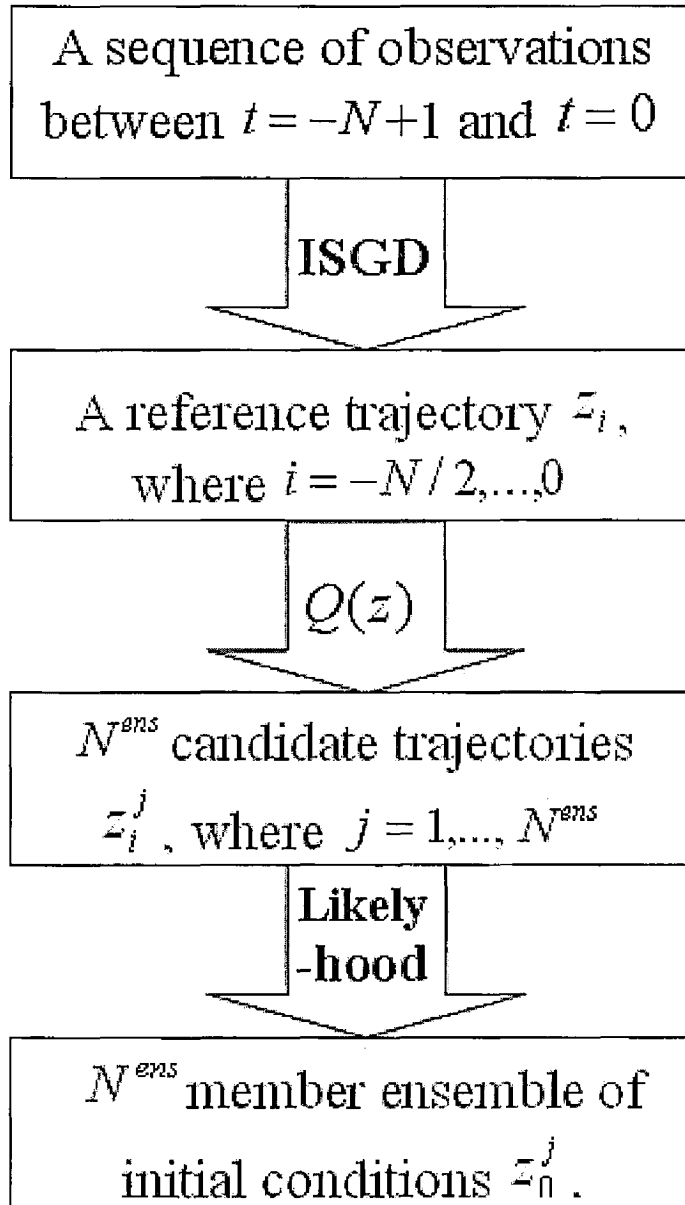
Figure 3.2: Schematic flowchart of the IS nowcasting algorithm

3.3.1 Reference trajectory

In our nowcasting methods, we define a *reference trajectory* to be the *analysis* about which an ensemble can be formed. Generally, any model trajectory might be a reference trajectory. The quality of the ensemble depends largely on how "good" the reference trajectory is [1].

In the PMS, as we discussed in Section 3.2, there is a set of indistinguishable states of the true state, i.e. $\mathbb{H}(\tilde{x})$. Let the reference trajectory end at x. One can form an ensemble of initial condition by drawing members from the set of indistinguishable states of the model state x, i.e. $\mathbb{H}(x)$. It is desired that such set of indistinguishable states $\mathbb{H}(x)$ contains the true state $\tilde{x}$, which means $Q(\tilde{x}, x) > 0$. And symmetrically the model state x is in the set of indistinguishable states of true state $\mathbb{H}(\tilde{x})$ [2]. Therefore the desirable reference trajectory we are looking for acts as a proxy of the true state.

We suggest using the Indistinguishable States Gradient Descent(ISGD) method (48) to find a reference trajectory which use the information both from model dynamics and the observations (details are discussed in the following section). In practice, the set of indistinguishable states of the reference trajectory we obtain by ISGD method, almost surely, does not contain the true state, nor would any other methods due to the fact that only finite sample is available. We are, however, interested in whether the reference trajectory we obtain provides a better ensemble of estimates of current states.

---

[1] or "are". We might take more than one reference trajectory in future work

[2] It does not mean that the set of indistinguishable states of the true state and that of the reference trajectory are identical but overlapped

3.3.2 Finding a reference trajectory via ISGD

Given a sequence of observations and a perfect model, we apply Indistinguishable States Gradient Descent algorithm (48) to find a reference trajectory. Judd and Smith (2001) demonstrate that the states produced by the ISGD method reflect the set of indistinguishable states of the true state. Here we give a brief introduction of how to apply such method (see (48) for more details). Let the dimension of our model state space be m and the number of observations be n; the sequence space is an $m \times n$ dimensional space in which a single point can be thought of as a particular series of n states $\mathbf{u}_i, i = -n+1, .., 0$. Some points in sequence space are trajectories of the model, some are not. We define a *pseudo-orbit* to be a sequence of model states that at each step differ from trajectories of the model, that is, $\mathbf{u}_{i+1} \neq F(\mathbf{u}_i)$. Particularly the observations being points of interest which, with probability one, are not a trajectory but a pseudo-orbit. We define the mismatch to be:

$$\mathbf{e}_i = \mid F(\mathbf{u}_i) - \mathbf{u}_{i+1} \mid \tag{3.6}$$

Model trajectories with probability 1 have $\mathbf{e}_i = 0$. We apply a gradient descent (GD) algorithm (details of GD can be found in appendix), initialised at the observations, i.e. $\mathbf{u}_i = \mathbf{s}_i$, and evolving the GD algorithm so as to minimise the sum of the squared mismatch errors. It has been proven (48) that the cost function

$$C(\mathbf{u}) = \sum \mathbf{e}_i^2 \tag{3.7}$$

28

has no local minima, while at points along every segment of trajectory the cost function has the value of zero. As the minimisation runs deeper and deeper, the pseudo-orbit $u_{-n+1}, ..., u_0$ is closer to be a trajectory of the model. In other words, the GD algorithm takes us from the observations towards a model trajectory. In practice, the GD algorithm is run for a finite time and thus not a trajectory but a pseudo-orbit is obtained. We denote the pseudo-orbit obtained from finite GD runs as $y_i, i = -n + 1, ..., 0$. In order to find our reference trajectory close to the pseudo-orbit obtained from GD algorithm, we iterate the middle point $y_{-n/2}$ [1] forward to create a segment of model trajectory $z_i, i = -n/2, ..., 0$ ($y-n/2 \equiv z_{-n/2}$). We treat such model trajectory to be the reference trajectory, in Meteorology this trajectory might be called "the analysis". It is important to notice that although the GD algorithm can be applied to any length of observation window, the reference trajectory will likely diverge from the pseudo-orbit when n is large due to the consequence of sensitivity to initial conditions. In the results shown in section 3.7, n is adjusted to provide the reference trajectory that is close to the pseudo-orbit y_i.

3.3.3   Form the ensemble via ISIS

In a fully Bayesian treatment one could use the natural measure as a prior and then update given the observations and the inverse noise model. Inasmuch as natural measure cannot be phrased analytically, in general, this approach is computationally intractable due to the cost of estimating the prior. The idea of ISIS is to select the ensemble members using the set of Indistinguishable States of the reference trajectory as an importance sampler (53). In order to do this, we firstly

---

[1] if n is odd, we take $y_{(-n+1)/2}$

generate a large number of model trajectories, called candidate trajectories, from which ensemble members can be selected. Ensemble members are drawn from the candidate trajectories according to their Q density relative to the reference trajectory. There are many ways to produce candidate trajectories. Here we suggest two methods of producing candidate trajectories. i) Sample the local space around the reference trajectory. One can perturb the starting point of the reference trajectory and iterate the perturbed point forward to create candidate trajectories. ii) Perturb the whole segment of observations $s_i, i = -n+1, ..., 0$ and apply the ISGD onto the perturbed orbit to produce the candidate trajectories, i.e. the same way that we produce the reference trajectory. Although method ii) may produce more informative candidates, it is obviously much more expensive than method i) since the ISGD involves a large number of model runs. The results shown in section 3.7 are produced by using method i) to generate candidate trajectories.

Given N^{cand} number of candidate trajectories, the Q density is then used to measure the indistinguishability between the candidate trajectories and reference trajectory. Since only a segment of reference trajectory is obtained, the Q density is calculated over the time interval $(-\frac{n}{2}, 0)$.

To form an N^{ens} member ensemble estimate of current state, we randomly draw N^{ens} trajectories from N^{cand} candidate trajectories according to their Q density, i.e. the larger its Q density is, the more likely the candidate trajectory is chosen. And the end point of each selected candidate trajectory is treated as the ensemble member. As the Q density depends not on the observations but on the noise model, in order to take account of the information in the particular observations we have, we weight the ensemble members using the likelihood of

the observations over the time interval $(-\frac{n}{2}, 0)$. The likelihood function is given by:

$$L(\mathbf{z}^j) = \frac{1}{2} \sum_{t=-\frac{n}{2}}^{0} (\mathbf{z}_t^j - \mathbf{s}_t)^T \Gamma^{-1} (\mathbf{z}_t^j - \mathbf{s}_t), \tag{3.8}$$

where $j \in \{1, ..., N^{ens}\}$, Γ^{-1} is the inverse of the covariance matrix of the observational noise, $\mathbf{z}^j$ denotes the chosen candidate trajectory and $\mathbf{z}_0^j$ is then taken to be the jth member of the ensemble estimates of the current state.

3.3.4 Summary

In this section, a new state estimation method based on applying IS theory is introduced in the perfect model scenario. A reference trajectory, which is expected to reflect the set of indistinguishable states of the true state, is identified by ISGD algorithm. Based on the reference trajectory (analysis), the ISIS method is then introduced to form ensemble members from model trajectories, therefore the ensemble members reflect the nonlinearity of the dynamics. Our methodology is aiming to enhance balance between the extracting information from the dynamic equations and information in the observations. Two state-of-the-art methods, Four-dimensional Variational Assimilation and Ensemble Kalman Filter, are discussed in the following sections. Results shown in Section 3.7 demonstrate that our method outperforms those two methods. The Perfect Ensemble as the optimal ensemble states is defined and discussed in Section 3.6. Comparison between the Perfect Ensemble and our method is provide in Section 3.7.

3.4 4DVAR

Four-dimensional Variational Assimilation (4DVAR) is a widely used method of noise reduction in data assimilation (18; 19; 90). The method provides an estimate of a system state by using the information in both model dynamics and observations. 4DVAR looks for initial conditions that are consistent with the system trajectory by taking account the observational uncertainty of the sequence of system observations. It aims to select the initial condition which minimises a cost function which measures the misfit between the model states and observations. During the application of 4DVAR, the minimisation is carried out over short assimilation windows rather than across all available data (Increasing the window length will not only increase the CPU cost but also introduce problems due to local minima (65; 71)).

3.4.1 Methodology

Assume the observations recorded within a time interval $t \in (-n, 0)$ will be used. Let $\mathbf{x}_t = F(\mathbf{x}_{t-1})$, the 4DVAR cost function is:

$$C_{4dvar} = \frac{1}{2}(\mathbf{x}_{-n} - \mathbf{x}_{-n}^b)^T \mathbf{B}_{-n}^{-1}(\mathbf{x}_{-n} - \mathbf{x}_{-n}^b) \tag{3.9}$$

$$+ \frac{1}{2}\sum_{t=-n}^{0}(H(\mathbf{x}_t) - \mathbf{s}_t)^T \mathbf{\Gamma}^{-1}(H(\mathbf{x}_t) - \mathbf{s}_t),$$

where $\mathbf{x}_{-n}$ is the model initial condition, $\mathbf{x}_{-n}^b$ is the first guess, or background state of the model and $\mathbf{B}_{-n}^{-1}$ is a weighting matrix that is the inverse of the covariance matrix of $\mathbf{x}^b$. The first term in the cost function is usually called the background

term. s_t is the observation at time t and Γ^{-1} is the inverse of the covariance matrix of the observational noise. Hence the second term in the cost function minimises the distance between the model trajectory and the observations.

By locating a minimum of the cost function, one finds initial conditions which defines a model trajectory that has the minimum distance from the observations. Such model trajectory is expected to be found in the perfect model case and the longer window is looked at, the better the global minima is expected to. In practice, increasing the window length will also increase the density of local minima which makes it much harder to locate the global minima (65; 71).

3.4.2 Differences between ISGD and 4DVAR

The 4DVAR method aims to produce a model trajectory consistent with observations. The 4DVAR analysis, whatever it may be in practice, can also be used as a reference trajectory to form an initial condition ensemble by ISIS. Although both ISGD method and 4DVAR method use the information of both model dynamics and observations to produce the model trajectories, there are fundamental differences between them.

- Both methods produce the model trajectories "close" to the observations but in a different way. The 4DVAR method tends to find a model trajectory close to the observations as the cost function minimises the distance between the model trajectory and the observations. If one initialises the cost function with the true state of the system, the minimisation algorithm will with probability 1 move away from the trajectory in order to minimise the distance between observations and the model trajectory. Only if the

window is infinite then this does not have to happen. In practice 4DVAR is applied to an assimilation window with finite length, the cost function forces the resulting model trajectory to be close to the observations, which may cause the estimate stay further away from the true state.

In the ISGD algorithm, the cost function itself does not contain any constraints to force the result staying close to the observations. The GD minimisation is, however, initialised with the observations in practice [1]. The states one achieves is on the attracting manifold that is close to the observations (48; 52). Unlike 4DVAR method, ISGD method does not require the pseudo-orbit to stay close to the observations and actually ISGD method forces the pseudo-orbit, on average, to move away from the observations as the minimisation goes further and further.

The results shown in section 3.7.1, indicate that 4DVAR method tends to produce the model trajectory closer to the observations than ISGD method.

- The behaviour of the 4DVAR cost function strongly depends on the assimilation window while ISGD does not. In practice, the number of local minima in the 4DVAR cost function increases with the length of the data assimilation window (71). The model trajectory defined by the local minima stays father away from the observations than the one defined by the global minima of the cost function. The results trapped in the local minima are very likely inconsistent with the observations. Gauthier(1992), Stensrud and Bao (1992) and Miller et al. (1994) have performed the 4DVAR experiments with Lorenz63 system (61). They all found that performance of

---

[1] One may initialise the GD minimisation with better analysis if it is available

assimilation varies significantly depending on the length of the assimilation window and difficulties arises with the extension of assimilation window due to the occurrence of multiple minima in the cost function. Applying the 4DVAR algorithm, one faces the dilemma of either from the difficulties of locating the global minima with long assimilation window or from losing information of model dynamics and observations by using short window.

The mismatch cost function in ISGD does not introduce such shortcomings. Although the cost function itself has more than one minima, each minima represents model trajectories where the mismatch cost function equals zero. Longer assimilation windows do not bring any trouble to the minimisation algorithm using GD. On the other hand, as longer assimilation window contains more information of the model dynamics and observations, the results in Section 3.7 show that the states obtained by ISGD method stay closer to the true state when the window length increases. The minima of the cost function are only model trajectories. And by initialising the minimisation algorithm with the observations, a pseudo-orbit on the attracting manifold which close to the observations can be found.

- The aim of 4DVAR is to locate a model trajectory through the available observations which minimises the distances between model states and observations, which is the second term of the cost function. The first term of the cost function, i.e. the background term, contains x^b, the estimation of the state at the initial time of the assimilation window. In practice x^b can be obtained from the previous assimilation window. By having the background term in the cost function, it not only makes the minimisation faster

but most importantly tries to help the minimisation algorithm avoid being trapped from the local minima. In the presence of multiple minima, the result of the minimisation will depend on the starting point of the minimisation (71). When the window length is very long, the second term of the cost function dominates the cost function. But when the window length is short, the background term forces the final estimate to stay close to the initial estimate, which means the quality of the assimilation depends critically on the initial estimate. While the ISGD method does not have to use any other initial estimates except the observation itself as the minimisation is initialised with the entire window of observations.

In the sense of forming the ensemble, we can also treat the model trajectory produced by 4DVAR as a reference trajectory and form the ensemble in the same way as ISIS method. Obviously the quality of the ensemble depends strongly on the quality of the reference trajectory. In section 3.7.1, we compare the quality of the model trajectory produced by 4DVAR and the one generated by ISGD in both low dimensional and higher dimensional case. The results show that the reference trajectory produced by ISGD is more consistent with the observations and closer to the true system trajectory than the 4DVAR results.

3.5   Ensemble Kalman Filter

Second well established class of algorithms has been defined for state estimation are sequential algorithms. In sequential algorithms, one integrates the model forward until the time that observations are available, the state at that time estimated by the model is usually called the first-guess, which is then corrected

with the new observations. The sequential algorithm, used in this chapter to compare with our methods, is based on the forms of Kalman filter (54). Although we only provide the comparison between ISIS method and a state of the art ensemble Kalman filter scheme (1; 2) later in the chapter, we first provide a brief overview of other versions of Kalman Filter methods including Kalman filter, Extended Kalman filter as background information on the ensemble Kalman filter being discussed later.

3.5.1 Kalman Filter

The Kalman filter (54) is a commonly used method of state estimation (86). It provides a sequential method to estimate the state of a system, with the aim of minimising the mean of the squared error of one step forecast. It gives the optimal estimate when the system dynamics are linear and the model is perfect (86).

The Kalman filter addresses the general problem of trying to estimate the state of the system $\mathbf{x}_t \in \mathbb{R}^m$, where the dynamics of the system is $\tilde{F}$:

$$\mathbf{x}_t = \tilde{F}(\mathbf{x}_{t-1}) \tag{3.10}$$

- Given a linear model F:

$$F(\mathbf{x}_t) = A\mathbf{x}_t, \tag{3.11}$$

where the model F need not be a perfect representation of the system's

dynamics $\tilde{F}$. It is assumed that model space and system space are identical. Any discrepancy between the model and the system can be written as:

$$\tilde{F}(\mathbf{x}_t) = F(\mathbf{x}_t) + \varpi_t, \tag{3.12}$$

where ϖ is understood to reflect the model error. When defining the Kalman Filter it is also assumed that ϖ is IID normally distributed with zero mean and variance Q^{err}.

- given observations $\mathbf{s} \in \mathbb{R}^{m^{obs}}$ we have

$$\mathbf{s}_t = h(\mathbf{x}_t) + \epsilon_t \tag{3.13}$$

where ϵ_t is the observational noise, assumed to be IID normally distributed with zero mean and variance Γ. The function h is the observation function, here assumed to be linear: $h(\mathbf{x}_t) = H\mathbf{x}_t$. The $m^{obs} \times m$ matrix H is a projection operator that gives the transformation from model space to observation space.

We define $\mathbf{x}_t^b \in \mathbb{R}^m$ to be the background or prior estimate of the system state at time t, and $\mathbf{x}_t^a \in \mathbb{R}^m$ to be the analysis or a *posteriori* estimate of the system state $\mathbf{x}_t$. The estimation error is then defined by

$$\mathbf{e}_t^b = \mathbf{x}_t - \mathbf{x}_t^b, \tag{3.14}$$

$$\mathbf{e}_t^a = \mathbf{x}_t - \mathbf{x}_t^a, \tag{3.15}$$

and the error covariances are given by

$$P_t^b = E(\mathbf{e}_t^b \mathbf{e}_t^{bT}), \tag{3.16}$$

$$P_t^a = E(\mathbf{e}_t^a \mathbf{e}_t^{aT}). \tag{3.17}$$

P^b and P^a are often called background-error covariance and analysis-error covariance. The Kalman filter provides an estimate of the updated state $\mathbf{x}_t^a$ as a linear combination of the first guess estimate $\mathbf{x}_t^b$ and a weighted difference between the actual observation and the prediction $H\mathbf{x}_t^b$, i.e.

$$\mathbf{x}_t^a = \mathbf{x}_t^b + K_t(\mathbf{s}_t - H\mathbf{x}_t^b), \tag{3.18}$$

where the $m \times m^{obs}$ matrix K_t, often called the Kalman gain, can be derived by minimising the posterior error covariance P_t^a. The Kalman gain is given by:

$$K_t = P_t^b H^T (H P_t^b H^T + \Gamma)^{-1}. \tag{3.19}$$

The application of the Kalman filter is as follows

$$\mathbf{x}_t^b = F(\mathbf{x}_{t-1}^a) \tag{3.20}$$

$$P_t^b = AP_{t-1}^a A^T + Q^{err} \tag{3.21}$$

$$K_t = P_t^b H^T (H P_t^b H^T + \Gamma)^{-1} \tag{3.22}$$

$$\mathbf{x}_t^a = \mathbf{x}_t^b + K_t(\mathbf{s}_t - h(\mathbf{x}_t^b)) \tag{3.23}$$

$$P_t^a = (I - K_t H)P_t^b \tag{3.24}$$

The equations above describe two phases, the first two equations are responsible for projecting the current state and error covariance estimates forward in time to obtain the first guess estimates for the next time step. Equations (3.22-3.24) are responsible for updating the estimates using the new observation. This results in the recursive nature of the Kalman filter. By doing so, the Kalman filter estimates the current state using the information of all past observations although not the same time.

3.5.2 Extended Kalman Filter

The Kalman filter addresses the state estimation problem of a process that is governed by a linear dynamics. But it is often the case that the process to be assimilated and (or) the observation operator is non-linear. A Kalman filter that linearises about the current mean and covariance is referred to as an extended Kalman filter (EKF) (29; 30; 47).

In the extended Kalman filter, the state transition model F and observation

model h need not be linear functions of the state. It is, however, assumed that these functions are differentiable.

The equations of EKF differs from KF in that H represents the $m^{obs} \times m$ Jacobian matrix of h: $H = \frac{\partial h}{\partial x}$ instead of the linear projection operator and A is the $m \times m$ Jacobian matrix of model F: $A = \frac{\partial F}{\partial x}$, often referred to as the transition matrix.

Similar to the Kalman filter, model errors are required to be uncorrelated with the growth of analysis errors through the model dynamics. This becomes a fundamental flaw of EKF as the distributions of the initial uncertainty are no longer normal after going through the nonlinear model. The linear assumption of error growth in EKF results in an overestimate of background error variance. Furthermore, estimating the model error covariance Q^{err} may be particularly difficult while the accuracy of the assimilation strongly depends on Q^{err} (37).

3.5.3   Ensemble Kalman Filter

The ensemble Kalman filter (EnKF) was first introduced by Evensen (23) as a method for avoiding the expensive calculation of the forecast error covariance matrix necessary for both KF and EKF in Numerical Weather Prediction. The mechanism of the EnKF's production of an analysis follows from the methods of the KF and EKF. It differs only in its method of using an ensemble to estimate the forecast error covariance matrix. No assumptions about linearity of error growth are made.

There are two general classes of ensemble Kalman filter, stochastic (37; 41; 42; 43) and deterministic (1; 7). Both filters propagate the ensemble of analyses

with non-linear models, the primary difference is whether or not random noise is applied during the update step to simulate observational uncertainty (37).

Let $X = (\mathbf{x}_t^1, ..., \mathbf{x}_t^{N^{ens}})$ be an N^{ens} member ensemble state estimation at time t. The ensemble mean $\bar{X}$ is defined as

$$\bar{X} = \frac{1}{N^{ens}} \sum_{i=1}^{N^{ens}} \mathbf{x}_t^i \tag{3.25}$$

and the variance $\hat{P}$ of a finite ensemble is given:

$$\hat{P} = \frac{1}{N^{ens} - 1} \sum (X - \bar{X})(X - \bar{X})^T \tag{3.26}$$

The EnKF uses the variance of nonlinear ensemble forecast $\hat{P}$ to estimate the background-error covariance P^b.

- Stochastic update methodology

  The traditional ensemble Kalman filter (37; 41; 42; 43) involves a stochastic update method. This algorithm updates each member according to different perturbed observations. As the perturbation involves randomness, the update is considered stochastic method.

  We define the perturbed observations $\tilde{\mathbf{s}}_i = \mathbf{s} + \eta_i$ where $\eta_i \sim N(0, \Gamma)$.

  For each ensemble member $\mathbf{x}_t^i$ the update equations are:

$$\mathbf{x}_i^a = \mathbf{x}_i^b + \hat{K}(\mathbf{s}_i - h(\mathbf{x}_i^b)) \tag{3.27}$$

$$\hat{K} = \hat{P}^b H^T (H\hat{P}^b H^T + \mathbf{\Gamma})^{-1} \tag{3.28}$$

As we can see from the equation, the perturbed observations are used to update the ensemble states, similar to the Kalman gain K in EKF (10), but using the ensemble to estimate the background-error covariance matrix.

If unperturbed observations are used in (15) without other modifications to the algorithm, the analysis error variance P^a will be underestimated, and observations will not be adequately weighted by the Kalman gain in subsequent assimilation cycles (37). Adding noise to the observations in the EnKF can, however, introduce spurious observation background error correlations that can bias the analysis-error covariances, especially when the ensemble size is small (92). Such shortage is overcome by deterministic update methodology.

- Deterministic update methodology

Deterministic algorithm like (1; 7) update in a way that generates the same analysis error covariance without adding stochastic noise. There are a number of different approaches, here in the case we are only going to talk about one. Here we briefly describe one of the methods called the ensemble square-root filter(EnSRF) (92) which is mathematically equivalent to the Ensemble Adjustment Kalman filter (1). We use this method to produce ensemble results comparing with the results obtained from IS method in Section 3.7.

Generally the EnSRF updates the ensemble mean and the deviation of each ensemble member from the the mean separately:

$$\bar{\mathbf{x}}^a = \bar{\mathbf{x}}^b + \hat{K}(\mathbf{s} - h(\bar{\mathbf{x}}^b)) \tag{3.29}$$

$$\mathbf{x}_i^a - \bar{\mathbf{x}}^a = \mathbf{x}_i^b - \bar{\mathbf{x}}^b - \tilde{K}h(\mathbf{x}_i^b) \tag{3.30}$$

$$\tilde{K} = \left(1 + \sqrt{\frac{\Gamma}{H\hat{P}^b H^T + \Gamma}}\right)^{-1} \hat{K} \tag{3.31}$$

Here $\hat{K}$ is the Kalman gain as in Eq.(16) and $\tilde{K}$ is called the *reduced gain* and is used to update deviations from the ensemble mean.

We can see that in order to obtain the correct analysis-error covariance with unperturbed observations, a modified Kalman gain, which is reduced relative to the traditional Kalman gain, has to be used to update the error covariance. Consequently, deviations from the mean are reduced less in the analysis using $\tilde{K}$ than using $\hat{K}$. In the stochastic EnKF, the excess variance reduction caused by using $\hat{K}$ to update deviations from the mean is compensated for by the introduction of noise to the observations (37).

3.6   Perfect Ensemble

Given a model F, there is a set of states consistent with the long term dynamics of the model, in the system with an attractor, this set will reflect the invariant measure on the attractor. The probability distribution of states in the set of invariant measure is called unconditional probability distribution. Generally a

perfect ensemble (80), is an ensemble of initial conditions which are not only consistent with the observational noise, but also consistent with the long term dynamics (as in "on the attractor"). The ensemble members are drawn from the posterior probability distribution of the model states given the observations. If only one observation s_0 is considered the posterior distribution of the current state x_0 given the observation can be derived from

$$p(x_0 \mid s_0) \propto \rho(s_0 \mid x_0)\Phi(x_0), \tag{3.32}$$

where $\rho(s \mid x)$ is the probability density function of the observational noise and $\Phi(x)$ is the unconditional probability density function of x. Figure 3.3 shows an example using Ikeda Map. In Figure 3.3, states (black) on the attractor are consistent with the long term dynamics of the Ikeda Map and those black states that inside the bounded noise region are members of the perfect ensemble. If a segment of n observations $s_{-n+1}, ..., s_{-1}, s_0$ is given, the perfect ensemble of current states are those states at $t = 0$ that are consistent with the long term dynamics and their trajectories backwards in time are consistent with the sequence of the observations. That is, the posterior distribution is then given by

$$p(x_0 \mid S) \propto \prod_{i=-n+1}^{0} \rho(s_i \mid x_i)\Phi(x_0), \tag{3.33}$$

Figure 3.4 shows examples of a segment observations are considered in the Ikeda Map case. As more observations are considered, the set of perfect ensemble becomes more concentrated to the true state of the system and stay the same attracting manifold as the true sate. When n approaches to infinity, the perfect
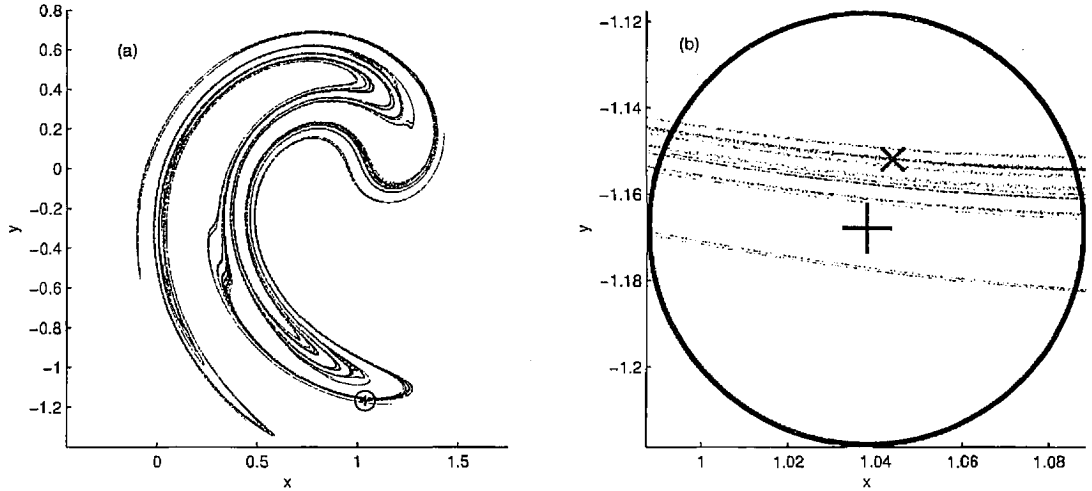
Figure 3.3: Example of perfect ensemble for the Ikeda Map when only one observation is considered. The observational noise is uniformly bounded. In panel a, the black dots indicate samples from the Ikeda Map attractor, the blue circle denotes the bounded noise region where the single observation is the centre of the circle. Panel b is the zoom-in plot of the bounded noise region. The red cross denotes the true state of the system

ensemble becomes actually "perfect", that is the ensemble members are consistent with infinite past observations which is the best ensemble one can obtain from the past observations. One might conjecture that this perfect ensemble is the set of indistinguishable states of the true state. In order to avoid confusion, in our thesis we call the perfect ensemble that based on finite number of observations, *dynamically consistent ensemble.*

$\Phi(x)$ can be known to be very complicated fractal without being known explicitly. In practice, to form the dynamically consistent ensemble, we simply integrate the system of interest and collect the states that are consistent with the observations considered (80). For bounded noise model, consistent means within the bounded region about the observations. For unbounded noise, one can, for
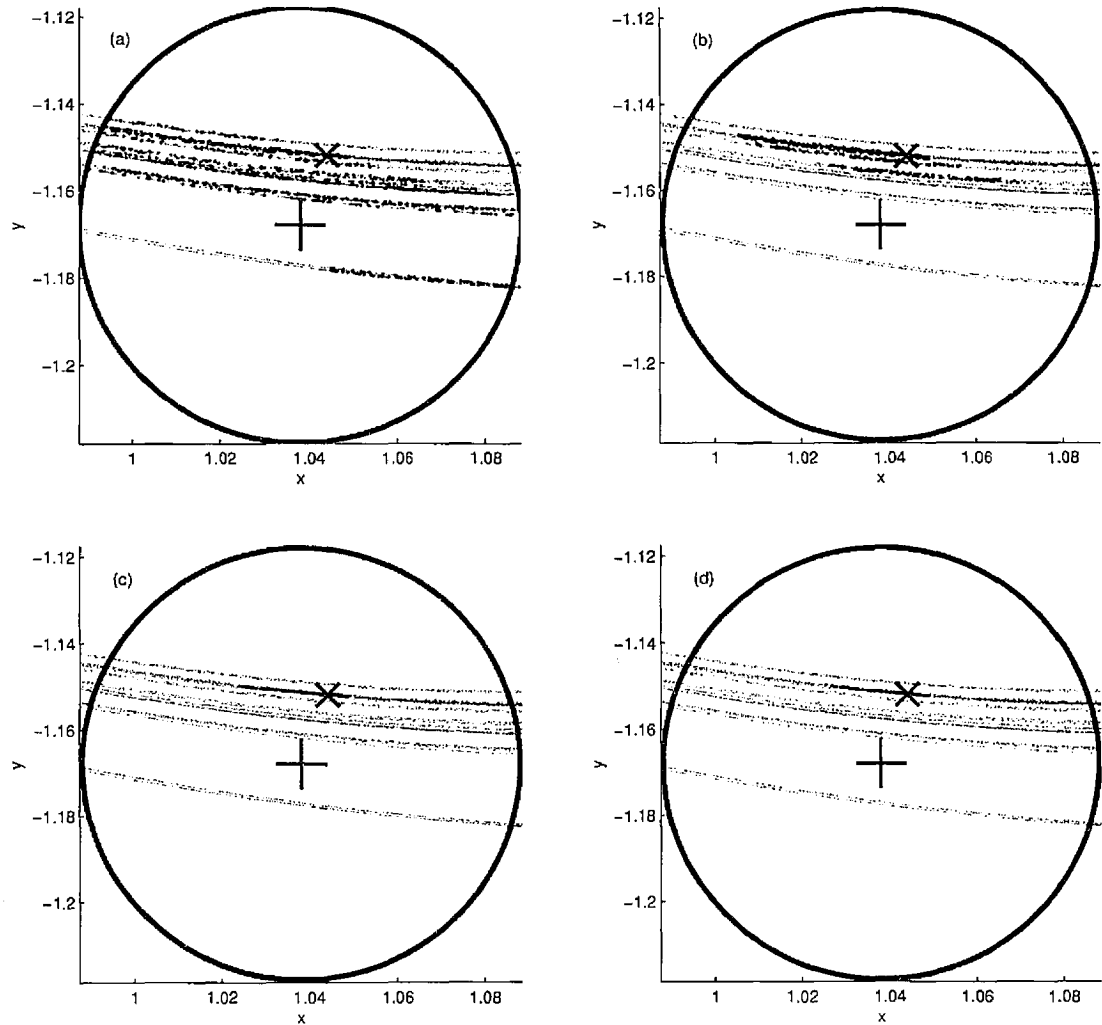
Figure 3.4: Following Figure 3.3, examples of perfect ensemble are shown for the Ikeda Map when more than one observation is considered. The perfect ensemble of different number observations are considered are plotted separately. Two observations are considered in panel (a), 4 in panel (b), 6 in panel (c) and 8 in panel (d). In all the panels, the green dots are indicates the members of perfect ensemble.

example, define consistent to be within the sphere centered on the observation. The radius of the sphere should be chosen depending on the number of obser-

vations, to increase as the number of observations increases. In practice we use 'within four standard deviations' (39) i.e. the states, treated to be consistent with observations, never farther than 4σ from the observations. Although the dynamically consistent ensemble produce a desirable ensemble state of the current state where the ensemble members are consistent with both model dynamics and the observations, it is extremely costly to construct such ensemble, when the model states are in the high dimensional state space. Even in low dimensional systems, it is prohibitively costly when a relative long observation window is considered.

3.7 Results

In this section we first compare the ISGD method with 4DVAR method by looking at the model trajectory each produces. We then compare the ISIS method with Ensemble Kalman Filter by comparing ensemble members in the state space and evaluating them using the new ϵ-ball method defined in Section 3.7.2. Finally we compare our method with the perfect ensemble.

3.7.1 ISGD vs 4DVAR

Since the 4DVAR method produces a model trajectory, we can use such model trajectory as a reference trajectory to form the ensemble in the same way as ISIS method. Here instead of comparing the ensemble nowcasting results, we simply compare the trajectory produced by 4DVAR with the reference trajectory generated by ISGD. We apply both methods to Ikeda Map (Experiment A) and the 18 dimensional Lorenz96 Model I (Experiment B). For each case three different length assimilation windows are tested. For Ikeda Map, the assimilation win-

dows are 4 steps, 6 steps and 8 steps. For Lorenz96, the assimilation windows are 8 hours (short window), 16 hours (median window) and 32 hours (long window). An hour indicates 0.01 Lorenz96 time unit (see Section 2.4). Details of the experiments are listed in Appendix B Table B.1 & B.2.

We use the second term of the 4DVAR cost function, i.e. the distance between observations and model trajectory (equation 3.34), and the distance between true states and model trajectory (equation 3.35) as diagnostic tools to look at the quality the model trajectories generated by each method.

$$\frac{1}{N+1} \sum_{i=0}^{N} (h(\mathbf{x}_{t_i}) - \mathbf{s}_{t_i})^T \Gamma_i^{-1} (h(\mathbf{x}_{t_i}) - \mathbf{s}_{t_i}), \tag{3.34}$$

$$\frac{1}{N+1} \sum_{i=0}^{N} (\mathbf{x}_{t_i} - \tilde{\mathbf{x}}_{t_i})^T \Gamma_i^{-1} (\mathbf{x}_{t_i} - \tilde{\mathbf{x}}_{t_i}) \tag{3.35}$$

From Table 3.1 and 3.2, we can see that when the assimilation window is short for both Ikeda and Lorenz96 experiments, both 4DVAR and ISGD tend to generate model trajectories that are closer to the true states than to the observations [1]. This is expected as both methods can be treated as noise reduction method. For ISGD method, the larger window length is considered, the better [2] model trajectories are produced. We expect the ensemble formed based on the reference trajectory to produce better ensemble forecast when the reference trajectory is closer to the true states of the system. For 4DVAR method, when the

---

[1] Although the trajectories is slightly father away from the observations, they are still consistent with the observational noise.

[2] closer to the true states of the system

Window length	a) Distance from observations					
	Average		Lower		Upper	
	4DVAR	ISGD	4DVAR	ISGD	4DVAR	ISGD
4 steps	1.58	1.66	1.51	1.59	1.63	1.73
6 steps	11.06	1.77	8.17	1.71	14.28	1.83
8 steps	51.84	1.85	46.16	1.80	58.54	1.90
Window length	b) Distance from truth					
	Average		Lower		Upper	
	4DVAR	ISGD	4DVAR	ISGD	4DVAR	ISGD
4 steps	0.52	0.61	0.48	0.55	0.55	0.67
6 steps	9.51	0.39	6.70	0.36	12.59	0.42
8 steps	50.04	0.28	43.59	0.25	55.77	0.31

Table 3.1: a) Distance between the observations and the model trajectory generated by 4DVAR and ISGD for Ikeda experiment, b) Distance between the true states and the model trajectory generated by 4DVAR and ISGD for Ikeda experiment, Average: average distance, Lower and Upper are the 90 percent bootstrap re-sampling bounds, the noise model is $N(0, 0.05)$ and the statistics are calculated based on 1024 assimilations and 512 bootstrap samples are used to calculate the error bars (Details of the experiment are listed in Appendix B Table B.1).

window length is relatively long, it suffers from the multiple local minima and produces the model trajectory which is both inconsistent with observations and far away from the truth although we expect to obtain more information of both observation and model dynamics from the longer window of observations. As we discussed in Section 3.4, applying the 4DVAR algorithm, one faces the dilemma of either from the difficulties of locating the global minima with long assimilation window or from losing information of model dynamics and observations by using short window. Without introducing such shortcomings, our ISGD method produces better model trajectories.

Window length	a) Distance from observations					
	Average		Lower		Upper	
	4DVAR	ISGD	4DVAR	ISGD	4DVAR	ISGD
8 hours	16.0	16.6	15.9	16.4	16.1	16.8
16 hours	16.8	17.0	16.7	16.9	16.9	17.2
32 hours	28.3	17.2	27.6	17.1	28.9	17.3
Window length	b) Distance from truth					
	Average		Lower		Upper	
	4DVAR	ISGD	4DVAR	ISGD	4DVAR	ISGD
8 hours	2.73	0.93	2.68	0.89	2.78	0.96
16 hours	1.35	0.41	1.33	0.40	1.37	0.42
32 hours	11.76	0.19	11.17	0.18	12.46	0.20

Table 3.2: a) Distance between the observations and the model trajectory generated by 4DVAR and ISGD for Lorenz96 experiment, b) Distance between the true states and the model trajectory generated by 4DVAR and ISGD for Lorenz96 experiment, Average: average distance, Lower and Upper are the 90 percent bootstrap re-sampling bounds, the noise model is $N(0, 0.4)$ and the statistics are calculated based on 1024 assimilations and 512 bootstrap samples are used to calculate the error bars (Details of the experiment are listed in Appendix B Table B.2).

3.7.2 ISIS vs EnKF

In this section we first explore the low dimensional case in order to provide easily visualised evidence. Then we evaluate the nowcasts using ϵ-ball method defined on following.

- Compare the results in the state space

  We applied both ISIS and EnKF in the 2 dimensional Ikeda Map (Experiment C) and plot the ensemble results in the state space (The details of the experiments are given in Appendix B Table B.3). Four nowcast examples are plotted in Figure 3.5. In all panels of Figure 3.5, the ensemble, produced by ISIS method, not only stays closer to the true state but also reflects the structure of the model's attractor as the ensemble members lies along the

model attractor. The EnKF ensemble, however, has its own structure as the ensemble members do not lie along the model attractor. In the top two panels of Figure 3.5, the EnKF ensemble manage to cover the true state and tends to stay close to the model's attractor. While in bottom two panels of Figure 3.5, the ensemble members are systematically off the attractor and tend to stay close to the observations and not covering the true state.

- Evaluate both methods via ϵ-ball

Here we introduce a simple new probabilistic evaluation method, which evaluate the ensemble forecasts without transforming it into probability distribution.

Given the verification corresponding to the forecast at time t, in this case the verification is the true state at $t = 0$. One can draw a hyper-sphere with radius ϵ (hereafter ϵ-ball) around the verification. For any methods, one can record the probability mass that is inside different size of ϵ-ball. One can compare the result between two methods by simply counting the proportion of times one method beats the other. If the methods tie, both methods win. When the size of the ϵ-ball is very small, we expect neither of the methods to be able to have ensemble members inside the ϵ-ball. When the size of the ϵ-ball is big enough, we expect all the ensemble members will fall inside the ϵ-ball. In both cases, both methods wins. When the size of the ϵ-ball is neither too large nor too small, we can investigate which method produces ensemble forecasts assigns more probability mass around the verification. The advantage of the ϵ-ball method is that it is simple and easy to implement. Note the weakness of this method is that it is not
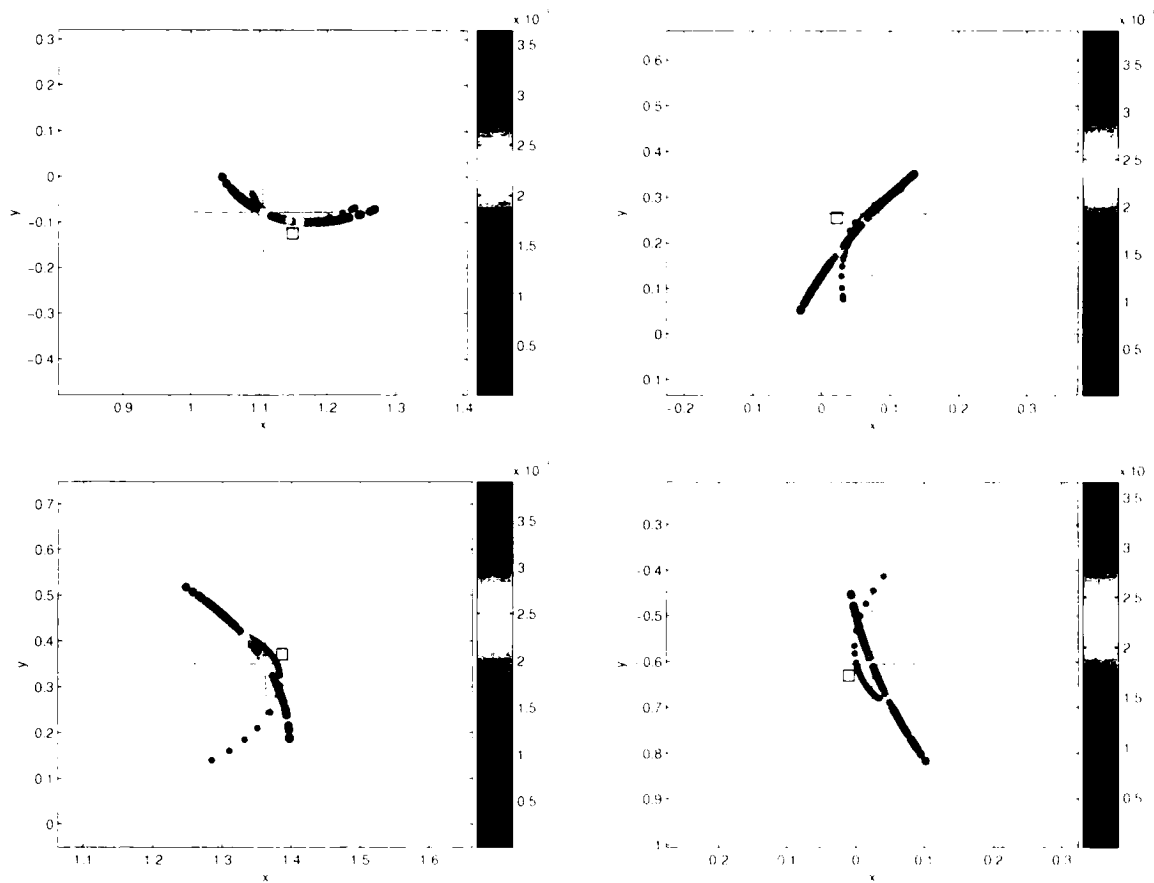
Figure 3.5: Ensemble results from both EnKF and ISIS for the Ikeda Map (Experiment C). The true state of the system is centred in the picture located by the cross; the square is the corresponding observation; the background dots indicate samples from the Ikeda Map attractor. The EnKF ensemble is depicted by 512 purple dots. Since the EnKF ensemble members are equally weighted, the same colour is given. The ISIS ensemble is depicted by 512 coloured dots. The colouring indicates their relative likelihood weights. Each panel is an example of one nowcast.

proper (12). We will discuss the weakness of the ϵ-ball method and compare it with the proper Ignorance Score in Section 6.1.3.

We compare our ISIS method with the EnKF method in both low dimen-

sional Ikeda Map (Experiment C) and higher dimensional Lorenz 96 model I (Experiment D). The details of the experiments are given in Appendix B Table B.3 & B.4. In both cases we evaluate the nowcasting performance using ϵ-ball. Figure 3.6 shows the comparison between EnKF and ISIS. From the figures, it appears that the ensemble generated by ISIS outperforms the one generated by EnKF for almost all different sizes of the epsilon balls in both higher dimensional Lorenz96 and low dimensional Ikeda Map experiments. [1]

3.7.3 ISIS vs Dynamically consistent ensemble

In this section, we compare the nowcasting performance of ISIS ensemble with that of the dynamically consistent ensemble (DCEn). For the purpose of simplicity and efficiency, in the following experiments only uniform bounded noise model is used to create the observations. Since finding the perfect ensemble members in the high dimensional case is extremely cost, we will only compare the results in the low dimensional Ikeda Map (Experiment E). Similar to the previous section, we first compare both methods by looking at the ensemble results in the state space and then we compare them by the ϵ ball method. As we mentioned in section 3.6, the more observations are considered, the better DCEn member can be found. In Figure 3.7, 3.8, 3.9, 3.10, we compare the ISIS results (with fixed window length, i.e. each window contains 12 observations) with the results produced by DCEn where different number of observations are considered. Details

---

[1]Note we expect both methods wins when the size of the ϵ-ball is very small or very large. In the Ikeda experiment, it happens when the size of the ϵ-ball less than 0.001 or larger than 1 although it is not seen in panel a) of Figure 3.6. And in the Lorenz96 experiment it happens when the size of the ϵ-ball larger than 6 although it is not seen in panel b) of Figure 3.6.
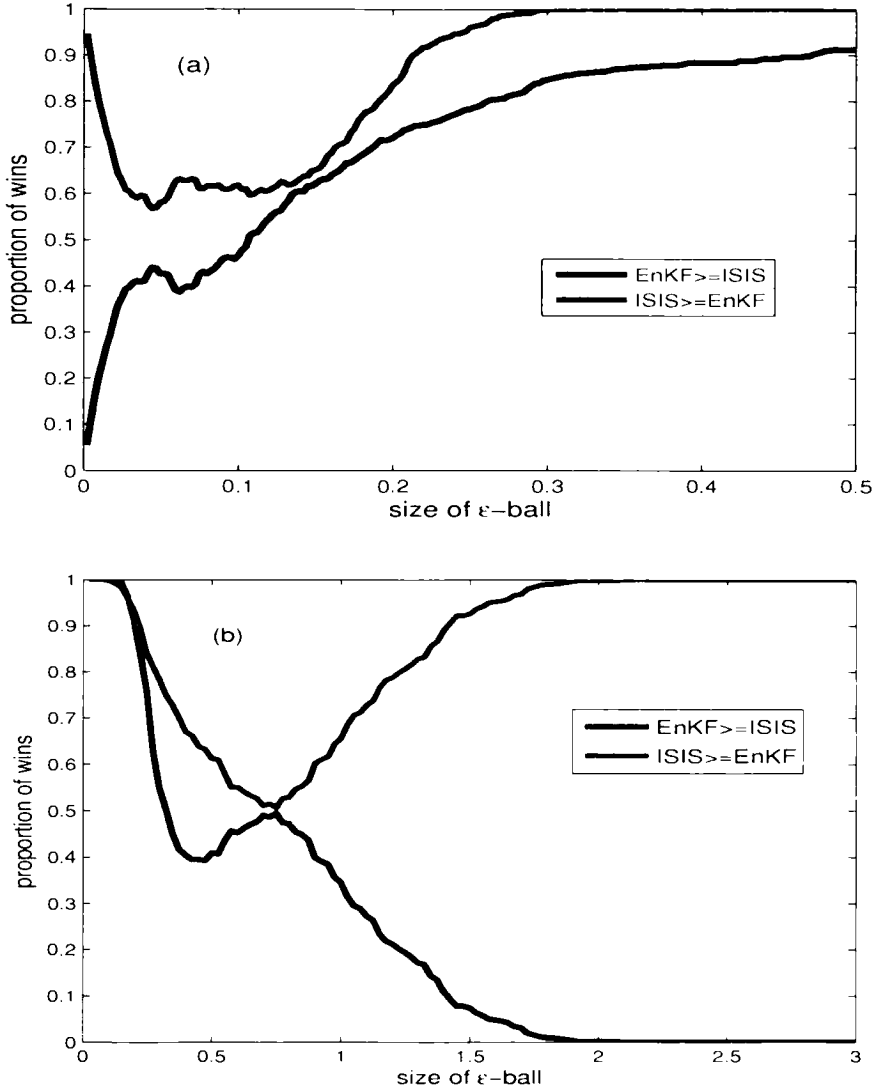
Figure 3.6: Compare the EnKF and ISIS results via ϵ-ball, the blue line denotes the proportion of EnKF method wins and the red line denotes the proportion of ISIS method wins a) Ikeda experiment. Noise level 0.05 (Details of the experiment are listed in Appendix B Table B.3); b) Lorenz96 experiment. Noise level 0.5 (Details of the experiment are listed in Appendix B Table B.4)

of the experiment are given in Appendix B Table B.5. It appears that when the DCEn is constructed by considering a small number of observations (e.g. 1 or 2), the ISIS ensemble built on 12 observations outperforms the DCEn as shown in Figure 3.7, 3.8. From the first four panels of Figure 3.7 and 3.8, we found that some of the DCEn members lie on the same model's attractor as the true state does, some are not while the ISIS ensemble seems to be lying on the right model's attractor. And by evaluating the nowcast ensemble using ϵ-ball method, we found the ISIS ensemble assigns more probability mass around the true state than the DCEn for almost all different sizes of ϵ ball. This is due to the fact that limited dynamical information are contained in such short window of observations. When more observations are considered the DCEn outperforms the ISIS ensemble. Figure 3.9 shows that even using half window-size of the observations, the DCEn outperforms the ISIS ensemble. The DCEn seems to be more concentrated and closer to the true state than the ISIS ensemble and assign more probability mass around the true state. Using the same length of the observations, with no surprise the DCEn again wins.

As we discussed in Section 3.6, the DCEn is the optimal ensemble estimates one may achieve. It is expected to outperform any other state estimation methods. Although our ISIS ensemble, with no doubt, underperforms the dynamically consistent ensemble, it seems to have similar structure as the dynamically consistent ensemble does. Note the ISGD algorithm is run for finite time, with more ISGD iterations, we conjecture the ISIS ensemble will converges to the DCEn. In practice, DCEn is computationally inapplicable while our IS methods can be applied in both low dimensional and high dimensional systems (53).
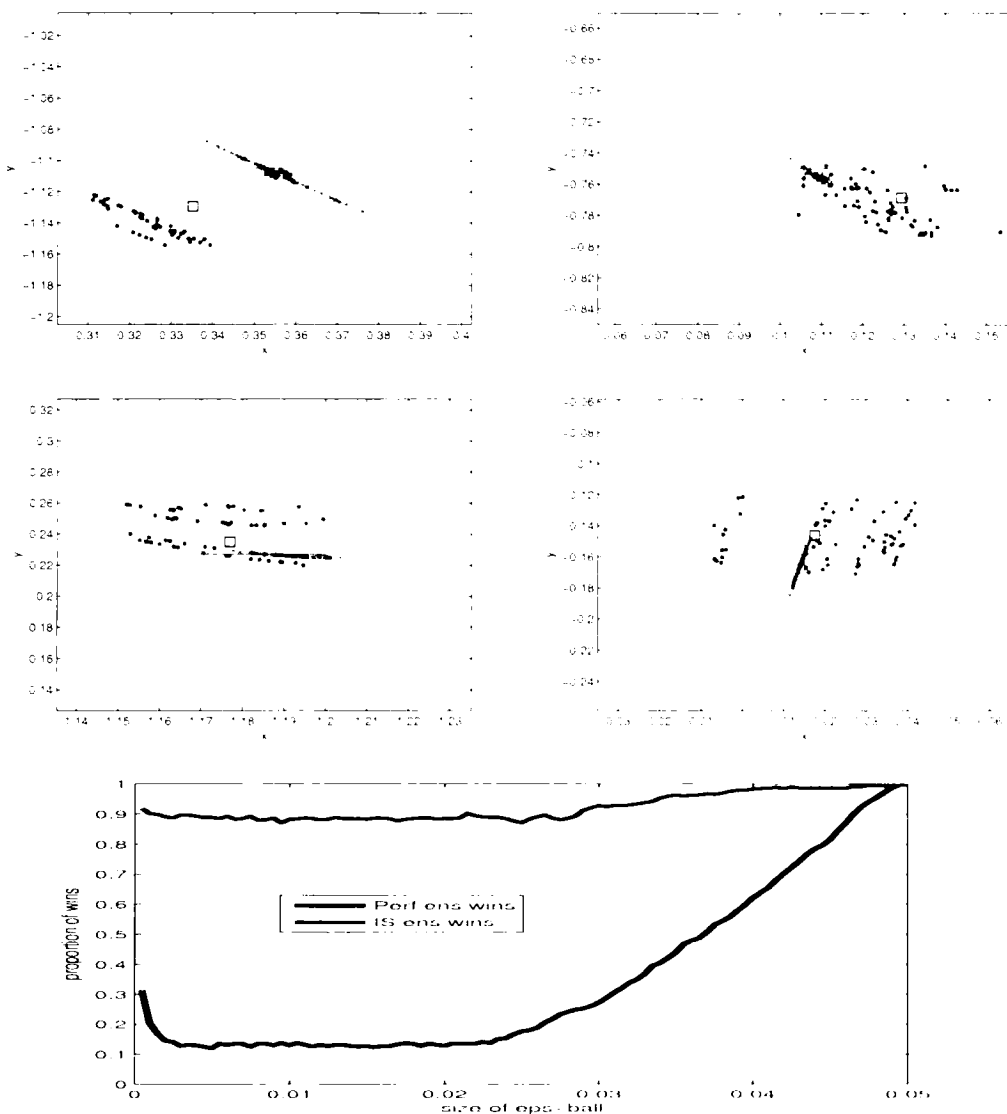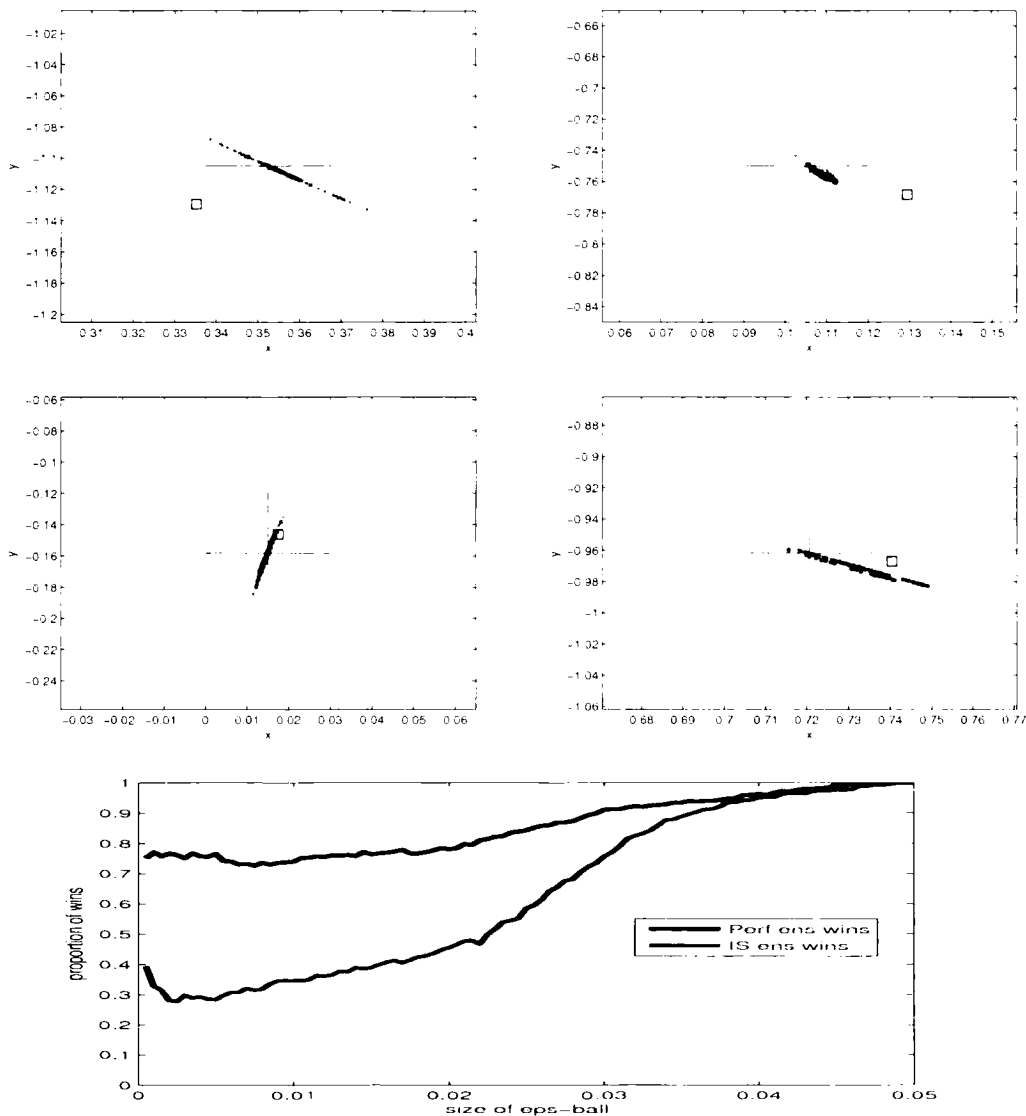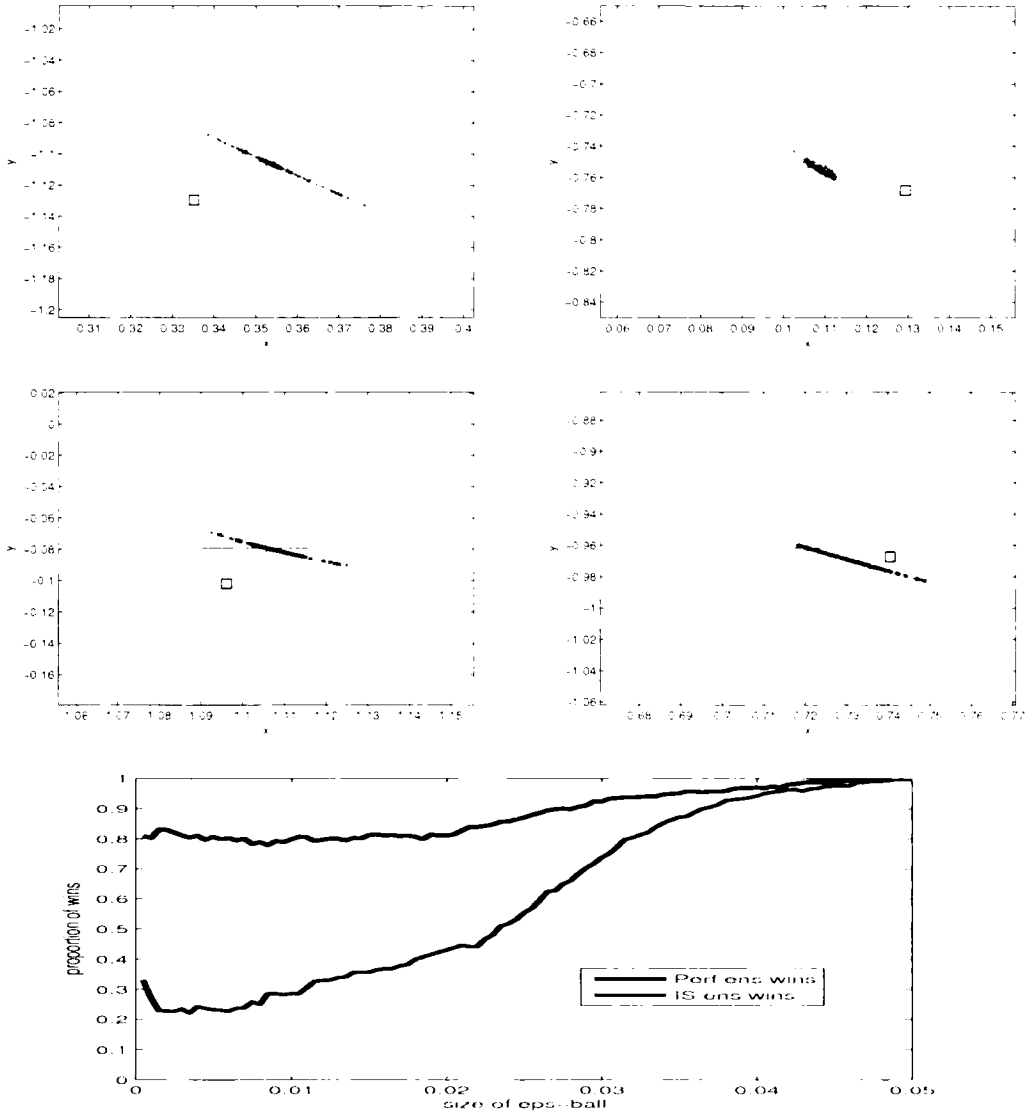
Figure 3.7: Dynamically consistent ensemble built on 1 observation compared with ISIS ensemble built on 12 observations. the noise model is U(-0.025,0.025). each ensemble contains 64 ensemble members. The top four panels following Figure 3.5. plot the ensemble in the state space. The ISIS ensemble is depicted by green dots. The DCEn is depicted by purple dots. The bottom panel following Figure 3.6 compare the DCEn and ISIS results via ϵ-ball. (Details of the experiment are listed in Appendix B Table B.5)
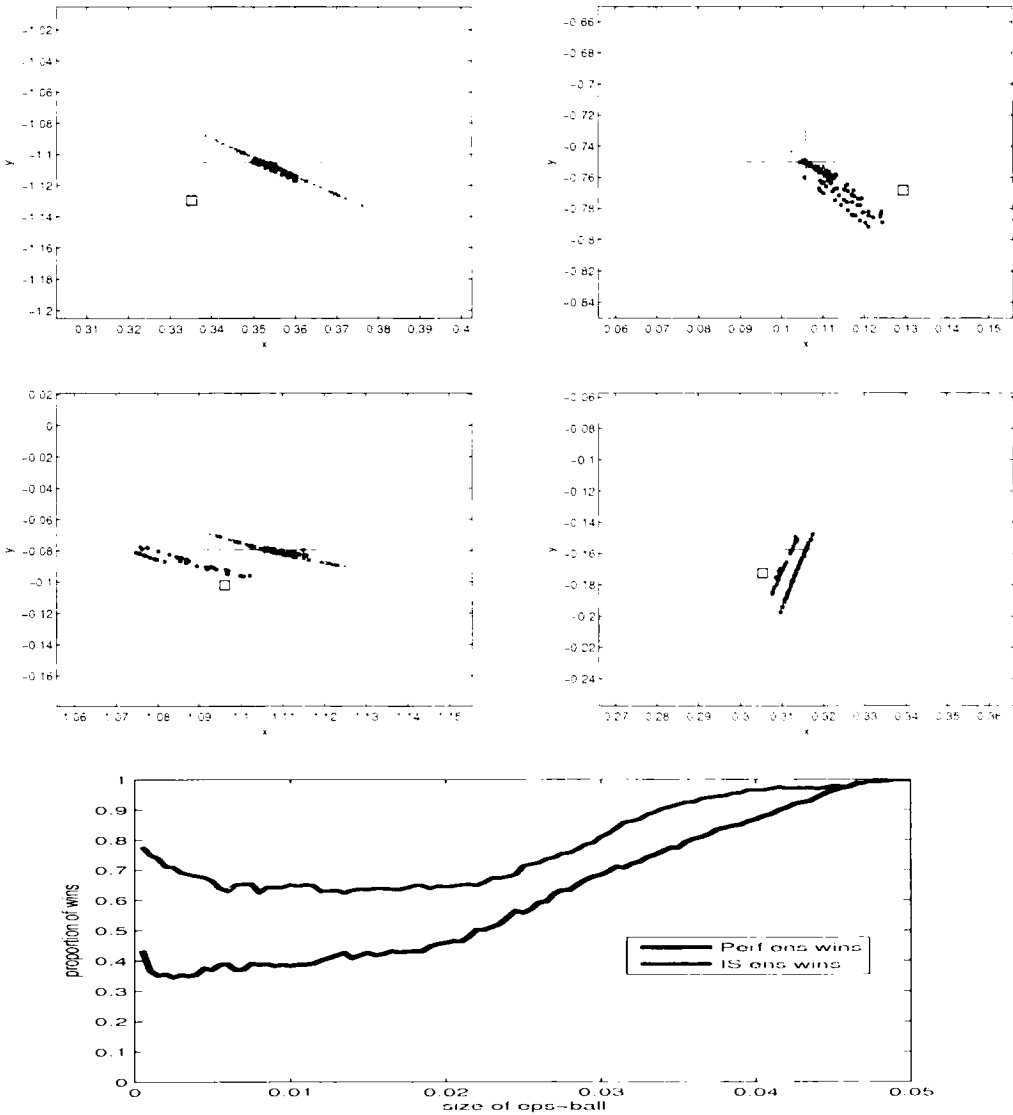
Figure 3.8: Dynamically consistent ensemble built on 2 observations compared with ISIS ensemble built on 12 observations. the noise model is U(-0.025,0.025). each ensemble contains 64 ensemble members. The top four panels following Figure 3.5. plot the ensemble in the state space. The ISIS ensemble is depicted by green dots. The DCEn is depicted by purple dots. The bottom panel following Figure 3.6 compare the DCEn and ISIS results via ε-ball. (Details of the experiment are listed in Appendix B Table B.5)

Figure 3.9: Dynamically consistent ensemble built on 6 observations compared with ISIS ensemble built on 12 observations. the noise model is U(-0.025.0.025). each ensemble contains 64 ensemble members. The top four panels following Figure 3.5. plot the ensemble in the state space. The ISIS ensemble is depicted by green dots. The DCEn is depicted by purple dots. The bottom panel following Figure 3.6 compare the DCEn and ISIS results via ϵ-ball. (Details of the experiment are listed in Appendix B Table B.5)

Figure 3.10: Dynamically consistent ensemble built on 12 observations compared with ISIS ensemble built on 12 observations. the noise model is U(-0.025,0.025). each ensemble contains 64 ensemble members. The top four panels following Figure 3.5. plot the ensemble in the state space. The ISIS ensemble is depicted by green dots. The DCEn is depicted by purple dots. The bottom panel following Figure 3.6 compare the DCEn and ISIS results via ε-ball. (Details of the experiment are listed in Appendix B Table B.5)

3.8 Conclusions

In this chapter, we considered the problem of estimating the current states of the model in the perfect model scenario. Based on the Indistinguishable States Theory, reviewed in Section 3.2, a new methodology is introduced to address the nowcasting problem. Our methodology involves first applying the ISGD algorithm to identify a reference trajectory which reflects the set of indistinguishable states of the true state. The ISIS method is then introduced to form the ensemble by selecting the model trajectories from the set of indistinguishable states of the reference trajectory.

The well established 4DVAR method is reviewed and the difference between 4DVAR method and ISGD method is discussed. Applying both method to Ikeda Map and Lorenz96 Model I, we demonstrate that the ISGD method produces more consistent results than 4DVAR method. This result comes with no surprise due to the fundamental shortcoming of the 4DVAR method, i.e. one faces the dilemma of either from the difficulties of locating the global minima with long assimilation window or from losing information of model dynamics and observations by using short window. The widely used sequential method EnKF is reviewed and discussed. Comparisons between ISIS method and EnKF method have been made in low dimensional Ikeda map and higher dimensional Lorenz96 model. By looking at the ensemble results in the state space, we find that the structure of the ensemble obtained by ISIS method is more consistent with the model dynamics than that of the ensemble produced by EnKF method. A new simple evaluation method, ϵ-ball, is introduced to evaluate the nowcasting results of both methods. We find that in both Ikeda Map and Lorenz96 model experi-

ments, our method systematically assigns more probability mass around the true state than the EnKF method.

The optimal ensemble, dynamically consistent ensemble (perfect ensemble), is described. Although the DCEn outperforms the ISIS ensemble, we found the ensembles they produce have similar structure as both methods produce the ensembles that reflect the dynamical information of the model. In practice, DCEn is computationally inapplicable while our IS methods can be applied in both low dimensional and high dimensional systems (53).

Chapter 4

Parameter estimation

In this chapter we consider the problem of parameter estimation of deterministic nonlinear models. The future evolution of the nonlinear dynamical models depend strongly on the initial conditions and parameter specifications. As forecast errors of nonlinear models will not be Gaussian distributed even if the observation errors are drawn from Gaussian distribution, tradition methods like least squares are not optimal. Methods have been developed to address the shortcomings of traditional methods, for example estimating model parameters by incorporating the global behaviour of the model into the selection criteria (64). Two new alternative approaches are introduced in this chapter within the perfect model scenario (PMS) where the mathematical structure of the model equations are correct and the noise model is known, but the true parameter values are unknown. The first approach forms the cost function based on probabilistic forecasting, we call it Forecast Based Estimates. The second approach focuses on the geometric properties of trajectories in short term while noting the global behaviour of the model in the long term, we call this method Dynamical Coherent Estimates. Dynamical

63

Coherent Estimates is also applicable to the case that only partial observations are available. We will first define the problem of parameter estimation in Section 4.1. The traditional Least Squares estimates method is then described and discussed in section 4.2. Forecast Based Estimates and Dynamical Coherent Estimates are presented in section 4.3 and section 4.4 respectively. Our approaches are compared with Least Squares Estimates and the numerical results are shown on several nonlinear models. Fundamental challenges remain in estimating model parameters when the system is not a member of the model class. Discussions of applying both methods to the case that the model structure is imperfect and defining optimal parameter values are presented in section 4.5.

4.1   Technical statement of the problem

Suppose the evolution of a system state $\tilde{x}_i \in \mathbb{R}^{\tilde{m}}$ is governed by finite dimensional discrete deterministic nonlinear dynamics:

$$\tilde{x}_{i+1} = \tilde{F}(\tilde{x}_i, \tilde{a}), \tag{4.1}$$

where the system's parameters are contained in the vector $\tilde{a} \in \mathbb{R}^{\tilde{l}}$. In the Perfect Model Scenario (see section 3.1), the model state space and system state space are identical. $F(x, a)$ of a model is known to match that of the system exactly, i.e. $F \equiv \tilde{F}$. Suppose the value for the vector of model parameters a is unknown and must be estimated from observations s_i of the state variables $\tilde{x}_i$. Assuming additive measurement error η_i yields observations $s_i = \tilde{x}_i + \eta_i$, where η_i is IID distributed. Without measurement error, $\tilde{l} + 1$ sequential measure-

ments $s_i, s_{i+1}, ..., s_{i+l}$ would, in general, be sufficient to identify the true parameter $\tilde{a}$ (64). In the presence of observational noise, the true state of the system $\tilde{x}_i$ can not be determined precisely even infinite observations are provided and the parameter values are known exactly (48). As we will see, this also makes the problem of parameter estimation much harder.

In this chapter we focus on addressing the problem of parameter estimation in the perfect model scenario. Our aim is to extract the information from a finite series of observations given the exact noise model and the functional form of the dynamic model to determine the model parameter values.

We never identify the true model parameter precisely of course; rather we introduce two methods for extracting significant information on parameter values, one via evaluating the probabilistic forecast performance that they produce; the other via the trajectories they admit. And how to report the parameter estimates based on our methods are discussed.

4.2 Least Squares estimates

The famous least squares method (8; 27; 56) estimates the parameter by testing the error in the forecast initialised at observations. The one-step least squares(LS) estimate gives the value of parameter which minimises the least squares cost function.

$$C_{LS}(\mathbf{a}) = \sum_{i=1}^{N-1} err_i^2,$$

(4.2)

where $err_i = s_{i+1} - F(s_i, a)$, the one-step prediction error. The LS cost function can be derived from Maximum Likelihood Estimate(MLE) (17). Assume the observational noise and the forecast error, i.e. $s_{i+1} - F(s_i, a)$, are IID Gaussian distributed with mean 0 and standard deviation σ. Given the observations $s_t, t = 1, ..., N$ the likelihood function of parameter a is then given by

$$L(a) = \frac{1}{(2\pi\sigma^2)^{N/2}} exp\{-\frac{1}{2\sigma^2} \sum_{t=1}^{N-1} (s_{t+1} - F(s_i, a))^2\}. \qquad (4.3)$$

By minimising the log likelihood function, i.e. $log(L(a))$, the Least Squares cost function is then derived. Mcsharry and Smith (64) proved that even with an infinite amount of data the optimal least squares solution is biased when it applied to the 1-D Logistic Map. Figure 4.1 plots the least square estimates against different noise level [1] for both Logistic map and Ikeda map. Figure 4.2 plots the Least Squares cost function in the parameter space for both Moore-Spiegel System and Henon Map experiments, given the noise level fixed. We can see from both figures that Least Squares Estimates systematically rejects the correct parameter value and from Figure 4.1, the higher the noise level is, the more bias in the estimate (20). The LSE method fails simply because the assumption of Independent Normal Distributed (IND) forecast errors does not hold even if the noise is IND.

---

[1]The different noise levels in the plots are defined by the ratio between the standard deviation of the observation noise and the standard deviation of the signal
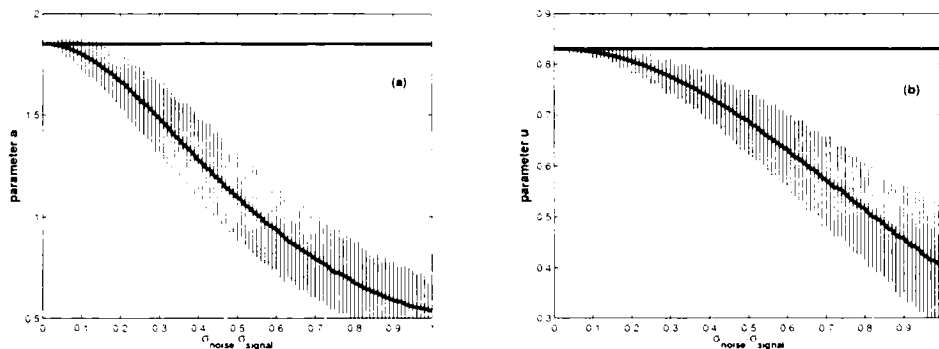
Figure 4.1: Parameter estimation using LS cost functions for different noise level. the black shading reflects the 95% limits and the red solid line is the mean. they are calculated from 1000 realizations and each cost function is calculated based on the observations with length 100. the blue flat line indicates the true parameter value (a) Logistic Map for $a = 1.85$ (b) Ikeda Map for $u = 0.83$

4.3   Forecast based parameter estimation

In this section we address the parameter estimation problem by looking at the forecast performance of different parameter values. Given the same initial conditions. the forecast performance varies as different parameter values are used. An illustration of the procedure used to obtain the forecast skill score is depicted in the schematic flow chart of Figure 4.3 (Details of each step of the procedure are described in the following sections): An ensemble of initial conditions is first formed to account the initial uncertainty. The forecast ensemble at lead time N is obtained by iterating the initial condition ensemble N times forward through the model for given parameter values. The ensemble forecast is then interpreted as a continuous forecast distribution by standard kernel dressing. In order to evaluate the probabilistic forecast in a more robust way. we blend the forecast distribution with the sample climatology. i.e. the historical distribution of the data. In the end we evaluate the forecast distribution via a probabilistic forecast
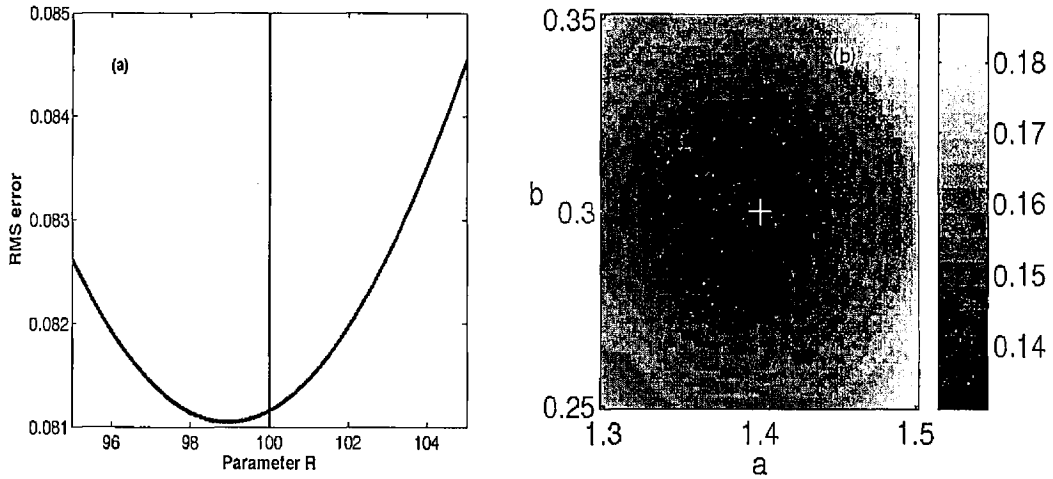
Figure 4.2: LS cost function in the parameter space, (a) Moore-Spiegel Flow with true parameter value R=100 (vertical line), Noise level=0.05; (b) Henon Map with true parameter values a=1.4 and b=0.3 (white plus), Noise level=0.05. In each case, LS cost function is calculated based on 2048 observations.

skill score, Ignorance. Such forecast score is treated as a cost function to obtain the estimate of the unknown parameter.

4.3.1 Ensemble forecast

Even with perfect knowledge of the model class of the system and the observational noise model, it is not possible to disentangle uncertainty in the dynamics from uncertainty in a given set of observations. Any parameter values, except the true parameter values, being used will introduce extra uncertainty in the dynamics. In order to partially account for those uncertainty in the initial condition, we suggest using ensemble forecast. An *ensemble forecast* is a forecast initialised with an ensemble of initial states. Methods, like ISIS, EnKF and Dynamically Consistent ensemble (introduced in Chapter 3) can be used to form an ensem-
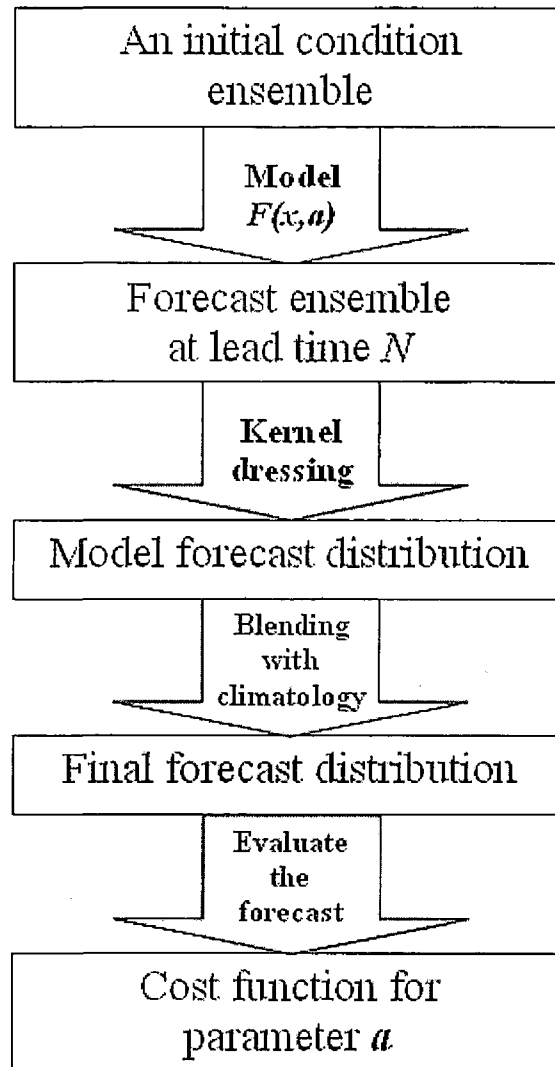
Figure 4.3: Schematic flowchart of obtaining forecast based cost function for parameter estimation

ble of initial states. Here we adopt another simple method, called Inverse Noise (Defined in the following paragraph), to form the initial condition ensemble.

69

Given a model of the observational noise, one can add random draws from the inverse of the observational noise model to the observation to define ensemble members. As each ensemble member is an independent draw from the inverse observational noise distribution, each ensemble member is equally weighted. This Inverse Noise method is an easy way to form the ensemble although the initial states are not guaranteed to [1] be consistent with the long term model dynamics i.e. the ensemble members are not on the attracting manifold of the model (if there is one). For purposes of illustration and simplicity, most results shown in section 4.3.4 are obtained by using Inverse Noise instead of other sophisticated state estimation methods (Discussed in chapter 3) to form the ensemble.

4.3.2 Ensemble interpretation

Ensemble members are often transformed into a distribution function which is easier to express the information contains in the ensemble members and it can be evaluated by forecast skill scores. Continuous forecast distributions can be produced from an ensemble by kernel dressing the ensemble forecast. In this section we give a brief introduction to standard kernel dressing which will be used to explain the problem in this section (see (13; 75) for more details). We define an N^{ens} member ensemble at time t to be $X_t = [x_t^1, ..., x_t^{N^{ens}}]$ and treat all ensemble members as exchangeable. In other words, the ensemble interpretation methods do not depend on the ordering of the ensemble members (13).

A standard kernel dressing approach is to transform the ensemble members into a probability density function:

---

[1]guaranteed not to, in the case of dispersive dynamics.

70

$$p(y : X, \sigma) = \frac{1}{N^{ens}\sigma} \sum_i^{N^{ens}} K\left(\frac{y - x^i}{\sigma}\right), \tag{4.4}$$

where

$$K(\zeta) = \frac{1}{\sqrt{2\pi}} exp(-\frac{1}{2}\zeta^2), \tag{4.5}$$

where y is a random variable corresponding to the density function p and $K(\cdot)$ is the kernel density function, for standard kernel dressing we use standard Gaussian density to be the kernel density function.

In this case a standard kernel dressed ensemble is a sum of Gaussian kernels. Each ensemble member is replaced by a Gaussian kernel centred at x^i. The width of each kernel, called the *kernel width*, is given by the standard deviation of the Gaussian kernel. The kernel width as one of the parameters of ensemble interpretation can be determined by optimising the expected performance, for example the ignorance score introduced in the next section, based on a training set of ensemble and its verification pairs.

We are aware that the variance of the standard kernel dressed ensemble is always larger than the variance of the raw ensemble, no matter how the kernel width is actually determined (93). When the ensemble is over dispersive, or in other words, the ensemble members are further away from each other than from the verification, the standard kernel dressing may even under-performs the Gaussian fit (93). In practice, ensembles tend to be under dispersive. Many advanced and complicated dressing methods exist, for example Brocker (13) introduced an

improved kernel dressing, called "affine kernel dressing" that is more flexible and robust kernel dressing method. In this chapter we use standard kernel dressing to produce the results as it is straightforward to understand and implement.

For any finite ensemble, there remains the chance that the verification lies outside the range of the ensemble. Even if the verification is selected from the same distribution as the ensemble itself, the probability of this happening is $\sim \frac{2}{N^{ens}}$. Given the nonlinearity of the model, these points may be very far from the ensemble, and appear as "outliers" or "bad busts". Those outliers will affect the kernel width significantly by making them wider in order to make the forecast distributions cover them which therefore degrades the performance of probability forecast where the outliers do not appear. To overcome such problems, we combine the forecast distribution with the sample climatology. As we mentioned in Section 2.3, the sample climatology [1] is the distribution of the historical data which can also be treated as an estimate of observed invariant measure of the system. The probability density function of climatology can be approximated from the historical data simply by kernel dressing the historical data. In this thesis we use standard kernel dressing to approximate the density function of climatology. The probabilistic forecast can be improved on average by blending model forecast distribution, which is obtained from the dressed ensemble, with the climatology. By blending with the climatology, defines the forecast distribution to be:

$$p(\cdot) = \alpha p_m(\cdot) + (1 - \alpha)p_c(\cdot) \qquad (4.6)$$

where p_m is the density function generated by dressing the ensemble and p_c is the

---

[1]We will often drop the word "sample" afterwards

estimate of climatological density, the subscript m denotes the model and c the climatology. $\alpha \in [0, 1]$, called blending parameter, denotes the weight assign to the model forecast distribution.

Note that comparing forecast performance of different models may provide a misleading comparison without blending climatology. As it might be the case that, without blending climatology Model A outperforms Model B while with blending climatology this is not the case.

4.3.3 Scoring probabilistic forecasts

A probability forecast describes our expectation of how likely an event is on a particular occasion. One may wish to ask whether a probability forecast is right or wrong. Unlike point forecasts, however, single probability forecasts have no such clear sense of "right" and "wrong". One can only measure how good the probabilistic forecasts are by looking at a large set of forecasts. Conventional diagnostics for evaluating deterministic forecasts, measures such as "root-mean-square error", are not useful with probabilistic forecasts (37).

A probabilistic forecast skill score is a function $S(p(y), Y)$, where Y is the verification and $p(y)$ is a probability density. Following Good (1950), Roulston and Smith (2001) introduced a measure of the quality of the forecasting scheme, which is called Ignorance. Ignorance is a logarithmic scoring rule that can be calculated for real forecasts and realizations. It is equivalent to the expected returns that would be obtained by placing bets proportional to the forecast probabilities (75). And Ignorance is the only proper local score for continuous variables (12; 75). The Ignorance Score is given by:

$$S(p(y), Y) = -log(p(Y)) \qquad (4.7)$$

The difference between the Ignorance scores of two forecast schemes, reflects the expected wealth doubling time under a Kelly Betting. [1] We employ the ignorance score to evaluate the probabilistic forecast in this thesis. In practice, we have to go to empirical since we have limited data. Given N forecast-verification pairs $(p_t, Y_t, t = 1, ..., N)$ (*forecast-verification pair* are a forecast and what actually happened, for example a forecast probability distribution of the temperature in London Heathrow and the temperature actually observed), the empirical average Ignorance skill score is given by:

$$S_{Emp}(p(y), Y) = \frac{1}{N} \sum -log(p(Y)) \qquad (4.8)$$

This empirical average Ignorance skill score is used as a cost function to estimate the parameter values of the model in the results shown in next section. In practice, we can get an idea how accurate of uncertainty in our empirical ignorance by bootstrapping.

---

[1]In a Kelly betting contest (57), one bets all of one's wealth on every outcome in proportion to the forecast probability of that outcome. More precisely, a fraction ω_i of ones wealth, where ω_i is the forecast probability of event E_i occurring, should be wagered on the ith outcome.

4.3.4   Results

In order to demonstrate the effectiveness of our method, parameter estimation by forecast performance is applied to both one and two dimensional systems and results are compared with Least Squares estimates. Figure 4.4a shows the cost function, i.e. Ignorance score, based on probabilistic forecast at lead time 4 for the logistic map, where initial condition ensemble is formed by Inverse Noise. Results of different noise levels are plotted separately. When the noise level is relative large for example 1/8, the information contained in the forecast is unable to tell the difference between the parameter values. When the noise level is small enough, estimates obtained by looking at the Ignorance score of the probabilistic forecast well identifies the parameter values as the minimum ignorance occurs at the vertical line that marks the true parameter value. Figure 4.4b plots the Ignorance cost function of forecast at lead time 4 in the parameter space for the Henon map, same observations are used as Figure 4.2b. The low ignorance region (black) captures the true parameter values. Comparing with LS estimates (Figure 4.2b), using Ignorance as a cost function produces more consistent results.

The forecast based parameter estimate results shown in Figure 4.4a and Figure 4.4b are based on the probabilistic forecast at lead time 4. The particular lead time was chosen because the cost functions at such lead time produce more consistent results. Figure 4.5 shows the forecast based parameter estimates for different lead times. Note there is a bias at short lead time. Also note that although estimates at longer lead time provides more consistent results, the cost function becomes less sharp as lead time gets larger. Examining graphs of several lead times (Figure 4.5), it was found that those of lead time 4 were consistent for
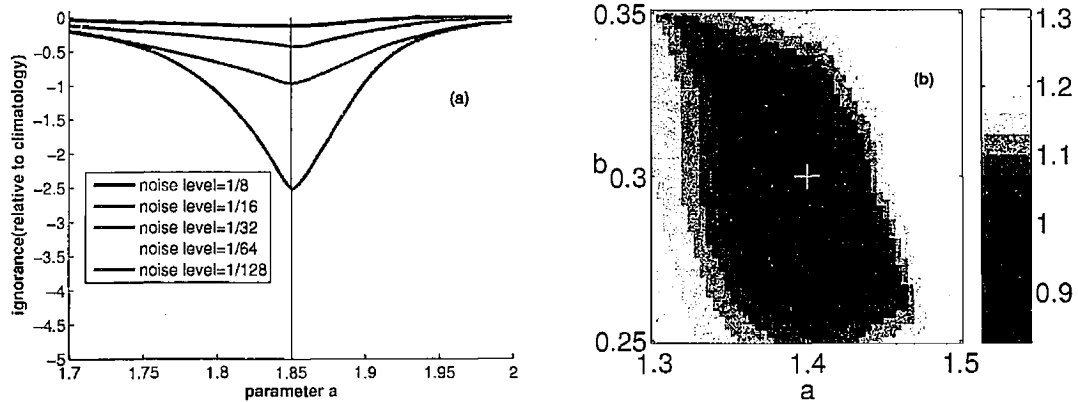
Figure 4.4: Parameter estimation based on ignorance score, 64-member initial condition ensemble is formed by inverse noise, the kernel parameter and blending parameter is trained based on 2048 forecasts and the empirical ignorance score is calculated base on another 2048 forecasts, the ignorance relative to climatology, i.e. 0 represents climatology, is plotted in the parameter space (a) Logistic Map with true parameter value a=1.85, results of different noise levels are plotted separately; (b) Henon Map with true parameter values a=1.4 and b=0.3, Noise level=0.05

this particular example and so these are presented.

The short lead time bias is due to the fact our initial condition ensemble does not contain the information of the model dynamics as explained in the following. The Logistic Map is a nonlinear chaotic map when a=1.85. A randomly observed state is expected to be on the attractor of the Logistic Map. It is almost always true that neither the observation itself (in the case that observational noise exists) nor the initial ensemble members formed by inverse noise lie on the model attractor. Using ensemble members not consistent with the long time dynamics cause the estimates to be biased. Figure 4.6 shows the dynamical consistent ensemble produces unbiased results at both short and long lead time.

Producing dynamical consistent ensembles, however, can be extremely costly.
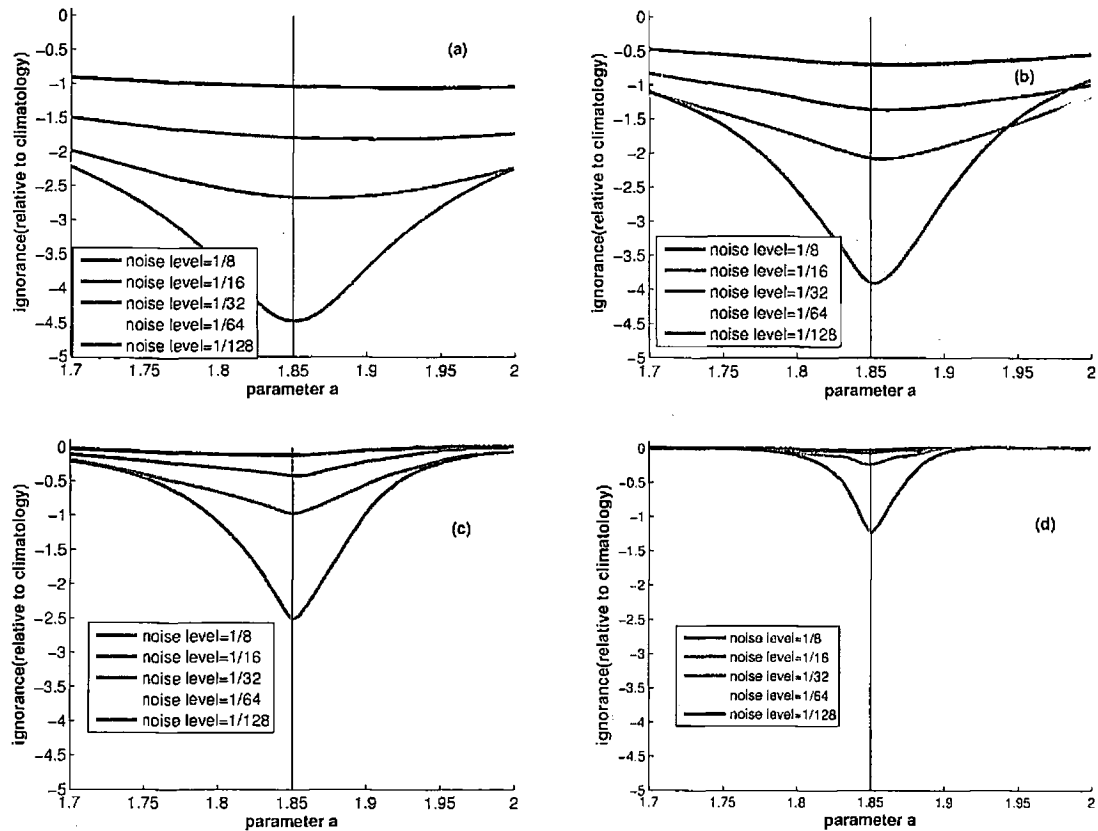
Figure 4.5: Following Figure 4.4a, Parameter estimation using ignorance for Logistic Map with alpha=1.85 (a) Lead time 1 forecast Ignorance(b) Lead time 2 forecast Ignorance (c) Lead time 4 forecast Ignorance (d) Lead time 6 forecast Ignorance.

There are other data assimilation methods which can form informative initial ensemble, for example Indistinguishable States methods introduced in Chapter 3. Using such methods may produce more skillful forecasts which may also help distinguish different parameter values. Nevertheless, when it is costly to run the model, as with weather or climate models, Inverse Noise provides a much faster and cheaper way to form the ensemble. It is presented here to illustrate the methodology for estimating parameter in a nonlinear deterministic model.

Figure 4.6: Follow Figure 4.5, Parameter estimation using forecast Ignorance Score for logistic map with a=1.85, initial condition ensemble formed by dynamical consistent ensemble, a) based on lead time 1 forecast b) based on lead time 4 forecast. Note scale change on y axis from Figure 4.4a and 4.5.

4.4 Parameter estimation by exploiting dynamical coherence

In this section we introduce a second new parameter estimation method which aims to balance the information provided by the dynamic equations and that from the observations. We consider this method as a "geometric" approach as emphasis is placed on model trajectories and their distributions rather than on traditional summary test statistics using observations and forecasts at particular lead times. This study is made in cooperation with Milena C. Cuellar, Leonard A. Smith and Kevin Judd and some of the principal results are presented in (20; 85).

For each parameter value, model trajectories and pseudo-orbits are firstly obtained by applying ISGD method upon the observations (see chapter 3), the parameter values are then evaluated upon how well the corresponding trajectories and pseudo-orbits mimic the observations. Instead of looking at only one statistic

or measurement, we measure i) the consistency between model trajectories and observations by shadowing time; ii) how well model pseudo-orbits approximate relevant trajectories by the mismatch error and iii) the consistency between the implied noise distribution (corresponding to the model pseudo-orbits) and the noise model.

Within the perfect model scenario, there exists a parameter set (for the dynamic model and the noise model) which admits the true trajectory which did, in fact, generate the observed data. Our method is aiming to identify such set by exploiting dynamical coherence. Outside PMS the preferred cost function will undoubtedly depend upon the application; parameters which admit long shadowing times seem a good choice for forecast models.

4.4.1 Shadowing time

Although superficially similar, the question of whether a model shadows a set of observations is a fundamentally different notion from the traditional question of whether or not one mathematical system can shadow the trajectories of another (26; 31; 33; 58; 77; 83). Traditional shadowing (77) involves two well-defined mathematical systems. Our ultimate interest here is between a set of observations and a proposed model. Given a segment of observations $s_0, ..., s_N$, we are interested whether there exists a model trajectory (for a given parameter value) $x_0, ..., x_N$ that the residuals defined by the trajectory and the observations, i.e. $s_i - x_i, i = 0, ..., N$, are consistent with the observational noise model. For an observation s_0 at initial time $t = 0$, the corresponding shadowing time τ_{s_0} is the largest K such that, there is some model state x_0, the time series

$r_i = s_i - F^{(i)}(x_0, a), i = 0, ..., K$ is consistent with the noise model.

In order to calculate the shadowing time, one must evaluate the consistency between a series of residuals and the noise model in some way. For uniform bounded noise this is straightforward: A series of residuals $r_0, ..., r_K$ is consistent with the noise model when every residual is inside the bound. For unbounded noise model, for example Gaussian distribution, there are a variety of approaches to test whether a series points are drawn from the given distribution, for example Chi-Square test and Kolmogorov-Smirnov test. In our methodology we adopt a simple method based on threshold exceedance to do the test. Given that the noise model is unbounded, any observation is conceivable; we look for relevant (9) shadows within a certain probability bound. For purposes of illustration and simplicity, we use the scalar to illustrate the procedure. We test the null hypothesis that the set of residuals $(r_i, i = 0, 1, 2, ..., K)$ is consistent in distribution with independent draw from the noise distribution. The shadowing time is then defined to be the largest K that the null hypothesis is not rejected at the 99.9% significant level. To accept the null hypothesis, we require both that the 90% isopleth of the residual distribution falls below the 99th percentile of the distributions of 90% isopleths given K draws from a Gaussian distribution, *and* that the median of the residual distribution falls below the corresponding 90th percentile for the median of the noise model (Note: The thresholds will vary with the size of the data set and the noise model). Together this implies that the chance rejection rate is 0.001, which will yield good results as long as the shadowing times we test are below 100 (as they are in the results presented in section 4.4.3).

For a given observation time, we are most interested in the trajectory which shadows the longest and is consistent with the observation made at that time.

In practice we consider only a finite set of candidate trajectory segments. Call these candidates $x_c^j, j = 1, ..., N_c$ where N_c is the number of candidates (the subscript c denotes candidate). For each observation define the shadowing time $\tau_s = \max_x \tau_s(x_c^j)$ where the maximum is taken over all candidates x_c values tested. Instead of random sampling around the observations, we derive more useful candidates from relative pseudo-orbits. Following section 3.3, given a sequence of observations, a pseudo-orbit of the model can be derived by ISGD method. Of course the quality of the pseudo-orbit strongly depends on the parameter values, which also links the quality of the parameter value to the candidates used to calculate shadowing time. Points along a pseudo-orbit can be used as candidate initial conditions of trajectory segments. In the results presented below in section 4.4.3, only three candidates per observation were tested: the corresponding point on the pseudo-orbit, the image of the previous point on the pseudo-orbit, and the point midway between these two.

As for each observation s_t, it has its corresponding shadowing time, for a segment of observations we have a distribution of shadowing time. Our idea is using the shadowing time distribution to estimate the parameter values by identifying the interest area in the parameter space. The parameter estimation method introduced in section 4.3 quantifies how well the dynamics of the model mimic the observations at a fixed lead time. The shadowing time distribution is a different flavour of quality statistic, quantifying the time scales over which the dynamics of the system reflect those of the data.

4.4.2 Further insight of Pseudo-orbits

As the model pseudo-orbits obtained by the ISGD method strongly depend on the parameter values, the dynamical information contained in the pseudo-orbits can help highlight areas where the estimates can be considered as candidates for "good" estimations in the parameter space (20). In this section we extract such information by looking at the remaining mismatch error and the implied noise of the model pseudo-orbits.

As the ISGD algorithm, introduced in Section 3.3, is iterated for a finite number of steps, the minimum of the mismatch cost function, i.e 0, is not reached and therefore a model pseudo-orbit is obtained instead of model trajectory. The remaining mismatch error after a fix number of iterations of the ISGD algorithm indicates how well the model pseudo-orbit converges to a model trajectory. For each parameter value, the speed of convergence also indicates how easily a corresponding model trajectory can be found. Therefore the magnitude of the remaining mismatch as a quality of the model pseudo-orbit can be used to identify the interesting areas in the parameter space.

As the model pseudo-orbit can be treated as the estimate of the true states in the model space, the quality of the pseudo-orbit can also be evaluated by the consistency of the corresponding implied noise (defined in section 3.3) distribution with the noise model. With finite ISGD iterations, it generally appears to be the case that the final pseudo-orbit obtained corresponding to the true parameter values has an implied noise level no more than the true noise level, inasmuch as we initialise the ISGD algorithm with the observations and aim to explicitly minimise the mismatch cost function. The pseudo-orbit corresponding to the

incorrect parameter values usually have an implied noise level larger than the true noise level as the implied noise has contributions from not only the observational uncertainty but also the inadequacy of the model dynamics caused by the incorrect parameter values. Figure 4.7 shows the standard deviation of implied noise changes as a function of number of ISGD iterations for Ikeda Map (the ISGD algorithm is applied 1024 observations). For the true parameter values, the implied noise level converges to the real noise level very fast. The implied noise level corresponding to the incorrect parameter values slowly converges to a relative larger noise level.
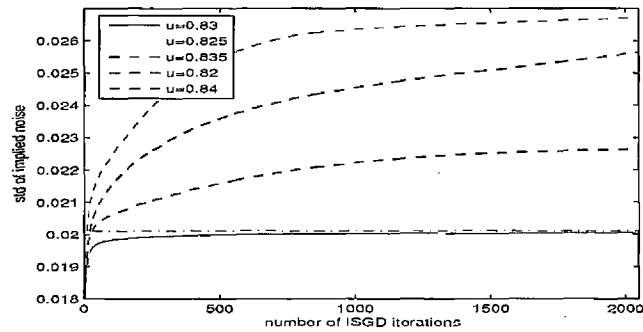
Figure 4.7: The standard deviation of implied noise as a function of number of ISGD iterations for Ikeda Map with true parameter value u=0.83, the black horizontal line denotes the noise level. The statistics for tests using different parameter values are plotted separately.

4.4.3 Results

Panels in Figure 4.8 show the standard deviation of mismatch and implied noise and the isopleths of shadowing time in the parameter space for both Ikeda Map and Moore-Spiegel System, the true parameter value is denoted by a vertical line. These figures establish that our approach can be effective in 2-dimensional

chaotic maps, 3-dimensional chaotic flows. Before discussing these individually, note that in each case the vicinity of the true parameter value is clearly indicated.

The distribution of shadowing time for several isopleths are shown for both the Ikeda system (panel a) and the Moore-Spiegel third order ODE (panel d) in Figure 4.8. The median and 90% contour provide good parameter estimates, while the 99% contour suffers from sampling effects. The choice of isopleth is not critical, although sampling noise will, of course, become an issue for extreme values of the distribution. Thresholds will vary with the size of the data set and the noise model; a simple bootstrap re-sampling approach can identify how high an isopleth can be robustly estimated. In addition to shadowing time, the vicinity of the true parameter value also provide small mismatch error (panel (b) and (e)) and their implied noise level is consistent with the true noise model (panel (c) and (f)). Note in Figure 4.8e, the true parameter does not provide the smallest mismatch error. As we mentioned in Section 4.4.2, the mismatch error is obtained by fixed number of iterations for each parameter value. It indicates how easily a corresponding model trajectory can be found. It is possible that for some parameter values other than the truth, it is easier for the pseudo-orbit to converge to a model trajectory under Gradient Descent. However the model trajectory may not consistent with the observations which can be testified by looking at the shadowing time distribution and implied noise distribution. We suggest looking at the distribution of shadowing time, the mismatch error and the distribution of implied noise together instead of looking at only one of them. Comparing with results shown in Figure 4.1(b) and Figure 4.2(a), our method outperforms least squares estimate approach significantly.

Figure 4.9 shows the results for simultaneous estimation of the two parameter
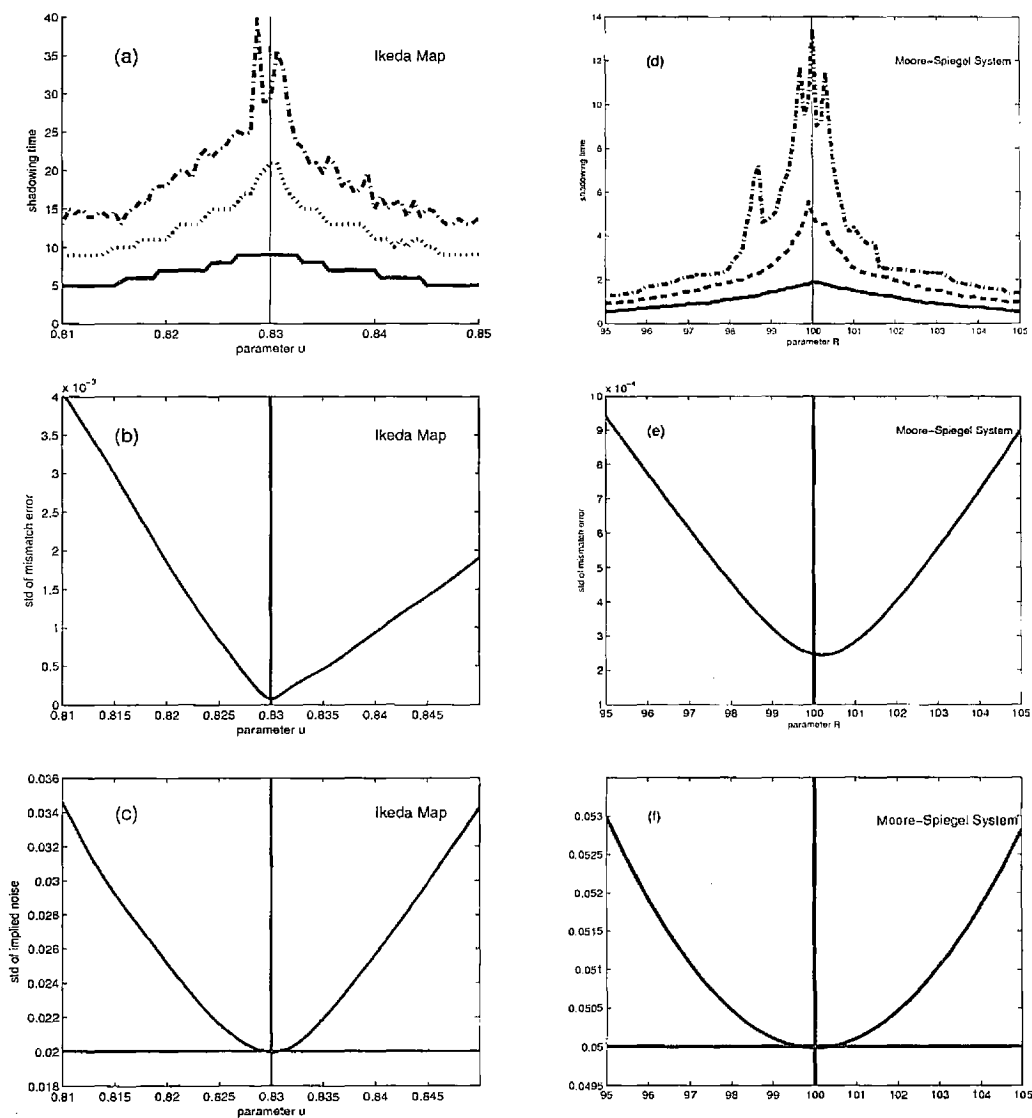
Figure 4.8: Parameter estimations for Ikeda Map with u=0.83 and noise level=0.02; Moore-Spiegel System with R=100 and noise level=0.05, the results are calculated base on 1024 observations, (a) and (d) The median (solid), 90% (dashed) and 99% (dash-dot) shadowing isopleths; (b) and (e) standard deviation of the mismatch; (c) and (f) standard deviation of the implied noise, the horizontal line denotes the real noise model. The vertical line represents the location of the unknown true parameter.

values in the Henon Map, where the standard deviation of the mismatch and the implied noise level are shown in addition to the median of the shadowing time distribution and a cost-function based on the invariant measure (after (64)). The fine structure ("tongues") in panel (c) is due to sensitivity to the parameters, nevertheless its minima are in the relevant regions. Contrasting panels (c) and (d) of figure 4.9 reveals that shadowing times provide information complimentary to that obtained by estimating the invariant measure (the C_{ML} of (64)). The shadowing time distribution provide complimentary information quantifying the time scales on which the model dynamics reflects the observed behaviour. Comparing the results with Figure 4.2b, our method provides more consistent results. Statistics of the shadowing time distribution provide and unambiguous indication of the range of relevant parameter values.

4.4.4 Application in partial observational case

Here we consider the case of parameter estimation in higher dimensional systems where the state vector is not completely observed, i.e. some components of the system are unobserved. In such case, i) we firstly estimate the unobserved components by simply random draw from the climatology of observed components. ii) We then initialise the ISGD algorithm with the observed components and the estimates of the unobserved components. A pseudo-orbit is obtained after a small number of ISGD iterations. iii) We then update the estimates of the unobserved components with the relative components of the pseudo-orbit. Repeating ii) and iii) several times in order to obtain an "good" estimates of the unobserved components. In the end we run a large number ISGD iterations to ob-
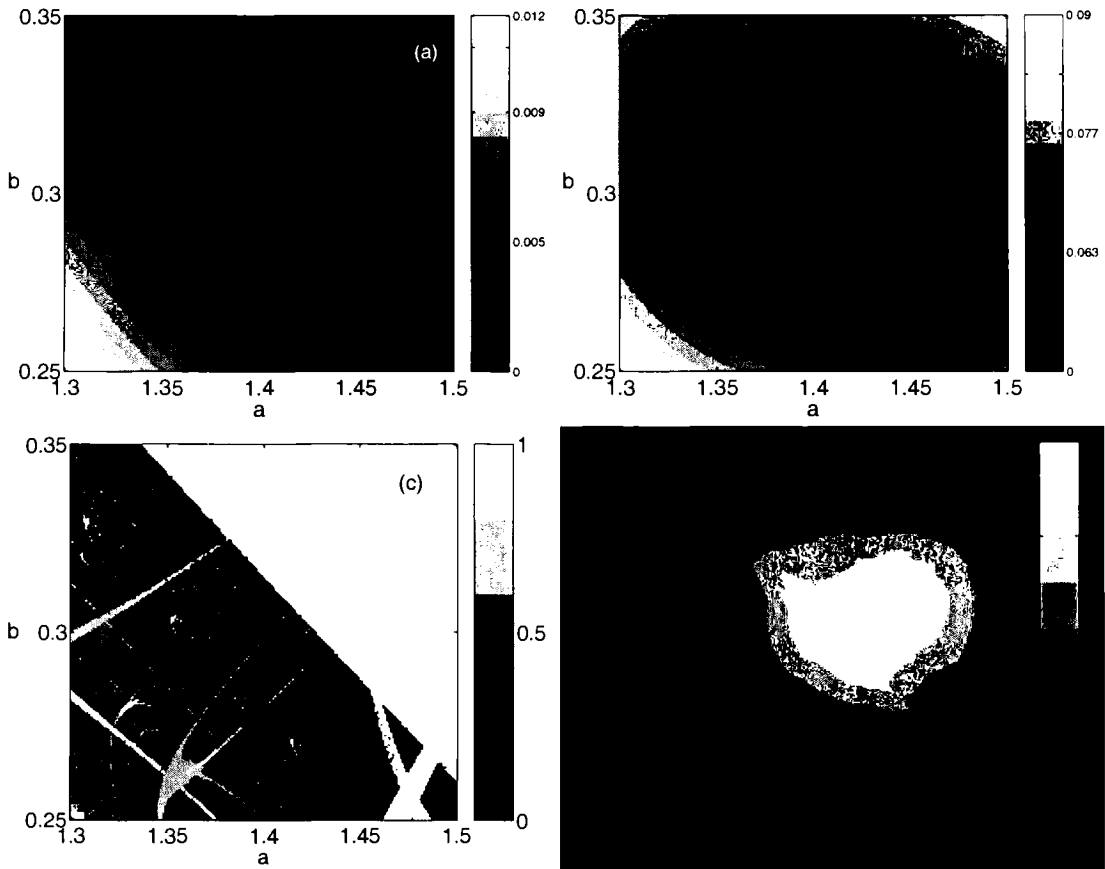
Figure 4.9: Information from a pseudo-orbit determined via gradient descent applied to a 1024 observations of the Hénon map with a noise level of 0.05. (a) standard deviation of the mismatch, (b) the implied noise level, (c) a cost function based on the model's invariant measure (after Fig.4(b) of ref ( )), (d) median of shadowing time distribution.

tain the pseudo-orbit which is used to calculate the shadowing time distribution. In such cases the shadowing-time is determined without placing any constraints whatsoever on the value taken by the unobserved component(s).
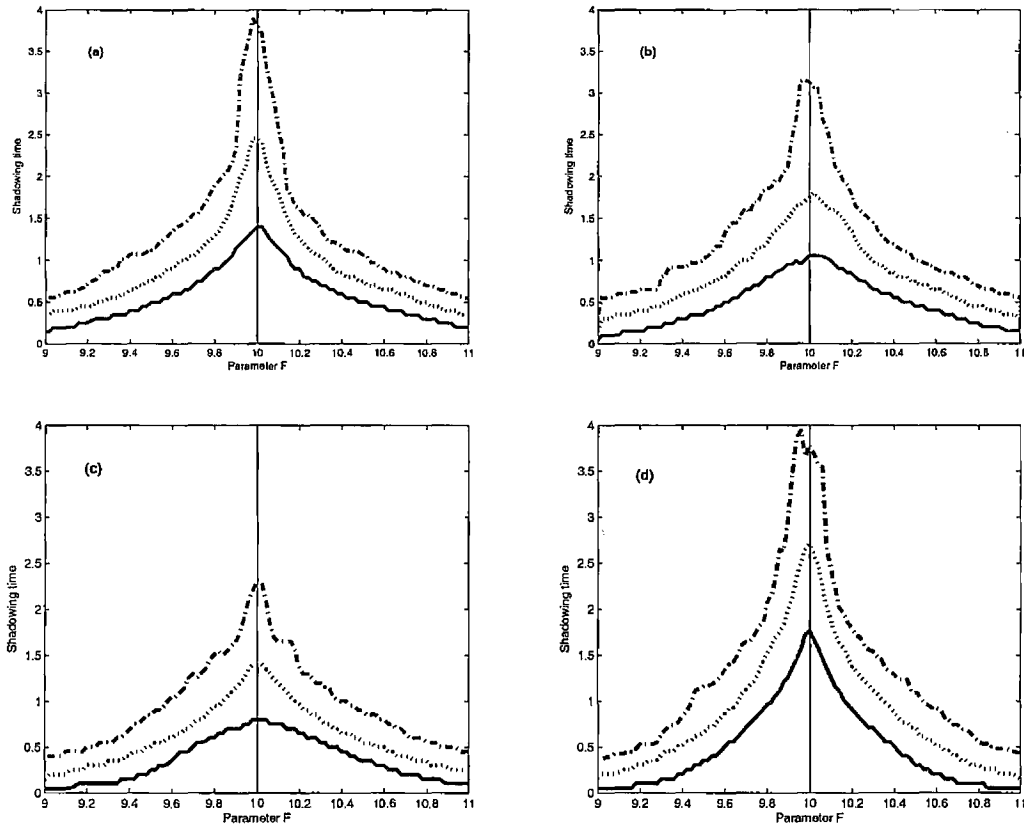
Figure 4.10: Shadowing time isopleths as in Figure 4.8 for 8-D Lorenz96 with parameter F=10 given only partial observations, a) the 8th component of the state vector is not observed; b) none of the 2nd, 5th or 8th variables are observed only the other five components; c) only 2nd, 5th or 8th variables are observed; d) all the components of the state vector are observed. In this experiment the noise level is 0.2.

Figure 4.10 shows the result of the application in the 8-D Lorenz96 system. Panel (d) shows the isopleths for the 8 dimension Lorenz96 system with states fulled observed. It appears that our method provides good parameter estimates

in the higher dimensional model case. In panel (a) seven of the eight components of the state vector are observed, in panel (b) 5 of the eight components are observed and in panel (c) only 3 components are observed. In all cases, the correct parameter values are well indicated although the length of shadowing time decreases as less components are observed.

4.5 Outside PMS

Large forecast-verification archives and lower observational noise level contain more information and thus yield better parameter estimates when the model structure is perfect. When the model class does not admit on empirically adequate model, the notation of a "true" parameter value is lost. It is important to note that even if the true parameter values are unknown, they are well defined within PMS; the question of defining optimal parameter values when the model structure is imperfect is more complex.

The experiment of forming probabilistic forecast to estimate parameter values is also useful at identifying "best" parameter in an imperfect model if a notation of best is defined as best forecast performance at certain lead time.

The geometric approach using shadowing time and additional statistics of the pseudo-orbit is also useful to identify parameter values which can mimic the dynamics, quantify the time scales on which they can shadow and extract information for improving the model class itself. Even in systems as unwieldily as multi-million-dimensional operational climate models, variations in parameters over the relevant range of uncertainties yield demonstrably nonlinear effects (87) in the most basic summary statistics (i.e. climate sensitivity). The ISGD methods

have been used on models of this level of complication (51). Outside PMS there may be no single optimal parameters, of course, but even in this case shadowing times have the advantage of providing information on likely lead times at which a forecast will have utility. Timescales on which the dynamics of the model are consistent with the noise model and the observations can be of use in setting the window of observations to be used, and the effectiveness of, variational approaches to data assimilation (51).

4.6   Conclusions

In this chapter, we considered the problem of estimating the parameter values of the model in the perfect model scenario. Traditional linear method, Least Squares estimates, is unable to produce consistent results due to the fact that the assumption of Independent Normal Distributed(IND) forecast does not hold when the model is nonlinear. To address the shortcomings of traditional methods, two new alternative approaches, Forecast Based estimates and Dynamical Coherent estimates, are introduced in this chapter.

For Forecast Based estimates, we estimate the parameter values based upon the probabilistic skill of the model as a function of parameter values. This straightforward procedure has been shown to yield good parameter estimation in several chaotic maps. Forecast based estimation using Inverse Noise ensembles is straightforward to implement and relatively computationally inexpensive. We have shown that it can suffer biases when the ensemble is not distributed consistently with respect to the models long term dynamics (invariant measure). We have also shown that, for addition computational investment to sample a perfect

90

ensemble this bias can be removed.

Dynamical Coherent estimates is presented which focuses on the geometry of trajectories of the model rather than the forecast performance at a given lead time. We estimate the parameter values based upon i) the ability of model trajectories to shadow by looking the shadowing time distribution; ii) how well model pseudo-orbits approximate relevant trajectories by measuring the mismatch error of the pseudo-orbits; iii) the consistency of the distribution of implied-noise with the noise model. ISGD method is applied to obtain candidates with longer shadowing time and the model pseudo-orbit. The technique is illustrated for both flows and maps, applied in 1, 2, 3 and 18 dimensional dynamical systems, and shown to be effective in a case of incomplete observation where some components of the state are not observed at all.

Outside PMS, although the optimal estimates of the parameter is not well defined, we suggest our approaches may still be able to produce robust results.

Chapter 5

Nowcasting Outside PMS

When forecasting real systems, for example the Earth's atmosphere as in weather forecasting, there is no reason to believe that a perfect model exists. Generally the model class from which the particular model equations are drawn does not contain a process that is able to generated the data. In this case we are in the Imperfect Model Scenario (IPMS), and it is crucial to distinguish the model(s) from the system which generated the data.

In the Perfect Model Scenario, given the infinite CPU power, one may be able to form a perfect ensemble (80), whose members are drawn from the same distribution as the system state. In the IPMS, however, such a perfect ensemble does not exist. Any ensemble data assimilation scheme is expected to result with an probabilistically unreliable state estimation. This chapter is concerned with how to forecast the current state using ensemble methods given the observations and imperfect model. In the IPMS, model state space and the system state are usually different. In this chapter we are aiming to estimate the initial states of the model for the purpose of forecasting. In this case not only the observational uncertainty

92

but also the model inadequacy need to be considered when an ensemble of initial conditions is constructed.

In the Imperfect Model Scenario, methods assuming the model is perfect may be inapplicable and in any event they would seem unlikely to produce the optimal results. It is almost certain that no trajectory of the model is consistent with an infinite series of observations (50), thus there is no consistent way to estimate the model states using trajectories. There are pseudo-orbits, however, that are consistent with observations and these can be used to estimate the model state (50). In this chapter we applying the same ISGD algorithm as discussed in previous chapter, but with a new stopping criteria to find relevant pseudo-orbits outside PMS.

The Imperfect Model Scenario is defined and two system-model pairs are set up in Section 5.1. Section 5.2 discusses various Indistinguishable States methods of finding a pseudo-orbit and demonstrates that our new methodology, i.e. applying the ISGD method with certain stopping criteria, can find better pseudo-orbits. Other method, such as Weakly Constraint 4DVAR, is discussed and compared with our method in Section 5.3. Results of comparing the pseudo-orbit produced by ISGD method and WC4DVAR method are presented in Section 5.5.1. This is the first time IS methods and the WC4DVAR method are compared in the IMPS. Methods of forming the ensemble based on the pseudo-orbits are introduced and discussed in Section 5.4 and the results of nowcasting is presented in Section 5.5.2.

5.1 Imperfect Model Scenario

Outside pure mathematics, the perfect model scenario is a fiction. Arguably, there is no perfect model for any physical dynamical system (50).

In the Imperfect Model Scenario (IPMS), we define a nonlinear system with state space $\mathbb{R}^{\tilde{m}}$, the evolution operator of the system is $\tilde{F}$, i.e. $\tilde{x}_{t+1} = \tilde{F}(\tilde{x}_t)$ where $\tilde{x}_t \in \mathbb{R}^{\tilde{m}}$ is the state of the system. An observation s_t of the system state $\tilde{x}_t$ at time t is defined by $s_t = h(\tilde{x}_t) + \eta_t$ where $s_t \in \mathbb{O}$, η_t represents the observational noise, in this thesis we assume η_t are IID distributed; $h(\cdot)$ is the observation operator, which projects the system state into the observation space $\mathbb{O}$. For simplicity, we take $h(\cdot)$ to be the identity. Consider a model, which represents the system approximately, with the form $x_{t+1} = F(x_t)$, where $x_t \in \mathbb{M}$, $\mathbb{M}$ is the model state space. Assume the system state $\tilde{x}$ can also be projected into the model state space by a projection operator $g(\cdot)$, i.e. $x = g(\tilde{x})$. In general, we don't know the property of this projection operator, we don't know even if $\tilde{x}$ exists. We are just going to assume that it maps the states of the system into somehow relevant states in the model. For the purposes of illustration and simplicity, unless otherwise stated, we assume $g(\cdot)$ is one-to-one identity. A better understanding of $g(\cdot)$ is beyond the scope of this thesis but it is an important point for additional work. Our aim is to estimate the current state of the model x_0 given the previous and current observations $s_t, t = -n + 1, ..., 0$.

In the imperfect model scenario, the model is inadequate. Following Smith and Judd (2004), two types of model inadequacy are investigated. One is structurally incorrect model inadequacy, the other is ignored subspace model inadequacy. For each type of model inadequacy, an example is given, where both the true system

94

and a class of models are listed. These model-system pairs are used to construct and compare the state estimation methods in the following sections.

- Structurally inadequacy

  This type of model inadequacy appears where the system dynamics are not known in detail and its mathematical structure is different from that of the model. Here we use the Ikeda Map and truncated Ikeda model as an example of this case (50). The Ikeda system is a two dimensional map (see section 2.4), $\tilde{F} : \mathbb{R}^2 \to \mathbb{R}^2$. The mathematical functions of the system are:

$$x_{n+1} = \gamma + u(x_n \cos\theta - y_n \sin\theta) \tag{5.1}$$

$$y_{n+1} = u(x_n \sin\theta + y_n \cos\theta), \tag{5.2}$$

where $\theta = \beta - \alpha/(1 + x_n^2 + y_n^2)$ and the parameter values used are $\alpha = 6, \beta = 0.4, \gamma = 1, u = 0.83$. The imperfect model F is obtained by using the truncated polynomial to replace the trigonometric function in $\tilde{F}$, i.e.

$$\cos\theta = \cos(\omega + \pi) \mapsto -\omega + \omega^3/6 - \omega^5/120 \tag{5.3}$$

$$\sin\theta = \sin(\omega + \pi) \mapsto -1 + \omega^2/2 - \omega^4/24 \tag{5.4}$$

where the change of variable to ω was suggested by Judd and Smith (2004) since θ has the approximate range -1 to -5.5, and $-\pi$ is conveniently near the middle of this range. In this case, the model state and the system state share the same state space.

Generally, the truncated Ikeda model is a good approximation to the Ikeda system. The model error is relevantly small but space correlated. Figure 5.1 (following Figure 1 of (50)) shows the one-step forecast error between the Ikeda system and the truncated Ikeda model.
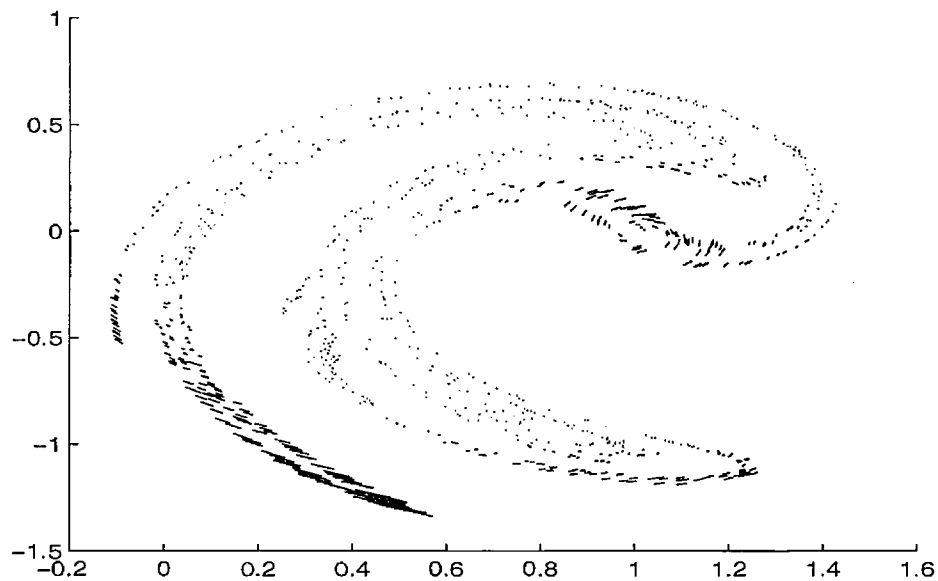
Figure 5.1: The one-step prediction errors for the truncated Ikeda map. The lines show the prediction error for 512 points by linking the prediction to the target.

- Ignored-subspace model inadequacy

  This type of model inadequacy appears where some component(s) of the system dynamics is(are) unknown, unobservable, or not included in the model. In this case, the system state space and model state space are different.

  Here we use the Lorenz96 flows (63) as an example of this case. We treat

the Lorenz96 model II as the system that generates the data (details of Lorenz96 models can be found in section 2.4). The mathematical functions of the system are

$$\frac{dx_i}{dt} = -x_{i-2}x_{i-1} + x_{i-1}x_{i+1} - x_i + F - \frac{h_x c}{b}\sum_{j=1}^{n} y_{i,j} \tag{5.5}$$

$$\frac{dy_{j,i}}{dt} = cby_{j+1,i}(y_{j-1,i} - y_{j+2,i}) - cy_{j,i} + -\frac{h_y c}{b}x_i \tag{5.6}$$

for $i = 1, ..., n$. The system used in our experiments containing $n = 18$ variables $x_1, ..., x_{18}$ with cyclic boundary conditions (where $x_{n+1} = x_1$). Like the large scale variables x_i, the small-scale variables $y_{j,i}$ have the cyclic boundary conditions as well(that is $y_{m+j,i} = y_{j,i+1}$) (in our experiments $m = 5$).

The Lorenz96 model I is treated as the imperfect model (details of Lorenz96 models can be found in section 2.4). From the mathematical function

$$\frac{dx_i}{dt} = -x_{i-2}x_{i-1} + x_{i-1}x_{i+1} - x_i + F \tag{5.7}$$

one can see that the small dynamical variables y in the system equation (5.5 & 5.6) are not included in the Lorenz96 model I. The magnitude of error made by the imperfect model depends on the coupling parameter h_x, h_y and in our experiments we set both h_x and h_y to be 1. In this system and model pair setting, the model state space and the system state space are different.

5.2 IS methods in IPMS

5.2.1 Assuming the model is perfect when it is not

What will happen if one ignores the model inadequacy and assumes that the model is perfect. Here we investigate whether this would degrade state estimation of the nonlinear system. And if so, how do the results from the perfect model scenario, as shown in chapter 3, change when applied to imperfect models?

In the Perfect Model Scenario, there are a set of indistinguishable states $\mathbb{H}(\tilde{x})$ that can not be distinguished from the system state $\tilde{x}$ (48). In IPMS, however, it is not necessary that $\mathbb{H}(\tilde{x})$ contains states other than itself. Even for the state $\tilde{x}$ itself, the projection [1] of the system trajectory defined by $\tilde{x}$ into the model space is not a trajectory of the model, which means no state of model is consistent with the observations. This situation can arise even when the model trajectory remains in proximity to (the observed part of) the system trajectory (50).

If we ignore the model inadequacy and apply the ISGD algorithm to find a model trajectory, we will find that the minimisation converges very slowly to zero when the window length is very long, which implies no model trajectory is "close" to the observations. In the results shown in 5.2.5, the results of state estimation by applying ISGD algorithm to minimise the mismatch degrade after certain iterations of gradient descent.

5.2.2 Model error

In this chapter we will consider the point-wise model error to be $\tilde{x}_{n+1} - F(\tilde{x}_n)$. It might be reasonable to assume the observational noise is IID distributed. But it

---

[1] assume the projection is one-to-one identity

is almost certain that the model error of a nonlinear model is not IID distributed. For example in Figure 5.1, the model error between the truncated Ikeda model and Ikeda system is spatially correlated; there are regions where the model error is small and regions where it is not. Understanding the distribution of the model error aids in model development. If systematic model errors are identified, one can improve the model by correcting some of the errors. In this chapter, we are less interested in improving the model than in how to obtain states of the model for initial conditions which, for insistence, serve the purpose of forecast given the imperfect model. Therefore, we assume that the model we use to approximate the system is the best model one can achieve and the model errors have been reduced to the minimum given the available information. In the later section, we will discuss how the information about the model error can also help to improve the quality of estimates of future states.

In the IPMS, to estimate the current state of the model, one need to account the uncertainty from both observational noise and model inadequacy. Without the observational noise, the model error can be derived from the observations directly. In the presence of observational noise, compounding of model error and observational noise prevent us identifying either of them precisely. Such unsolvable problem also causes the state estimation more or less biased in the IPMS.

5.2.3 Pseudo-orbit

Since no state of the model has a trajectory consistent with an infinite sequence of observations of the system in the IPMS, any model trajectory must eventu-

ally be unable to maintain consistency between the observations and the model dynamics. There are pseudo-orbits, however, that are consistent with observations and these can be used to provide better estimates of the projection of the system state. *Pseudo-orbits* (50) are sequences of states of the model $\mathbf{x}_t$ that at each step differ from trajectories of the model, that is, $\mathbf{x}_{t+1} \neq F(\mathbf{x}_t)$. We define the imperfection error of the pseudo-orbit $\mathbf{x}_t$ to be $\omega_t = \mathbf{x}_{t+1} - F(\mathbf{x}_t)$. Note the imperfection error does not necessarily correspond to the model error, however the projection of a system trajectory [1] in the model state space forms a pseudo-orbit of the model where the imperfection error is exactly the model error in the model state space. Recall that in the PMS, there are a set of indistinguishable states $\mathbb{H}(x)$ of the system state x. Each indistinguishable state defines a system trajectory that consistent with both the observations and the system dynamics. In the IPMS, the system trajectories are pseudo-orbits of the model in the model space and these "true pseudo-orbits" are consistent with the observations and the model dynamics and most important the imperfection error reflects the model error exactly. Unfortunately, such desirable pseudo-orbits cannot be found in the Imperfect Model Scenario, because of the confounding between observational noise and model error. One can, however, find relevant (useful) pseudo-orbits of the model that are consistent with observational noise and the imperfection error of those pseudo-orbits can be treated as estimates of the model error or at least provide some information about the model error. Methods, adopted based on ISGD method, of finding relevant pseudo-orbits are introduced and discussed in the next two sections.

---

[1] assume the system states are one-to-one identically projected onto the model space

5.2.4   Adjusted ISGD method in IPMS

Judd and Smith (2004) introduced a method of finding relevant pseudo-orbits by adjusting the ISGD method to include the model imperfection. A brief description of this method is given here in order to introduce and compare with a new method introduced in the next section.

Similar to the ISGD method introduced in section 3.3, Following Judd and Smith (2004), Gradient Descent algorithm is applied to minimise the adjusted mismatch error by including the model imperfection error term. For a finite sequence of observations, $s_t, t = -N + 1, ..., -1, 0$, we define the *adjust mismatch error* for a sequence of pseudo-orbit z_t to be

$$e_t = \mid z_{t+1} - \omega_{t+1} - F(z_i) \mid, \tag{5.8}$$

where ω_t is the imperfection error.

Define the implied noise, δ to be the difference between the pseudo-orbit and the observations, i.e.

$$\delta_t = s_t - z_t. \tag{5.9}$$

Hence fore, the mismatch equation 5.8 can be written as

$$e_t = \mid s_{t+1} - \delta_{t+1} - \omega_{t+1} - F(s_t - \delta_t) \mid . \tag{5.10}$$

Consider cost function $CM(\delta, \omega)$, where

$$CM(\delta, \omega) = \sum_{t=-N}^{0} \mathrm{e}_t^T \mathrm{e}_t, \qquad (5.11)$$

is defined in order to find relevant pseudo-orbit by GD algorithm.

Following Judd and Smith (2004), one can find a pseudo-orbit from the sequence of observations by applying Gradient Descent to minimise the cost function $CM(\delta, \omega)$. It is necessarily that $CM(\delta, \omega)$ attains a minimum of zero. To solve the minimisation by gradient descent, one need to solve the differential equations

$$\dot{\delta} = -\frac{\partial L}{\partial \delta}, \dot{\omega} = -\frac{\partial L}{\partial \omega} \qquad (5.12)$$

to compute the asymptotic values of (δ, ω) by initialising the cost function with both δ and ω equal to 0. The resulting values of δ and ω defines a certain pseudo-orbit.

Ignoring the model inadequacy, one may attempt to minimise $CM(\delta, 0)$, which equals to applying the ISGD method (see Section 3.3.2) to look for model trajectory assuming that the model is perfect. Although the cost function $CM(\delta, 0)$ always has the minimum of zero regardless the model is perfect or not, the model trajectory obtained when $CM(\delta, 0)$ reaches 0, is expected to be far away from the true states and be inconsistent with the observations as long as N is large enough.

Recall that the relevant pseudo-orbits we are looking for are those consistent with the observations and their corresponding imperfection errors contains information about the model error or somehow reflects the model error. The implied noise δ provides an estimate of the observational noise and the imperfection error ω provides an estimate of the model error. In order to improve the method and find *better* pseudo-orbits, we measure the quality of the pseudo-orbit by looking at the RMS distance between pseudo-orbit and the projection of the true trajectory of the system and testing the statistical consistency both between the implied noise and the observation noise and between the imperfection error and the model error. We are aware that when the system is nonlinear, linear measurement like RMS has systematic bias (64) (see Chapter 4). The distance between the pseudo-orbit and the true states may not reflect forecast skill in the Imperfect Model Scenario. We only use this measurement as a diagnostic tool to help explain how to construct a better method to locate relevant pseudo-orbit.

We investigate the quality of the pseudo-orbits generated by minimising the cost function $CM(\delta, 0)$ and $CM(\delta, \omega)$ in both Ikeda and Lorenz96 system and model pairs experiments.

Cost function	No. of GD runs	$CM(\delta, \cdot)$	std of δ_t	std of ω_t	RMS distance
$CM(\delta, 0)$	4096	0.025	0.051	0	0.0154
$CM(\delta, \omega)$	128	0.0002	0.037	0.02	0.012

Table 5.1: Statistics of the pseudo-orbits obtained by minimising the cost function $CM(\delta, 0)$ and $CM(\delta, \omega)$ for the experiment of Ikeda system-model pair. Minimisations are applied upon 4096 observations, the noise level is 0.05 and the sample standard deviation of the model error is 0.018.

From Table 5.1 and 5.2 one can see that firstly in both experiments, it is much more difficult to minimise $CM(\delta, 0)$ than $CM(\delta, \omega)$ and the cost function

Cost function	No. of GD runs	$CM(\delta,\cdot)$	std of δ_t	std of ω_t	RMS distance
$CM(\delta,0)$	4096	0.11	1.69	0	1.38
$CM(\delta,\omega)$	128	0.0006	0.63	0.46	0.52

Table 5.2: Statistics of the pseudo-orbits obtained by minimising the cost function $CM(\delta,0)$ and $CM(\delta,\omega)$ for the experiment of Lorenz96 system and model pair. The length of the sequence of observations is 102.4 time unit and the sampling rate is 0.025 time unit. The noise level is 1 and the sample standard deviation of the model error is 0.25.

$CM(\delta,0)$ does not appear to converge to zero. Secondly for both methods the standard deviations of the implied noise and the imperfection error are very different from that of the observational noise and the model error (We are aware that neither the model error nor the imperfection error is IID, there are information of them beyond the second moment of their distribution. For simplicity we use the standard deviation, as a diagnostic tool, to test consistency between imperfection error and model error). The pseudo-orbit generated by minimising $CM(\delta,0)$ stays too far away from the observations as the standard deviation of implied noise is much larger than that of the observational noise, which indicates that the pseudo-orbit obtained by minimising $CM(\delta,0)$ is not consistent with observations. While the pseudo-orbit generated by $CM(\delta,\omega)$ seems to stay too close to the observations according to the standard deviation of implied noise. The standard deviation of the imperfection error is larger than that of the model error between the system and the model which indicates that the model error is over-estimated by the imperfection error. From the RMS distance between pseudo-orbit and true states in table 5.1 & 5.2, minimising $CM(\delta,\omega)$ produces pseudo-orbit closer to the truth. But apparently this method doesn't tackle the problem of confounding between observational error and model error very well as neither the implied noise is a good estimate of observational noise nor the

imperfection error is a good estimate of model error which may indicate that the estimates of the model states are highly biased.

5.2.5 ISGD with stopping criteria

The GD method introduced by Judd and Smith (2004) is unable to produce a desirable estimation of the projection of the system state as the implied noise and imperfection error of the relevant pseudo-orbit are not consistent with the observational noise and model error. Confounding between observational noise and model error makes it impossible to produce pseudo-orbits whose implied noise and imperfection error are consistent with observational noise and model error respectively. We found that applying the ISGD method with proper stopping criteria can, however, reduce such inconsistency and obtain less bias state estimation results.

As we mentioned in the previous section, applying the ISGD method is equivalent to minimise $CM(\delta, 0)$ cost function, i.e. the mismatch cost function defined in Section 3.3.2 and Equation 5.11 are the same. Examples shown in previous section demonstrate that the minimisation does not converge to zero easily and the pseudo-orbit produced eventually is not consistent with the observations and stays farther away from the true pseudo-orbit than even the observations. When the $CM(\delta, 0)$ is greater than zero after finite iterations of GD, the mismatch error e_t is actually the imperfection error. In other words, minimising the $CM(\delta, 0)$ is actually minimising the imperfection error. If the imperfection error goes to zero, the pseudo-orbit becomes a model trajectory. Since we treat the imperfection error as the estimate of the model error which is known to exist when the model

is imperfect. Our purpose is not minimising the imperfection error but producing better or more consistent estimate of the model error. Figure 5.2 shows the statistics of pseudo-orbit changes as a function of the number of iterations of Gradient Descent minimising mismatch cost function $CM(\delta, 0)$ in both higher dimensional Lorenz96 system-model pair experiment and low dimensional Ikeda system-model pair experiment (Details of the experiments are list in Appendix B Table B.6.

Figure 5.2 shows that as the Gradient Descent minimisation iterates further and further, the standard deviation of implied noise is getting larger and larger which indicates that the pseudo-orbit is moving farther away from the observations. By comparing the standard deviation of implied noise with that of the real noise model, we found that at the beginning of the minimisation, the observational noise is underestimated by the implied noise since the pseudo-orbit stays too close to the observations. This makes sense because the minimisation algorithm is initialised at the observations. As the minimisation proceeds, the implied noise becomes more consistent with the observational noise and the pseudo-orbit gets closer to the true pseudo-orbit. After a certain number of iterations, however, the implied noise tends to overestimated of the observational noise and the distance between the pseudo-orbit and the projection of true system trajectory gets larger. This is due to the model inadequacy. The minimisation makes the imperfection error smaller. When the imperfection error of the pseudo-orbit becomes smaller than the actual model error, the implied noise has to compensate for the imperfection error to account for the uncertainty caused by the model inadequacy which makes implied noise too large and the pseudo-orbit inconsistent with the observations.
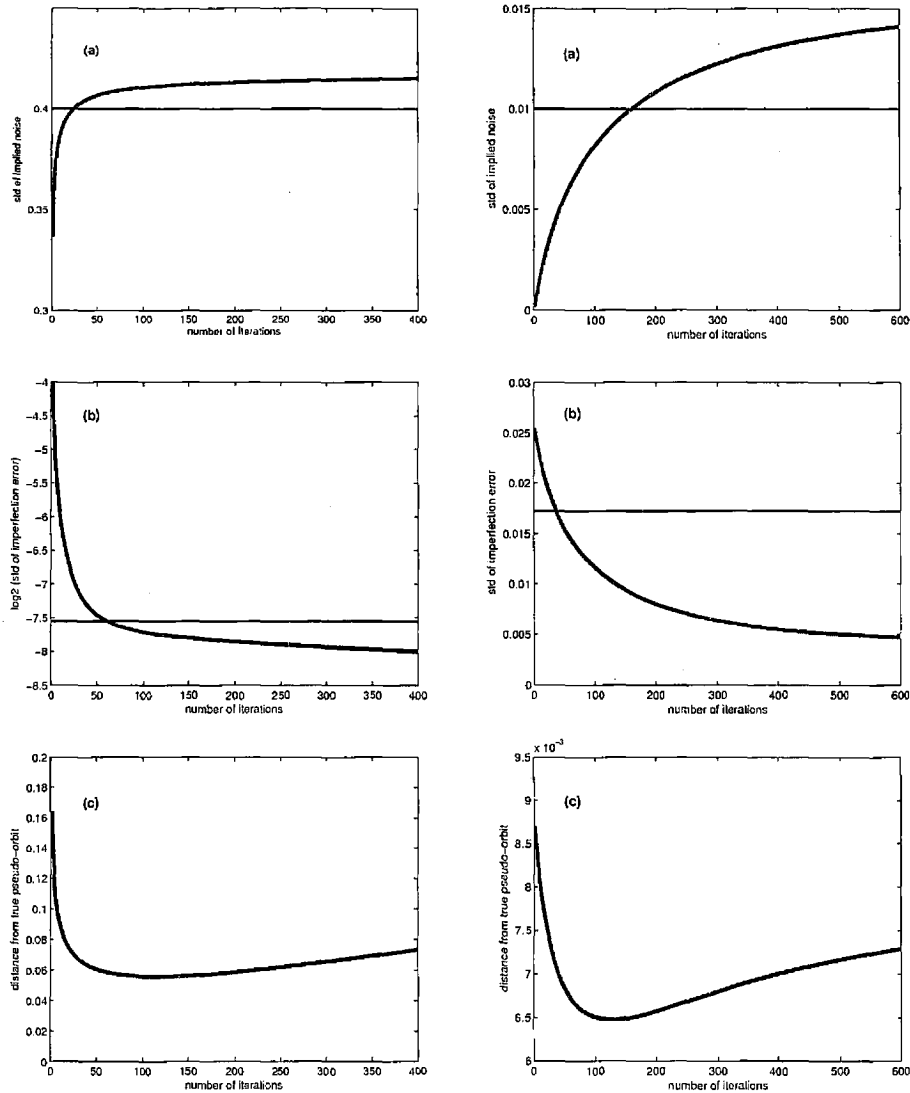
Figure 5.2: Statistics of the pseudo-orbit as a function of the number of Gradient Descent iterations for both higher dimension Lorenz96 system-model pair experiment (left) and low dimension Ikeda system-model pair experiment (right). (a) is the standard deviation of the implied noise (the flat line is the standard deviation of the noise model); (b) is standard deviation of the model imperfection error (the flat line is the sample standard deviation of the model error); (c) is the RMS distance between pseudo-orbit and the true pseudo-orbit.

Since the model error is neither IID nor Gaussian distributed, how well the imperfection error mimics the model error should not be judged only by the statistics of the second moment. Figure 5.1 shows that the model error is spatially correlated. As an estimation the model error, we expect the imperfection error has similar spatial correlations as the model error. Figure 5.3 plots the imperfection error in the state space with different GD iterations for the Ikeda Map. To make comparison easier, Figure 5.1 is re-ploted in the fourth panel. The pictures show that at the beginning of the minimisation, the imperfection error is larger than the model error in most places. The pattern of spatial correlation can only be seen around $(0.5, -1.3)$, which suggests the imperfection error is not a good estimate of the model error. This is because at the beginning of the minimisation, the imperfection error contains both the observational error and model error. Similarly after too many iterations, the imperfection error is forced to be small and lose the spatial correlation it should have. One can see very little spatial correlation of imperfection error in the third panel. With a intermediate number of iterations [1], however, the imperfection error seems better estimate the model error, the pattern in the second panel and fourth panel are very similar.

It might be asked whether the imperfection error estimates the model error precisely? Unfortunately, it does not. Confounding between model error and observational noise prevents us identifying either of them precisely (50). We also found that how well the model error can be estimated strongly depends on the signal magnitude between observational noise and model error. Figure 5.4 plots the imperfection error in the state space with intermediate GD iterations at

---

[1]The number of iterations set up based on the statistics of imperfection error, generally we match the standard deviation of the imperfection error with that of the model error
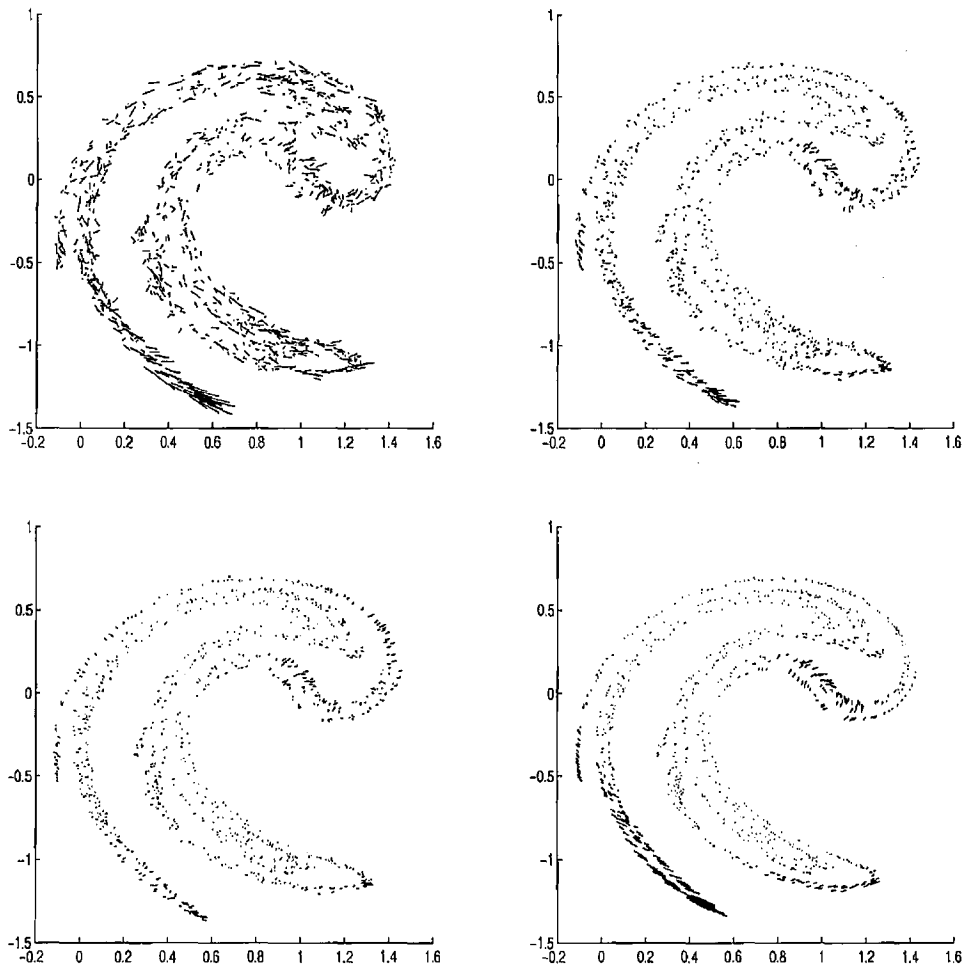
Figure 5.3: Imperfection error during the Gradient Descent runs for Ikeda Map case is plotted in the state space. (a) after 10 GD iterations, (b) after 100 GD iterations, (c) after 400 GD iterations (d) the real model error in the state space for comparison.

another two different noise levels. When the observational noise is much smaller than the model error, the model error can be well estimated by the imperfection error. When the observational noise is much bigger than the model error, the imperfection error looks very close to random.

109
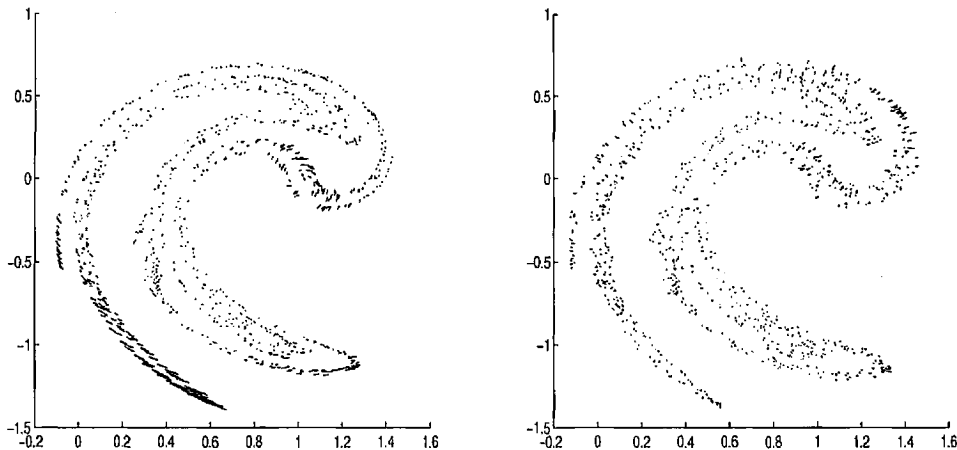
Figure 5.4: Imperfection errors after intermediate Gradient Descent runs for Ikeda system-model pair are plotted in the state space. (a) Noise level=0.002, (b) Noise level=0.05.

Generally we conclude from the above experiments that the ISGD minimisation with intermediate runs produces "better" pseudo-orbits than the minimisation with both short runs and long runs and the IS Adjusted method (50). When shall we stop the ISGD minimisation in order to obtain the relevant pseudo-orbit? Certain criteria need to be defined in advance to decide when to stop. Such criteria have to be defined based on the meaning of "better" (pseudo-orbit). For example if "better" means the pseudo-orbit is more consistent with the observations, the stopping criteria can be built by testing the consistency between implied noise and the noise model; if "better" means the initial condition ensemble, formed based on the pseudo-orbit, produces "better" forecast at certain lead time, the stopping criteria can be built by fitting the number of iterations with the forecast performance. We call the ISGD method with certain stopping criteria to be $ISGD^c$. In the experiments whose results shown in section 5.5, we stops

the ISGD iterations when the implied noise becomes larger than the standard deviation of the noise model. There are many potential criteria that can be used for stopping, here we use a simple one which no doubt could be improved upon. Most importantly, in this chapter we demonstrate that using certain stopping criteria can provide more consistent state estimation results.

5.3 Weak constraint 4DVAR Method

In the traditional 4DVAR method (see section 3.4), the model is assumed to be perfect and the model dynamics is treated as a strong constraint (90), i.e. only model trajectories are considered. In the Imperfect model scenario, in order to account for the model error, one should apply the model as a weak constraint, rather than as a strong constraint in the 4DVAR method (76). Recent research (4; 5) shows that applying the model dynamics as a weak constraint in a 4DVAR data assimilation method outperforms the one with strong constraint.

Here we give a brief introduction of Weak Constraint 4DVAR (WC4DVAR) method. Differences between WC4DVAR method and $ISGD^c$ method are discussed and comparisons are made in both low dimensional model and higher dimensional model experiments.

5.3.1 Methodology

The weak constraint 4DVAR method looks for pseudo-orbits instead of trajectories that are consistent with sequence of system observations. Following (Lorenc 1986), the weak constraint 4DVAR method can be derived as follow. Given a sequence of observations within a time interval $(0, N)$, $s_0, ..., s_N$ and a background

111

state x_0^b at time $t = 0$, we want to produce the optimal estimate of the model states $x_0, ..., x_N$. Assuming the observational noise and the model error are both IID Gaussian distributed. Follow the maximum likelihood principle, the probability of $x_0, ..., x_N$ given x_0^b and $s_0, ..., s_N$, i.e. $p(x_0, ..., x_N \mid x_0^b; s_0, ..., s_N)$ is proportional to

$$e^{-\frac{1}{2}(x_0-x_0^b)^T B_0^{-1}(x_0-x_0^b)} \times e^{-\frac{1}{2}\sum_{i=0}^{N}(H(x_i)-s_i)^T \Gamma_i^{-1}(H(x_i)-s_i)} \times \qquad (5.13)$$

$$e^{-\frac{1}{2}\sum_{i=1}^{N}(x_i-F(x_{i-1}))^T Q_i^{-1}(x_i-F(x_{i-1}))}.$$

Matrices Γ, B and Q are observational, background and model error covariances. The weak constraint 4DVAR cost function is then derived by taking the logarithm of the above equation, i.e.

$$C_{4dvar} = \frac{1}{2}(x_0 - x_0^b)^T B_0^{-1}(x_0 - x_0^b) + \frac{1}{2}\sum_{i=0}^{N}(H(x_i) - s_i)^T \Gamma_i^{-1}(H(x_i) - s_i) \quad (5.14)$$

$$+\frac{1}{2}\sum_{i=1}^{N}(x_i - F(x_{i-1}))^T Q_i^{-1}(x_i - F(x_{i-1})).$$

Note that although the expression of the first and the second term in the cost function is same as the original 4DVAR cost function (Equation 3.9), they are different in the sense that the estimate of the system states $x_0, ..., x_N$ are components of a single trajectory of the model in the original 4DVAR case i.e. $x_i - F(x_{i-1}) = 0$. While in the WC4DVAR case those estimates form a pseudo-orbit. And it is assumed that difference between x_i and $F(x_{i-1})$ is IID Gaussian distributed with covariance matrix Q. In order to make difference from the real model error which

is $\tilde{x}_i - F(\tilde{x}_{i-1})$ and to be consistent with the terminology in the previous section, we call the difference between x_i and $F(x_{i-1})$, the imperfection error of the pseudo-orbit $x_0, ..., x_N$ which is expected to be minimised by the third term of the cost function. Generally WC4DVAR looks for pseudo-orbit of the model by maintaining the balance that such pseudo-orbit stays close to the observation but with small imperfection error. Similar to the original 4DVAR, the application of WC4DVAR is carried out over short assimilation windows as increasing the window length will not only increase the CPU cost exponentially but also suffer from the increasing density of local minimums.

5.3.2 Differences between $ISGD^c$ and WC4DVAR

There is some similarity between the $ISGD^c$ method and WC4DVAR method. i) Both methods can be applied to an assimilation window to produce an estimate of model states (analysis); ii) The analysis produced by both methods is a pseudo-orbit of the model with its corresponding sequence of imperfection error. There are, however, fundamental differences between them.

- The WC4DVAR method forces the pseudo-orbit to stay close to the observations by the second term of its cost function. As the imperfection error brings extra freedom to the pseudo-orbit, the pseudo-orbit produced by WC4DVAR might be stay too close to the observations and the distribution of the difference between pseudo-orbit and the observations, the distribution of implied noise, might not be consistent with the observational noise model. In the $ISGD^c$ algorithm, the cost function itself does not contains any constraints to force the pseudo-orbit staying close to the

observations. The observations are only used to initialise the GD minimisation. By setting up the relevant stopping criteria, the implied noise is found to be more consistent with the observational noise.

- Both methods produce a sequence of imperfection error besides the pseudo-orbit, such imperfection error could be treated as the estimation of the real model error. In this case, WC4DVAR can be shown not to be self consistent (52). Within the process of deriving the WC4DVAR, the model error is assumed to be IID Gaussian distributed. Such assumption appears unlikely to hold if the model is nonlinear (52) and can be tested after the fact. As we discussed in section 5.2.2, we expect this model error to be space correlated and not necessarily to be Gaussian distributed. Even were this assumption to hold, the covariance matrix $\mathbf{Q}$ has to be predetermined in order to initialise the WC4DVAR cost function. Without knowing the true states of the system, it is impossible to obtain the model error covariance matrix. Therefore an estimation has to be used. As the imperfection error is the estimation of the model error, we expect the imperfection error produced by WC4DVAR is IID Gaussian distributed with covariance $\mathbf{Q}$. In the $ISGD^c$ algorithm, no assumption of the model error is made and the covariance matrix of model error is never needed, the imperfection error is the remaining mismatch after certain number of GD minimisation runs.

- It is shown in section 5.5.1 that the performance of the WC4DVAR method degrades as the length of the assimilation window increases while $ISGD^c$ does not. In section 3.4, we discussed that the 4DVAR method suffers from the problem of local minimums when it is applied to a long data

assimilation window of observations. Miller et al. (1994) also anticipated difficulties in finding global minima of the WC4DVAR cost function similar to those encountered in the 4DVAR case. For the WC4DVAR method, it appears to be difficult to demonstrate analytically whether the number of local minima of the cost function increases as the length of the data assimilation window increases. Results, shown in section 5.5.1, indicate that WC4DVAR method suffers from the local minima when the assimilation window increases. As the cost function tries to minimise the *linear* sum of the distance between the pseudo-orbit and the observations and the squared imperfection error, it might be the case that the local minima of the cost function defines the pseudo-orbit that is too far away from the observations in order to have small imperfection error. In other words, in such cases the WC4DVAR is trying to find a model trajectory (i.e. imperfection error is 0) close to the observations while for the imperfect model of a nonlinear chaotic system, it is often the case that no model trajectory is close to the observations if large assimilation window is considered. Results, shown in section 5.5.1, suggest this might be the reason WC4DVAR performs badly when the assimilation window is large. The $ISGD^c$ method does not have this deficiency. Results, shown in section 5.5.1, demonstrate that a longer assimilation window does not cause problems; on the contrary better estimates are produced by $ISGD^c$ method.

The analysis produced by $ISGD^c$ and WC4DVAR can be used to form an ensemble of initial conditions. The quality of the ensemble depends on the quality of the analysis. In section 5.5.1, we compare the quality of pseudo-orbits produced by $ISGD^c$ and those produced by WC4DVAR. Our results demonstrate

that WC4DVAR still suffers from the local minimum when applying to longer assimilation window while our $ISGD^c$ method doesn't have such shortcoming and produces pseudo-orbits closer to the true pseudo-orbit.

5.4 Methods of forming an ensemble in IPMS

In this section, we introduce and discuss the methods of forming an ensemble of model states at $t = 0$ based on the pseudo-orbit, $\mathbf{z}_i, i = -N, ..., 0$, which can be produced by methods like $ISGD^c$ and WC4DVAR. Such ensemble is treated to be the solution of nowcast.

5.4.1 Gaussian perturbation

An easy way to form the ensemble is perturbing the current estimate $\mathbf{z}_0$ with Gaussian distribution. To form an N^{ens} member ensemble, one can draw N^{ens} samples from $N(0, \sigma^2)$ and add onto $\mathbf{z}_0$. The parameter σ can be chosen to obtain the best nowcast skill or simply use the standard deviation of the noise model. The problem of this method is that it assumes the error of the analysis is Gaussian distributed, which is often not the case even in the perfect model case. It is, however, a simple straightforward method to form the ensemble to cover the error of the analysis.

5.4.2 Perturbing with imperfection error

In this section we introduce a method to form the ensemble by perturbing the image of second last component of the pseudo-orbit, i.e. $F(\mathbf{z}_{-1})$, using the historical imperfection error. This method needs a large amount of historical data in

116

order to record a large set of imperfection error for future sampling. As we mentioned before, our state estimation method $ISGD^c$ produces a set of imperfection errors along with the pseudo-orbit. We apply the state estimation method to the historical data and record all the imperfection errors. To form an N_{ens} member ensemble, we randomly draw N_{ens} samples from the historical set of imperfection errors and add them onto $F(z_{-1})$. The advantage of this method is that the ensemble members tend to cover the uncertainty of model error. The disadvantage are i) the imperfection error is usually not IID distributed, they usually have strong spatial correlations as shown in Figure 5.3. As simple random sample of imperfection errors may lose this useful information; ii) the results are also strongly depending on how good the second last component of the pseudo-orbit estimates the true state. We believe better methods can be found by extracting more information in the imperfection error. In this chapter we give an example to suggest that imperfection error might be useful to produce nowcast ensemble.

5.4.3 Perturbing the pseudo-orbit and applying $ISGD^c$

Another way to form the initial condition ensemble is perturbing the pseudo-orbit and applying $ISGD^c$. As we discussed in Section 5.2.5, given a sequence of observation, $s_{-n}, s_{-n+1}, ..., s_0$, we can find a pseudo-orbit, $z_{-n}, z_{-n+1}, ..., z_0$, by the $ISGD^c$ method. One may consider the last component of the pseudo-orbit, z_0, as a point estimation of the current state. To form an N^{ens} member ensemble, we perturb the pseudo-orbit with the distribution of the observational noise N^{ens} times, apply the $ISGD^c$ method on the perturbed pseudo-orbits and finally record the last component of each pseudo-orbit produced by the $ISGD^c$

method as one of the ensemble member. Each ensemble member can be treated equally or weighted according to the likelihood of its corresponding pseudo-orbit given the observations. The results presented in section 5.5.2, show that this method produces better nowcasting ensembles than the other two methods. It is, however, very costly to run the $ISGD^c$ method to generate each ensemble member.

5.5 Results

In this section we first compare the $ISGD^c$ method with WC4DVAR by looking at the pseudo-orbits they provide. Results are then shown the comparison among the ensemble formation methods. Finally we compare the ensemble nowcasts based on $ISGD^c$ with an Inverse Noise ensemble.

5.5.1 $ISGD^c$ vs WC4DVAR

Both the $ISGD^c$ and WC4DVAR produce a pseudo-orbit from which an ensemble of the current state estimates can be constructed. In this section instead of comparing ensemble nowcasting results, we compare the quality of the pseudo-orbit each produces. We apply both methods in the higher dimensional Lorenz 96 system-model pair experiment and the low dimensional Ikeda system-model pair experiment. And in each case, different lengths assimilation windows are tested.

Firstly we measure the distance between observations and pseudo-orbit (equation 5.15), and the distance between true states and pseudo-orbit (equation 5.16) as diagnostic tools to look at the quality the model trajectories generated by each method.

Window	Distance from observations					
length	Average		Lower		Upper	
	WC4DVAR	$ISGD^c$	WC4DVAR	$ISGD^c$	WC4DVAR	$ISGD^c$
4 steps	1.52	1.19	1.45	1.13	1.60	1.24
6 steps	2.89	1.29	2.27	1.24	3.60	1.34
8 steps	4.61	1.34	3.80	1.30	5.52	1.37
Window	Distance from true states					
length	Average		Lower		Upper	
	WC4DVAR	$ISGD^c$	WC4DVAR	$ISGD^c$	WC4DVAR	$ISGD^c$
4 steps	0.70	0.67	0.65	0.63	0.76	0.71
6 steps	2.07	0.55	1.43	0.52	2.81	0.58
8 steps	4.01	0.50	3.19	0.47	4.88	0.52

Table 5.3: Ikeda system-model pair experiment (Experiment G): a) Distance between the observations and the pseudo-orbits generated by WC4DVAR and $ISGD^c$, b) Distance between the true states and the pseudo-orbits generated by WC4DVAR and $ISGD^c$ in Ikeda system-model pair experiment. Average: average distance, Lower and Upper are the 90 percent bootstrap re-sampling bounds, the statistics are calculated based on 1024 assimilations and 512 bootstrap samples are used to calculate the error bars. (Details of the experiment are listed in Appendix B Table B.7)

$$\frac{1}{N+1}\sum_{i=0}^{N}(H(z_{t_i}) - s_{t_i})^T R_i^{-1}(H(z_{t_i}) - s_{t_i}), \qquad (5.15)$$

$$\frac{1}{N+1}\sum_{i=0}^{N}(z_{t_i} - \tilde{x}_{t_i})^T R_i^{-1}(z_{t_i} - \tilde{x}_{t_i}) \qquad (5.16)$$

From Table 5.3 and 5.4 we can see that when the assimilation window is short, e.g. 4 steps, both WC4DVAR and $ISGD^c$ produce similar results that the pseudo-orbits are closer to the true states than the observations except the pseudo-orbit produced by $ISGD^c$ is slightly closer to the observation and the

Window	Distance from observations					
length	Average		Lower		Upper	
	WC4DVAR	$ISGD^c$	WC4DVAR	$ISGD^c$	WC4DVAR	$ISGD^c$
6 hours	16.42	14.00	16.24	13.85	16.59	14.14
12 hours	20.60	14.40	20.41	14.30	20.78	14.50
24 hours	81.11	14.52	78.17	14.45	84.17	14.59
Window	Distance from true states					
length	Average		Lower		Upper	
	WC4DVAR	$ISGD^c$	WC4DVAR	$ISGD^c$	WC4DVAR	$ISGD^c$
6 hours	5.87	4.15	5.76	4.08	5.98	4.23
12 hours	7.92	3.06	7.77	3.01	8.10	3.10
24 hours	74.29	2.45	71.04	2.42	77.61	2.47

Table 5.4: Lorenz96 system-model pair experiment (Experiment H): a) Distance between the observations and the pseudo-orbits generated by WC4DVAR and $ISGD^c$, b) Distance between the true states and the pseudo-orbits generated by WC4DVAR and $ISGD^c$. Average: average distance, Lower and Upper are the 90 percent bootstrap re-sampling bounds, the statistics are calculated based on 1024 assimilations and 512 bootstrap samples are used to calculate the error bars.(Details of the experiment are listed in Appendix B Table B.8)

true states than that produced by WC4DVAR. As longer assimilation window being used, the pseudo-orbit generated by $ISGD^c$ become father away from the observations and closer to the true states while the pseudo-orbit generated by WC4DVAR become father away from the observations and the true states. This is important because we expect to obtain more information from the observations and model dynamics by using longer assimilation window. In the $ISGD^c$ case, the pseudo-orbit moves closer to the true states as we expected. The WC4DVAR method, however, fails to produce better pseudo-orbit when applying on longer assimilation windows. We suggest without proof that such failure is due to increase of the density of local minima of the cost function, especially when the minimisation tends to obtain small imperfection error; as the WC4DVAR cost function depends on not only the initial state but also the imperfection errors, we

are unable to plot the cost function against the initial state to demonstrate the appearance of local minimums. To support our suggestion, however, we apply the WC4DVAR method on different realizations of observations of the true states. If the WC4DVAR cost function does not have multiple local minimums, we expect that the pseudo-orbit produced by WC4DVAR should not varies much for different realizations of observations. Table 5.5 and 5.6, shows the standard deviation of both middle point and end point of the pseudo-orbits [1], The WC4DVAR method is compared with $ISGD^c$ method. It appears that for $ISGD^c$ method the standard deviation does not vary much for different length of assimilation windows while for WC4DVAR method different realization of observations effect the results more when the assimilation window becomes larger, which also indicates that more local minimums appears.

5.5.2 Evaluate ensemble nowcast

In this section we compare nowcast performance of the three ensemble methods based on $ISGD^c$ with the Inverse Noise ensemble. For the purpose of illustration, we call the Inverse Noise ensemble Method I; the ensemble formed by dressing the end point of the pseudo-orbit with Gaussian distribution Method II; the ensemble formed by perturbing the image of the second last component with imperfection error Method III and the ensemble formed by perturbing the pseudo-orbit and applying $ISGD^c$ Method IV. The three ensemble methods based on $ISGD^c$ are introduced and discussed in section 5.4. The Inverse Noise ensemble is formed by sampling the inverse noise distribution and adding onto the observations (details

---

[1]We expect the middle point provides better estimate of the model state than the end point as the end point only has information from the past, the middle point has information of both past and future.

121

Window	STD of the middle point of the pseudo-orbit					
length	Median		10th percentile		90th percentile	
	WC4DVAR	$ISGD^c$	WC4DVAR	$ISGD^c$	WC4DVAR	$ISGD^c$
4 steps	0.0153	0.0155	0.0113	0.0105	0.0259	0.0274
6 steps	0.0271	0.0126	0.0121	0.0087	0.0595	0.0264
8 steps	0.0431	0.0126	0.0242	0.0086	0.0905	0.0262
Window	STD of the end point of the pseudo-orbit					
length	Median		10th percentile		90th percentile	
	WC4DVAR	$ISGD^c$	WC4DVAR	$ISGD^c$	WC4DVAR	$ISGD^c$
4 steps	0.0260	0.0301	0.0124	0.0147	0.0417	0.0407
6 steps	0.0369	0.0296	0.0228	0.0147	0.0841	0.0407
8 steps	0.0590	0.0299	0.0363	0.0147	0.1294	0.0406

Table 5.5: Ikeda system-model pair experiment, following Table 5.3: Statistics of the standard deviation of the pseudo-orbits' components for different lengths of assimilation window, for each assimilation window, pseudo-orbits are produced by WC4DVAR and $ISGD^c$ based on 512 realizations of observations. Median, 10th percentile and 90th percentile are calculated based on 512 assimilation windows. a) Standard deviation of the middle point of the pseudo-orbit, as the chosen window length contain even numbers of components we treat $(Length/2) - 1$ as the middle point; b) Standard deviation of the end point of the pseudo-orbit.

can be found in section 4.3.1). We apply each method in the Ikeda system-model pair experiment with two different noise level. For each method, the ensemble estimate of the current states, i.e. nowcasting, contains 64 equally weighted ensemble members. We use both ϵ-ball method (Figure 5.5 and Figure 5.6) and ignorance skill score (Table 5.7) to evaluate the results.

Figure 5.5, 5.6 and Table 5.7 shows the comparison among four ensemble nowcasting methods in both Ikeda system-model pair experiment and Lorenz96 system-model pair experiment. In both cases, the ϵ-ball method and ignorance score indicates Method IV and III performs better than Method II and Method II performances better than Method I. As Method I and Method II use the same Gaussian distribution to form the ensemble, the difference is that the ensemble

Window	STD of the middle point of the pseudo-orbit					
length	Median		10th percentile		90th percentile	
	WC4DVAR	$ISGD^c$	WC4DVAR	$ISGD^c$	WC4DVAR	$ISGD^c$
6 hours	0.0489	0.0402	0.0391	0.0295	0.0815	0.0697
12 hours	0.0540	0.0314	0.0411	0.0236	0.1045	0.0674
24 hours	0.2132	0.0309	0.1642	0.0227	0.3505	0.0662
Window	STD of the end point of the pseudo-orbit					
length	Median		10th percentile		90th percentile	
	WC4DVAR	$ISGD^c$	WC4DVAR	$ISGD^c$	WC4DVAR	$ISGD^c$
6 hours	0.0563	0.0480	0.0429	0.0243	0.0934	0.0744
12 hours	0.0743	0.0477	0.0573	0.0238	0.1332	0.0741
24 hours	0.2444	0.0477	0.1859	0.0236	0.3949	0.0740

Table 5.6: Lorenz96 system-model pair experiment, following Table 5.4: Statistics of the standard deviation of pseudo-orbits' components for different lengths of assimilation window, for each assimilation window, pseudo-orbits are produced by WC4DVAR and $ISGD^c$ based on 512 realizations of observations. Median, 10th percentile and 90th percentile are calculated based on 512 assimilation windows. a) Standard deviation of the middle point of the pseudo-orbit, as the chosen window length contain even numbers of components we treat $(Length/2) - 1$ as the middle point; b) Standard deviation of the end point of the pseudo-orbit.

formed by Method I is centred at the observation while the ensemble formed by Method I is centred at the end point of the pseudo-orbit. Whichever wins merely indicates which centre tend to be closer to the true state. Here the results indicate that the end point of the pseudo-orbit obtained by $ISGD^c$ method falls closer to the true state than the observation. Therefore the $ISGD^c$ method can also be treated as a useful noise reduction method. Although Method IV did the best, it is much more costly. Method III seems to work better than Method I & II which indicates using the imperfection error to form the initial condition ensemble is useful. And we expect such ensemble works better in the case that the observational noise is relatively large. As we discussed in section 5.2.5, when the observational noise is relatively larger than the model error, the geometrical
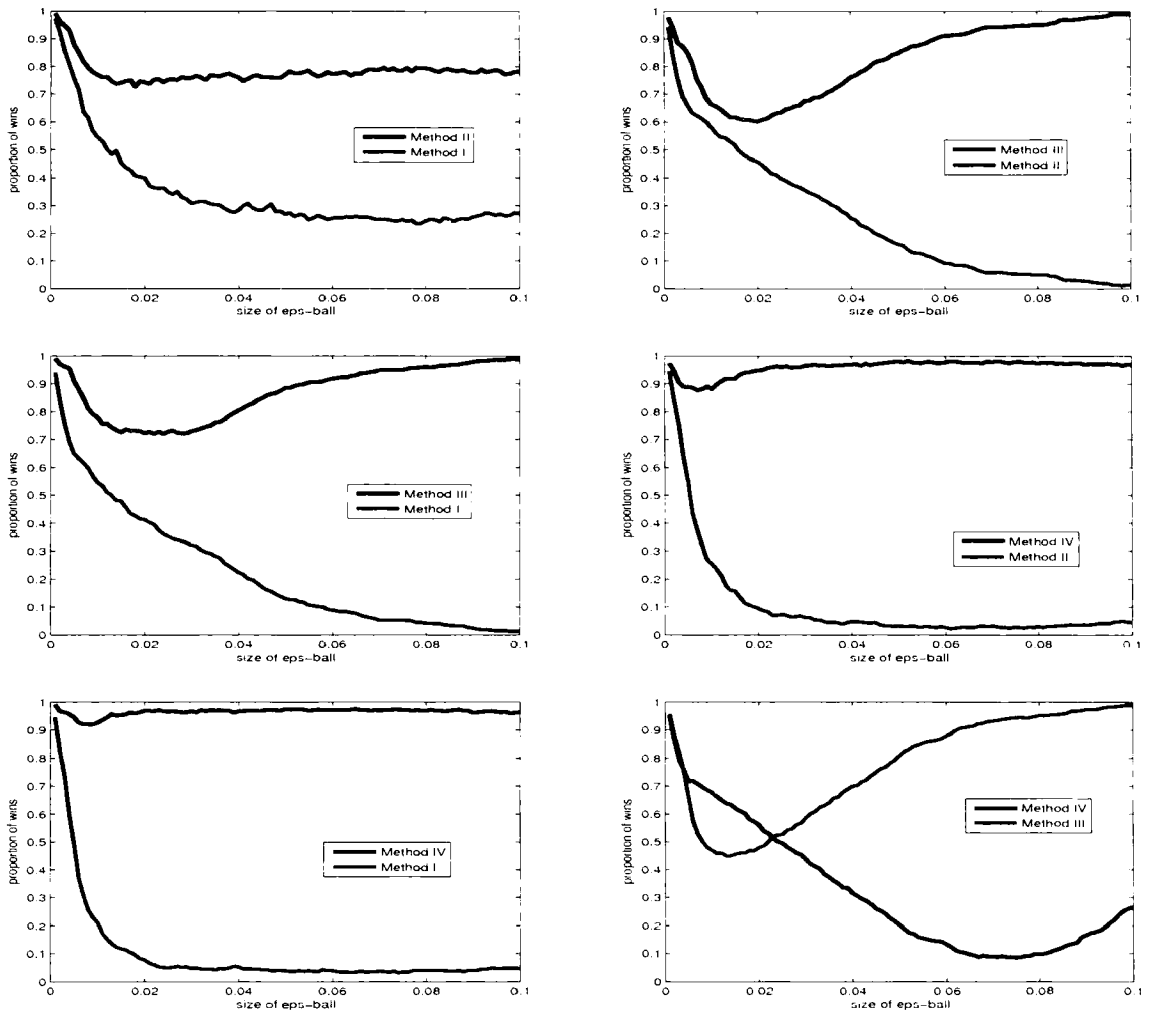
Figure 5.5: Comparing nowcasting ensemble using ϵ-ball. Observations are generated by Ikeda Map with observational noise $N(0, 0.05)$. The truncated Ikeda model is used to estimate the current state. We compare the nowcasting ensemble formed by Method I, Method II, Method III and Method IV. All the ensemble contains 64 ensemble members.

information of the model error is hard to extract. In this case the estimation of model error, i.e. imperfection error, will more or less look like random noise. As we mentioned in section 5.4, the disadvantage of Method III is that it as-
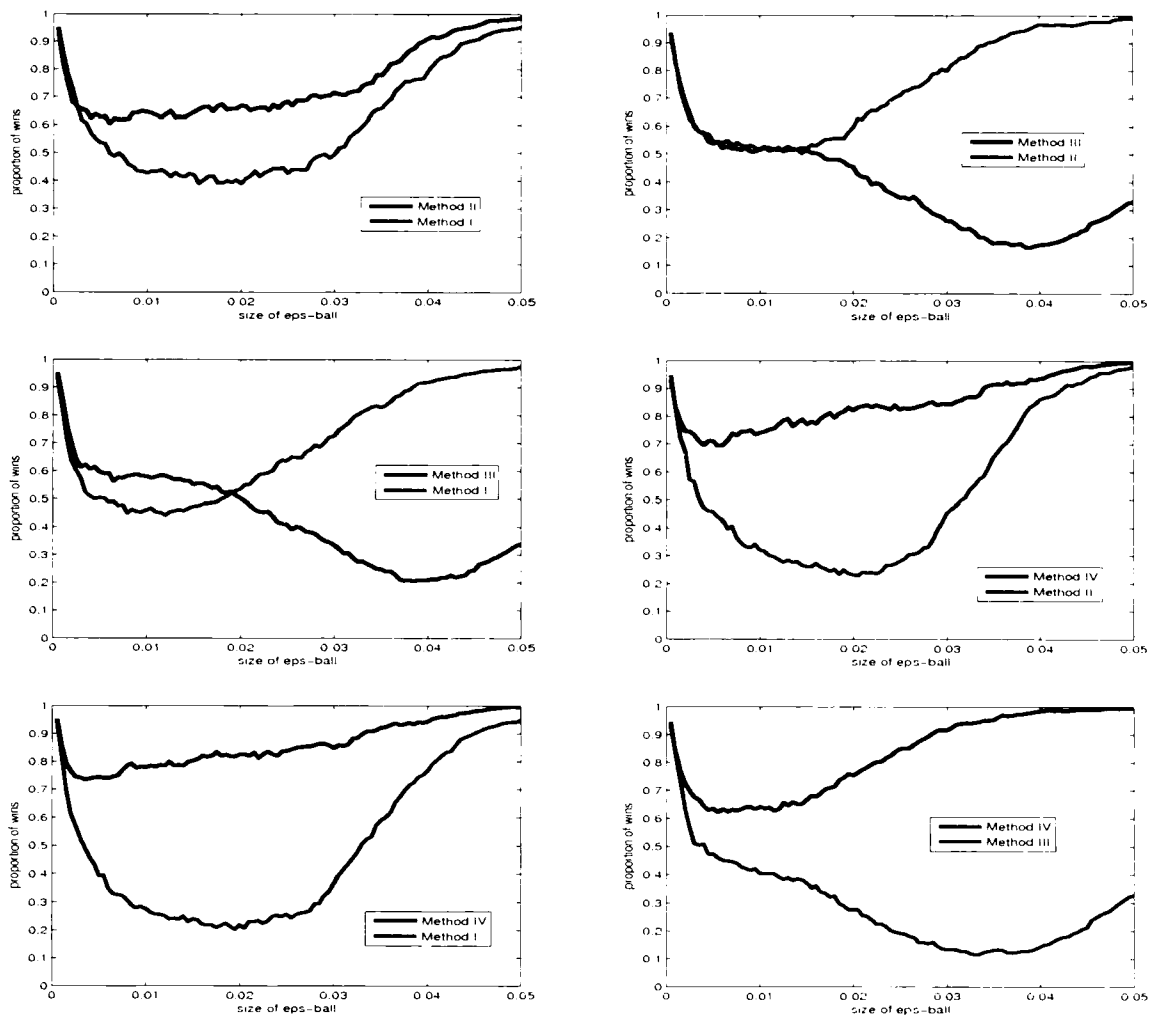
Figure 5.6: Comparing nowcasting ensemble using ϵ-ball. Observations are generated by Lorenz96 Model II with observational noise $N(0,0.1)$. The Lorenz96 Model I is used to estimate the current state. We compare the nowcasting ensemble formed by Method I, Method II, Method III and Method IV. All the ensemble contains 64 ensemble members.

sume the imperfection error is IID distributed. the assumption become less of a disadvantage when the observational noise is relatively larger than the model error.

	Ignorance skill score					
	Ikeda system-model pair			Lorenz96 system-model pair		
	Average	Lower	Upper	Average	Lower	Upper
Method I	-2.1863	-2.248	-2.1233	-4.4901	-4.5519	-4.4252
Method II	-2.5351	-2.5857	-2.4854	-4.6042	-4.6682	-4.5349
Method III	-2.9782	-3.0665	-2.891	-4.6345	-4.6886	-4.5966
Method IV	-3.0267	-3.0981	-2.9249	-4.9227	-4.9964	-4.8181

Table 5.7: Following Figure 5.5 and 5.6 experiments setting, Ignorance skill score of the nowcasting results of each methods for both Ikeda system-model pair experiment and Lorenz96 system-model pair experiment. Average: is the empirical ignorance score over 1024 nowcasts , Lower and Upper are the 90 percent bootstrap re-sampling bounds, 512 bootstrap samples are used to calculate the error bars.

5.6 Conclusions

In this chapter, we considered the problem of estimating the current states of the model outside PMS. Methods assuming the model is perfect are shown to be unable to produce the optimal results outside PMS. The adjusted ISGD method (50) is also found unable to produce consistent results. Using the ISGD method but with certain stopping criteria is then introduced to address the problem of nowcasting. The $ISGD^c$ method produces pseudo-orbit that are consistent with the observations and imperfect error which well estimate the model error.

The well established WC4DVAR method is reviewed and the differences between WC4DVAR method and ISGD method are discussed. Applying both methods to the Ikeda system-model pair and Lorenz96 system-model pair, we demonstrate that the $ISGD^c$ method produces more consistent results than WC4DVAR method. By measuring the variation of the WC4DVAR estimates based on different sizes of assimilation window, we demonstrate that similar to 4DVAR method, the WC4DVAR method also encounters the problem that the density of local

minima increases as the length of assimilation window increases.

Three methods are introduced to form the initial condition ensemble based on the pseudo-orbit provided by $ISGD^c$ method. Using the information of imperfection error are found to be useful to produce better initial condition ensemble. Forming the ensemble by applying $ISGD^c$ on perturbed pseudo-orbit are found to produce the best initial condition ensemble among these three methods.

Chapter 6

Forecast and predictability
outside PMS

In this penultimate chapter we discuss how to produce better forecast based on the initial condition ensemble given the fact that our model is imperfect. By showing the results in the Ikeda system-model pair experiment, we demonstrate first that forecast with relevant adjustment, which could be obtained from the imperfection error (see section 5.2.3), can produce better forecast than ignoring the existence of model error. Secondly we discuss how to interpret predictability outside PMS. Traditional ways of evaluating the predictability of one model, Lyapunov exponents and doubling time for example, provide the information of error growth but they implicitly assume the model is perfect. Outside PMS these measurements would systematically overestimate the predictability. We suggest using the probability forecast skill to interpret the predictability. Such forecast skill not only depends on the system, and model, and observation method but also depends on the way that initial conditions are formed and forecasts are

determined from the ensemble.

6.1 Forecasting using imperfect model

6.1.1 Problem setting up

We set up the forecast problem in the imperfect model scenario following (50). As in section 5.1, the trajectory of system states, $\tilde{x}_t, t = -n, ..., 0, ..., n^f$ where $\tilde{x}_t \in \mathbb{R}^{\tilde{m}}$, where $\mathbb{R}^{\tilde{m}}$ is the state space of the system, is governed by the nonlinear evolution operator $\tilde{F}$, i.e. $\tilde{x}_{t+1} = \tilde{F}(\tilde{x}_t)$. An observation s_t of the system state $\tilde{x}_t$ at time t is defined by $s_t = h(\tilde{x}_t) + \eta_t$ where $s_t \in \mathbb{O}$, η_t represents the observational noise, which we assume is IID distributed, and $h(\cdot)$ is the observation operator, which projects the system state into the observation space $\mathbb{O}$. For simplicity, we take $h(\cdot)$ to be the identity. Let the model be $x_{t+1} = F(x_t)$, where $x_t \in \mathbb{M}$, $\mathbb{M}$ is the model state space. Assume the system state $\tilde{x}$ can also be projected into the model state space by a projection operator $g(\cdot)$, i.e. $x = g(\tilde{x})$. In general, we don't know the property of this projection operator, we don't know even if $\tilde{x}$ exists. We are just going to assume that it maps the states of the system into somehow relevant states in the model. For the purposes of illustration and simplicity, unless otherwise stated, we assume $g(\cdot)$ is one-to-one identity. Our aim is to forecast the future model states $x_t, t = 1, ..., n^f$ given the model and the previous and current observations $s_t, t = -n, ..., 0$. Chapter 3 and Chapter 5 have discussed methods to estimate the current state using ensemble. In the following sections, we will treat the ensemble for the current states as the initial condition ensemble and use them to forecast the future states $x_t, t = 1, ..., n^f$.

The experimental results discussed in this section will based on the Ikeda system-model pair, i.e treat the Ikeda Map as the system and the truncated Ikeda Map as the model. Details of this system-model pair can be found in Section 5.1 and 2.4.

6.1.2 Ignoring the fact that the model is wrong

Given an initial condition ensemble, the simplest way to produce the forecast ensemble is to iterate the initial condition ensemble forward by the model, we call this the *direct forecast*. Unfortunately no matter how good the initial condition ensembles are, by simply iterating them forward the forecast ensembles are expected to move far away from the observations eventually. This failure of producing a relevant forecast results from ignoring the fact that the model is imperfect. Usually the invariant measure of the system in the model space and that of the model are rather different, and iterations of the initial condition under the model will, however, only approach the model attractor (if there is one) eventually, which essentially cause the irrelevance of the forecast.

6.1.3 Forecast with model error adjustment

As discussed in section 5.2, a system trajectory provides a pseudo-orbit of the model instead of a model trajectory in the model space. The mismatch $\tilde{x}_{t+1} - F(\tilde{x}_t)$, i.e. the model error $\tilde{\omega}_t$, distinguishes a system trajectory from being a model trajectory. Forecasting by iterating the initial condition ensemble forward by the model ignores the existence of model error. Given an initial condition ensemble at time 0, the ideal forecast at time 1 would be obtained by adjusting

the iteration of the initial condition ensemble with the corresponding model error.

If one has a large sample of historical model errors $\{\tilde{\omega}_j\}$, these could be used to improve the forecasting. One could, for example, adjust the iterations of initial condition ensemble with random draws from the set of relevant historical model errors (79). Let the initial condition ensemble be $\mathbf{x}_0^i, i = 1, ...N^{ens}$, where N^{ens} is the number of ensemble members. The forecast ensemble member at lead time t is then given by $\mathbf{x}_t^i = F(\mathbf{x}_{t-1}^i) + \zeta_t^i$ where ζ_t^i is random drawn from the set of historical model error. we call this the forecast with *random adjustment*. This method is equivalent to transferring the deterministic model F to a stochastic model by adding the dynamical noise term ζ_t. And this method assumes that the model error is IID distributed when usually it is not the case.

Model error is usually correlated, for example see Figure 5.1. Randomly drawing from the set of global historical model error discards the geometrical information about model error. Another approach by using historical model error that doesn't discard geometrical information is to employ a local analogue model to determine the adjustments ζ_t^i. For each model error $\tilde{\omega}_j$, it corresponds to two sequential states $\tilde{x}_j$ and $\tilde{x}_{j+1}$ as $\tilde{\omega}_j = \tilde{x}_{j+1} - F(\tilde{x}_j)$. To construct ζ_t^i, we can first find K nearest neighbours of $\mathbf{x}_t^i$ from the historical set $\{\tilde{x}_j\}$ and record their corresponding $\tilde{\omega}_j$, we then randomly choose one model error from the K $\tilde{\omega}_j$ to be ζ_t^i. We call this method forecast with *analogue adjustment*. There are many other analogue models one can use (details of analogue models can be found in Section 2.5), our interest here is not finding a better analogue model but to demonstrate that by extracting information from the model errors the forecast performance can be improved.

For computational reasons, we illustrate both methods taking only one ad-

justment ζ_t^i for each ensemble member x_t^i. Note that in future work, one could sample more than one from the set of historical model error or from the K local model error (70). Taking large samples will be more useful, but will lead to exponentially growing ensemble size, which is interesting but beyond the scope of current thesis.

The experiment results discussed below are based on two different initial condition ensembles. One is inverse noise (see section 4.3.1), which is a computationally cheap and easy way to form the initial condition ensemble but which ignores the information of the dynamics. The other is the dynamical consistent ensemble (see section 3.6), in our experiment the ensemble members are consistent with the system dynamics and a segment of observations, $s_i, i = -5, -4, ..., 0$. In the imperfect model scenario, such initial condition ensemble is not achievable as the system dynamics is unknown. We use such "perfect" initial condition ensemble as an example of the best initial condition ensemble one might hope to achieve. Results shown below demonstrate that forecasting with the adjustment of model error improves the forecast performance in both cases.

Figure 6.1 shows four examples of the one step forecast ensemble in the model state space when the initial condition ensemble is formed by inverse noise. In all the examples, forecasting with random adjustment produces ensemble members with too much spread. In panel (a), forecasting were made in a place where the model error is very small, which makes the difference between direct forecast and forecast with analogue adjustment very small. Panel (b) shows an example where the model error is small but not negligible, direct forecast ensemble fails to capture the true state to a slight extent. Panel (c) and (d) are cases that the model error is moderate and relatively large, in both cases direct forecast

132
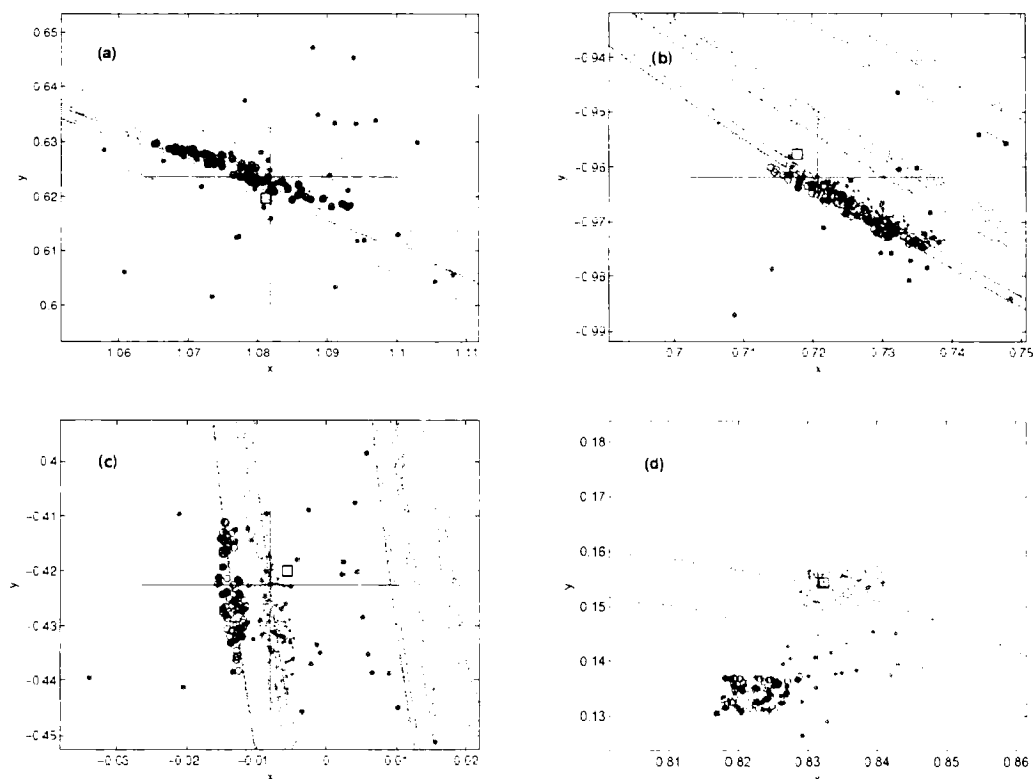
Figure 6.1: One step forecast ensemble in the state space. Observations are generated by Ikeda Map with IID uniform bounded noise $U(0, 0.01)$. The truncated Ikeda model is used to make forecast. The initial condition ensemble is formed by inverse noise with 64 ensemble members. Four 1-step forecast examples are shown in four panels. In each panel, the background dots indicate samples from the Ikeda Map attractor, the red cross denotes the true state of the system, the blue square indicates the observation, the direct forecast ensemble is depicted by purple circles, the forecast with random adjustment ensemble is depicted by orange dots and the forecast with analogue adjustment ensemble is depicted by cyan stars.

ensemble fails significantly to capture the true state, while the forecast with

analogue adjustment ensemble is still able to capture the true state very well.

The forecast with random adjustment sometimes produces ensemble members

that stay closer to the true state than all the ensemble members produced by

direct forecast.

Figure 6.2 shows the comparison between the three methods discussed above using the ϵ-ball test at different lead times (Details of ϵ-ball method can be found in Section 3.7). It appears that forecasts with analogue adjustment almost always outperform the direct forecasts for different lead times and different sizes of ϵ-ball. At lead time 1 and 2, direct forecasts outperform the forecasts with random adjustment no matter what the size of ϵ-ball is. At lead time 4, the proportion of wins for these two methods are close when the diameter of ϵ-ball is less than 0.03, beyond 0.03 direct forecast wins. At lead time 8 and lead time 16, however, forecast with random adjustment outperforms the direct forecast. The reason of direct forecast winning at short lead time and losing at longer lead time is that at short lead time although the direct forecast may not capture the true state, the forecast ensemble members are still stay relatively close to the true state. For longer lead time, a direct forecast ensemble is not only unable to capture the true state but also further way from the true state.

Following Figure 6.1, Figure 6.3 shows the same four examples of the one step forecast ensemble but based on the initial condition ensemble that is a dynamical consistent ensemble in the state space. Forecasts with random adjustment still produce ensemble members with too much spread. Although the initial conditions are consistent with both observations and system dynamics, the direct forecast fails to capture the true state with the appearance of model error. Forecast with analogue adjustment ensemble members not only cover the true state but also lie closer to the relevant system attractor.

Following Figure 6.2, Figure 6.4 shows the ϵ-ball test for the three forecasting methods at different lead time where the initial condition ensemble is formed by
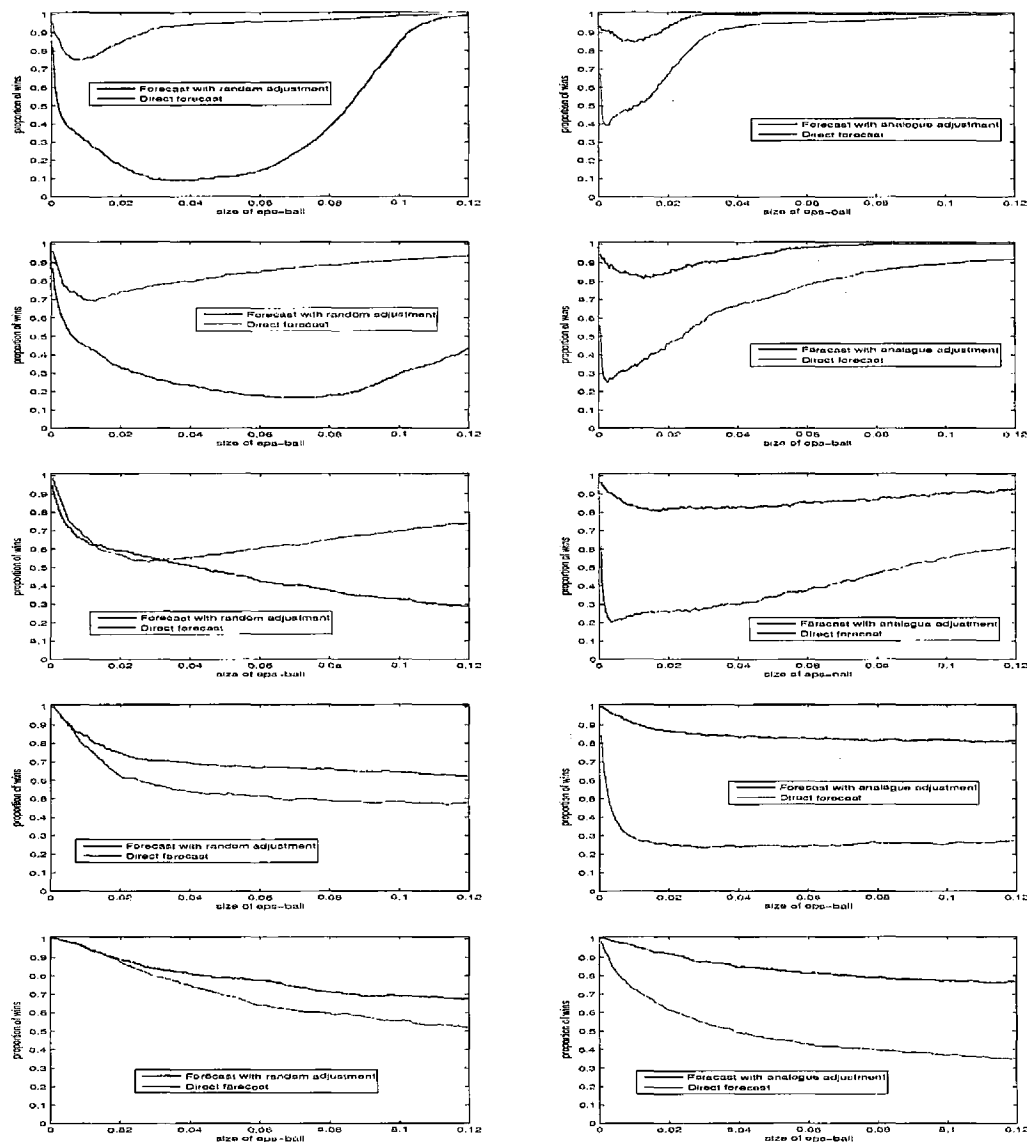
Figure 6.2: Following Figure 6.1 experiment setting, compare forecast ensemble using ϵ-ball. Direct forecasts are compared with forecasts with random adjustment (left) and forecasts with analogue adjustment (right). The initial condition ensemble is formed by inverse noise with 64 ensemble members. For each forecast method, 2048 forecasts are made. Each row shows the comparison for different lead time. First row denotes lead time 1, second lead time 2, third lead time 4, forth lead time 8 and fifth lead time 16.
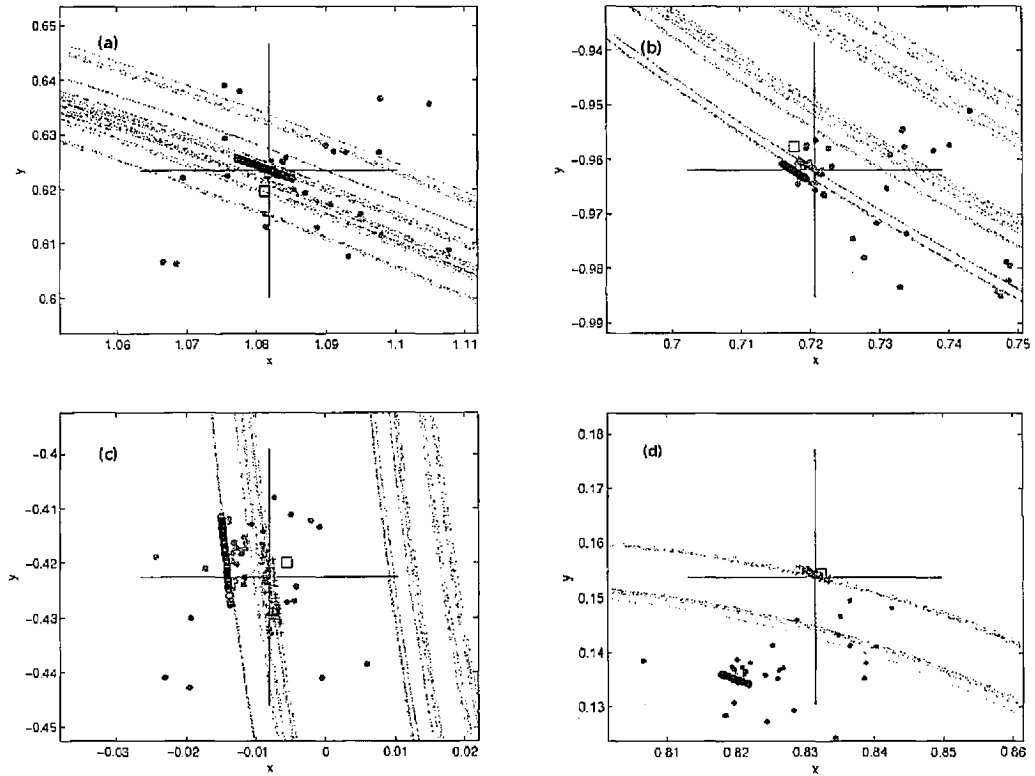
Figure 6.3: Following Figure 6.1 one step forecast ensemble in the state space. The initial condition ensemble is formed by dynamical consistent ensemble with 64 ensemble members.

a dynamical consistent ensemble. The results are almost the same as seen in Figure 6.2 did. Comparing with Figure 6.2, the advantage of using adjustment at longer lead time becomes more obvious as the dynamical consistent initial conditions are more concentrated than inverse noise ensemble which makes the forecast ensemble less likely to capture the true state using a direct forecast.

Figure 6.1 and Figure 6.3 have compared the results of three forecasting methods in the state space at lead time 1. And Figure 6.2 and Figure 6.4 compare their forecast performance at different lead times by looking at the probability mass
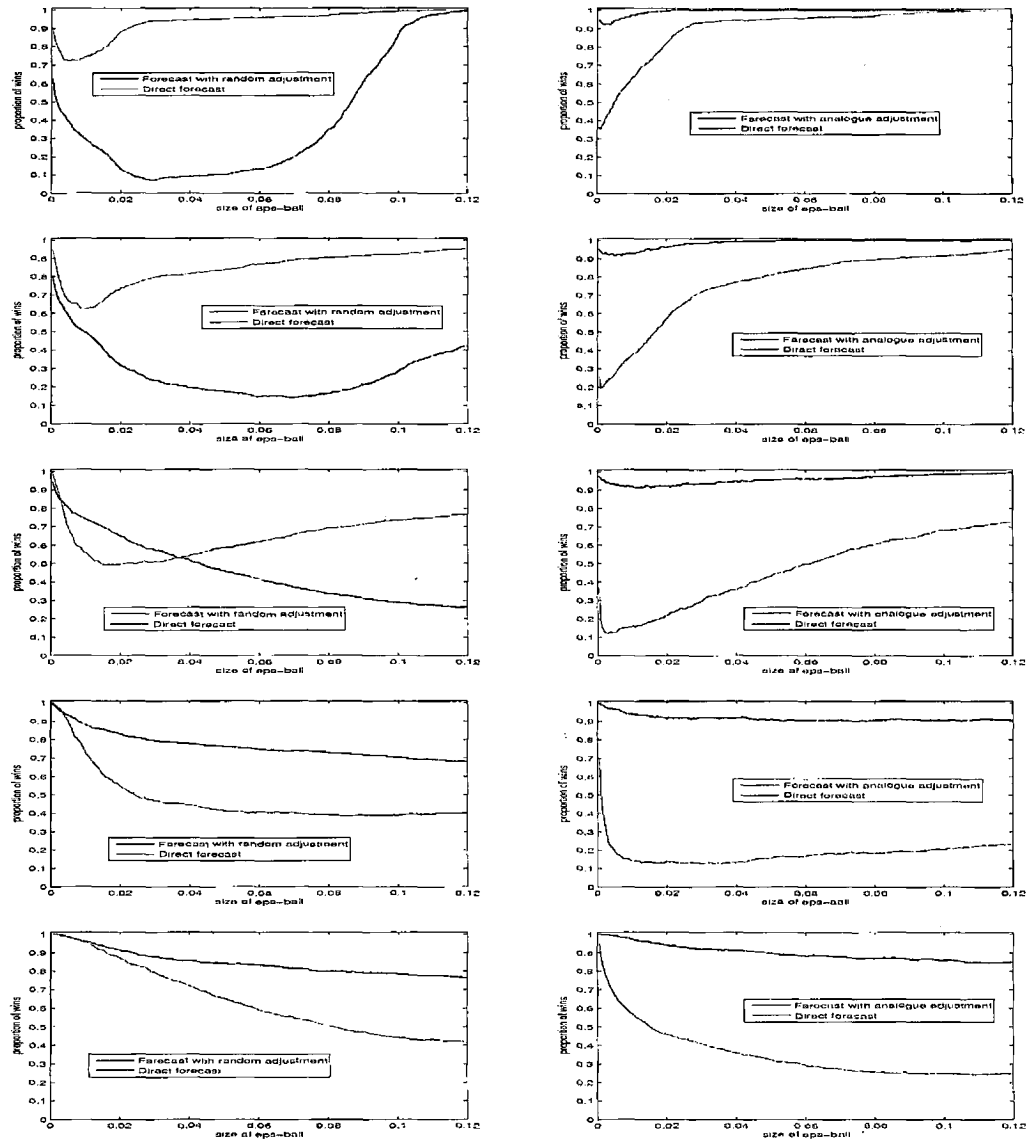
Figure 6.4: Comparing forecast ensemble using ϵ-ball. Observations are generated by Ikeda Map with IID uniform bounded noise $U(0, 0.01)$. The truncated Ikeda model is used to make forecast. The initial condition ensemble is formed by dynamical consistent ensemble with 64 ensemble members. Each row of pictures shows the comparison for different lead time. First row denotes lead time 1, second lead time 2, third lead time 4, forth lead time 8 and fifth lead time 16.

around the true state. We now look at their forecast performance at different lead times using the ignorance score. Following section 4.3.2, we first transform the forecast ensemble into a probability distribution by standard kernel dressing, and we use the historical observations for a climatology which is blended with forecast distribution generated by forecast ensemble. we evaluate the final forecast probability distribution by the ignorance score. Figure 6.5 plots the ignorance score of three forecasting methods for different lead times. In panel (a) the forecasts are based on an inverse noise initial condition ensemble. In panel (b) the forecasts are based on a dynamical consistent initial condition ensemble. In both cases, the forecasts with random adjustment appears slightly better than direct forecast, and forecasts with analogue adjustment outperforms the other two methods significantly. Panel (c) combines the panel (a) and panel (b) in order to compare the difference between different initial condition ensembles. From panel (c), it appears that using a dynamical consistent ensemble for the initial condition is only slightly better than using inverse noise ensemble for both direct forecast and forecasting with random adjustment, while for the forecast with analogue adjustment a dynamical consistent ensemble initial condition can improve the forecast perform significantly which indicates that the information of the initial condition is well maintained.

From Figure 6.2, 6.4 and 6.5, it seems that ϵ-ball test and ignorance score do not indicate a single best approach in the case of comparing direct forecast and forecast with random adjustment, especially at short lead times. Comparing these two methods by ϵ-ball test, the proportion of wins of direct forecast is never smaller than that of forecast with random adjustment for any size of ϵ-ball at lead time 1 and 2. By comparing the ignorance score, however, forecasts with random
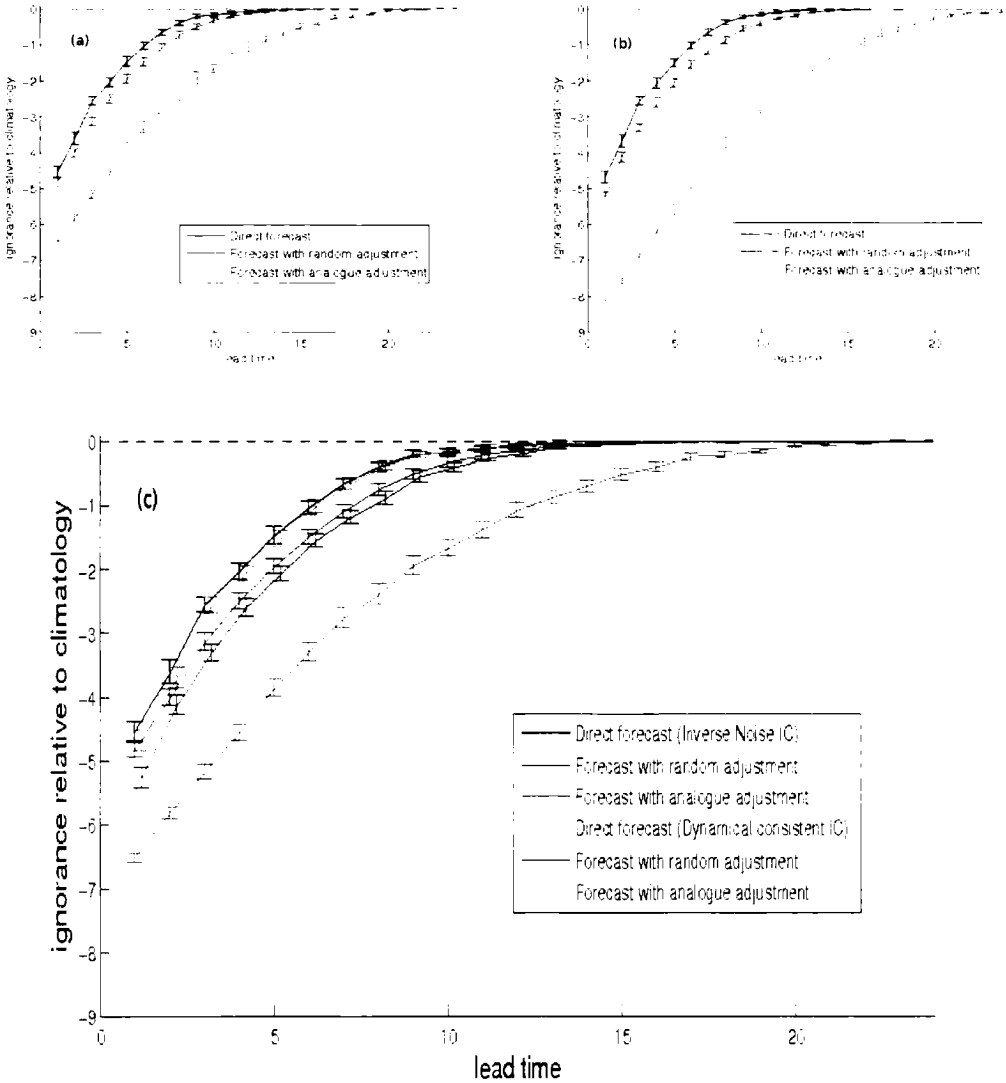
Figure 6.5: Following Figure 6.1 experiment setting. Ignorance score of three forecasting methods relative to climatology is plotted vs lead time. The error bars are 90% bootstrap re-sampling bars. In panel (a), the initial condition ensemble is formed by inverse noise with 64 ensemble members. In panel (b), the initial condition ensemble is formed by dynamical consistent ensemble with 64 ensemble members. Panel (c) is the combination of panel (a) and (b). Ignorance is calculated based upon 2048 forecasts.

adjustment have slightly lower ignorance than direct forecasts. The reason for such inconsistent results is that there are fundamental differences between these two evaluation methods, as now explained. The ϵ-ball method measures the probability mass that stays inside different sizes of ϵ-balls and counts the proportion of times one method beats the other (on a tie, both win). For each forecast, an ϵ-ball test only counts which method wins regardless of how significantly the win is, which means ϵ-ball treats an overwhelming win and slight win the same. The empirical ignorance score discussed in section 4.3.3, on the other hand, averages the ignorance of each forecast, i.e how much one method wins in one forecast matters. In our experiments, although direct forecasts have a lager proportion of wins, it loses a lot when it loses to forecast with random adjustment. This can also be seen from Figure 6.1 and Figure 6.3, where the model error is large, direct forecast miss the target (true state) completely while forecast with random adjustment may produce some ensemble members are close to the true state; for this kind of forecast, ignorance score punishes direct forecast heavily.

6.1.4 Forecast with imperfection error adjustment

It is clear that forecasts with adjustment using the model error can improve the forecast performance compared to direct forecast. Unfortunately, identifying the actual model error is not achievable except the noise free case. With observational noise, model error cannot be precisely determined (see section 5.2.2). One can, however, estimate the model error and use the estimates to improve the forecast. The $ISGD^c$ method we introduced in section 5.2.5 is not only a state estimation method, it also provides estimates of model error, i.e. the imperfection error (see

Section 5.2). In this section we consider using the imperfection error to adjust the forecast and compare with direct forecasts. The experiment results discussed below are based on initial condition ensemble obtained by inverse noise [1].

Figure 6.6 shows six examples of the one step forecast ensemble in the state space, the initial condition ensemble is formed by inverse noise. Instead of using the actual model error we use the model imperfection error obtained from the $ISGD^c$ method to adjust the forecast. In all examples, forecasts with random adjustment still produce ensemble members with too much spread. Similar to Figure 6.1, the first 4 panels present the four cases where the model error is very small, small, moderate and large. Forecasts with analogue adjustment outperform the direct forecast as long as the model error is not negligible. Panel (e) shows an example where the model error is small but the forecast with analogue adjustment ensemble is unable to capture the true state. This failure occurs because the model error in this case is overestimated by the imperfection error. Panel (f) shows an opposite example where forecasts with analogue adjustment did not capture the true state because the model error in this case is underestimated by the imperfection error. Figure 6.7 shows the comparison between three methods via ϵ-ball method (see section 3.7) at different lead time, the forecast adjustment is obtained from the imperfection error instead of model error. Similar to the adjustment using model error, the forecasts with analogue adjustment almost always outperform the direct forecast for different lead time and different sizes of ϵ-ball. Direct forecasting outperforms the forecasts with random adjustment at short lead times while underperforms at longer lead times. As the result of using

[1] dynamical consistent ensemble is not employed this time since if method can improve the forecast based on inverse noise it is expected to do so for other initial condition ensemble and it might be too costly to form an dynamical consistent ensemble in practice
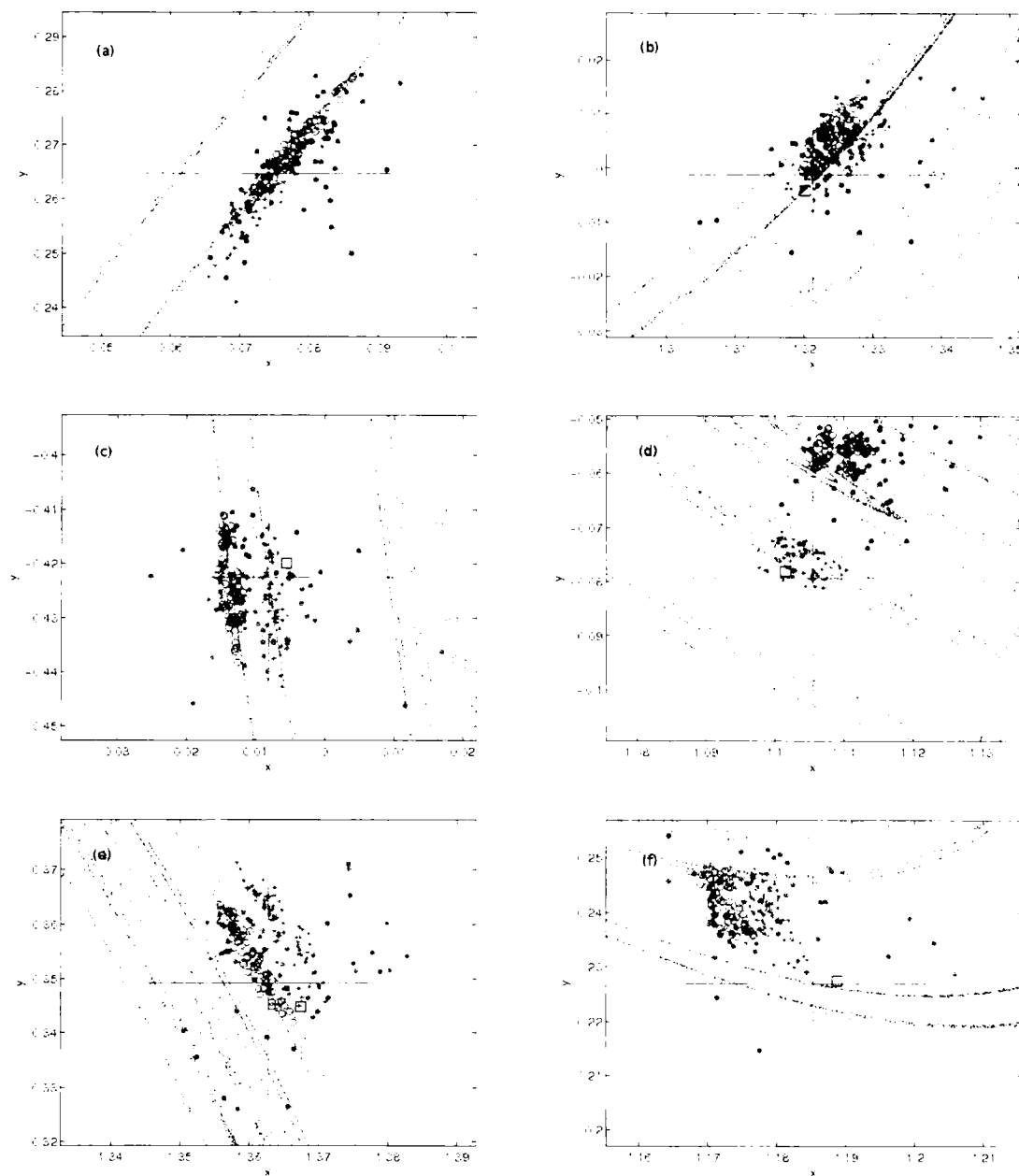
Figure 6.6: Following Figure 6.1, six 1-step forecast examples are plotted in the state space. Here the adjustment is obtained from imperfection error instead of model error.
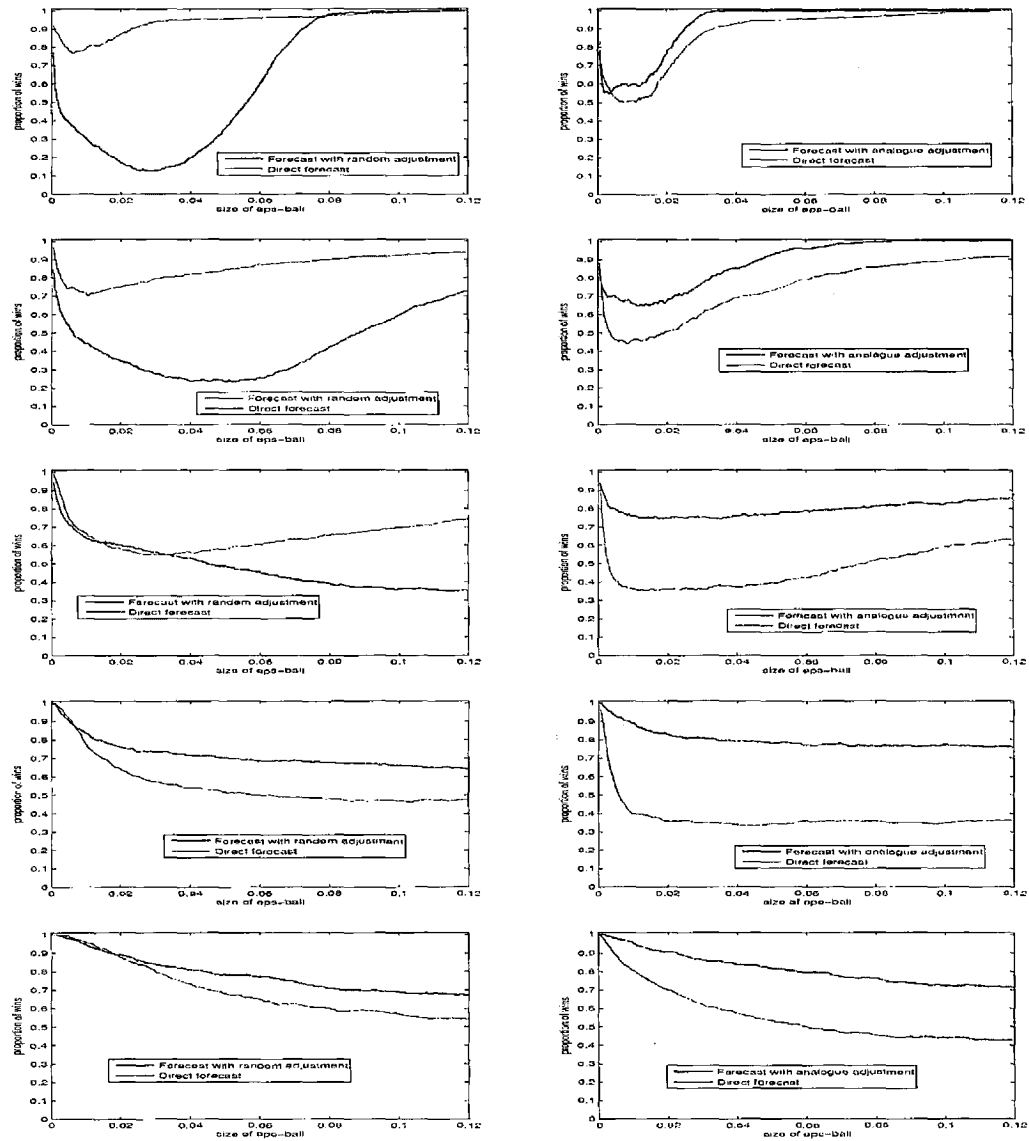
Figure 6.7: Following Figure 6.2, comparing three forecast ensemble results using ϵ-ball. Here the adjustment is obtained from imperfection error instead of model error.

imperfection error, forecasts using analogue adjustment outperform the direct forecast less significantly than using the actual model error. Figure 6.8 plots the ignorance score of three forecasting methods for different lead time. Similar to

143
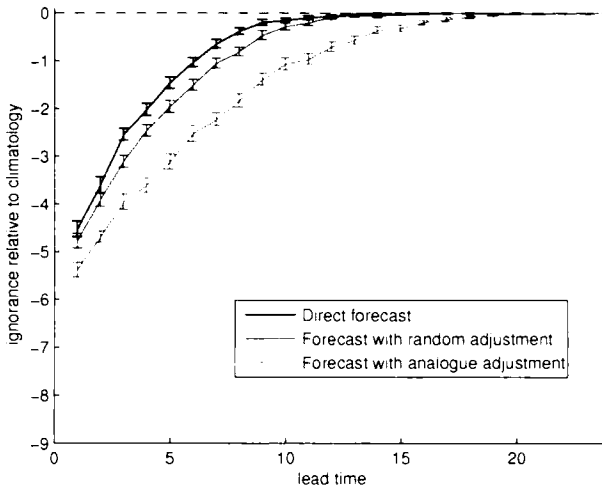
Figure 6.8: Following Figure 6.5a. Ignorance score of three forecasting methods relative to climatology is plotted vs lead time. Forecast adjustment is obtained from imperfection error.

Figure 6.5 forecasts with random adjustment appear to be slightly better than direct forecasts. and forecasts with analogue adjustment outperform the other two methods significantly. Compared with Figure 6.5. by using imperfection error the forecast with analogue adjustment gives higher ignorance score than using the actual model error.

As we mentioned in section 5.2.5. the quality of the estimates of the model error using imperfection error is strongly dependent on the observational noise level. When the model error is relatively larger than the observational noise. then the model error can be well estimated by the imperfection error. On the other hand. when the model error is relatively small corresponding to the observational noise. then the model error will be poorly estimated by the imperfection error. In general the smaller the observational noise is. the better the model error can be estimated. Figure 6.9 plots the ignorance score of forecast with adjustment
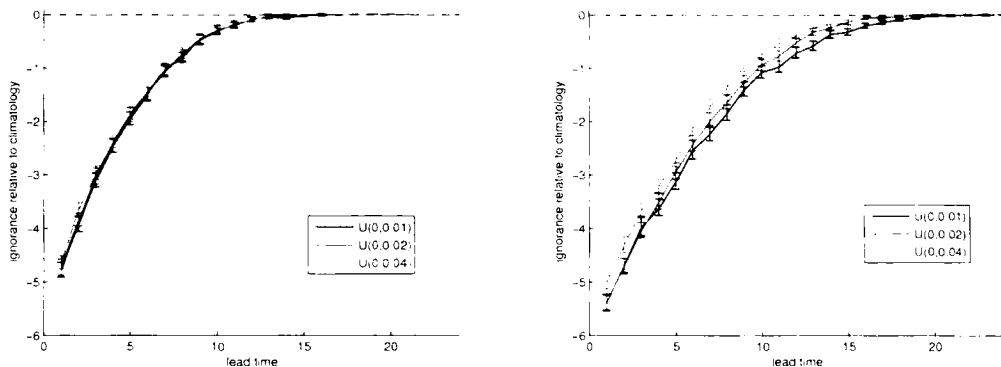
Figure 6.9: Ignorance score of forecast with adjustment where the adjustment is generated from the observations with different noise level. The initial condition ensemble is formed by inverse noise with fixed noise level $U(0, 0.01)$ so that the observations with different noise level only affect the imperfection error. The error bars are 90% bootstrapped error bars. In panel a, the forecast is made by random adjustment; in panel b, the forecast is made by analogue adjustment

where the imperfection error is produced of different noise levels. It appears that forecasts with random adjustment are not affected much by having higher observational noise. Doubling the observational noise, however, decreases the forecast performance of using analogue adjustment.

Overall, we conclude that forecasting with adjustments can improve the forecast performance from direct forecast as the adjustment is able to account the model inadequacy partially. The adjustments can be obtained from estimates of the model error. Such estimates can be obtained for example using $LSGD^c$ method. Forecasts with random adjustment ignores the geometric information of model error by assuming it is IID distributed. Forecast with analogue adjustment extracts such information and as a result, outperforms forecast with random adjustment and direct forecast significantly.

6.2 Predictability outside PMS

If the dynamics of a deterministic system are completely understood and the exact initial state is observed, then there is no limit to predictability and the future holds no surprises. When there is uncertainty in the initial condition, sensitive dependence on initial conditions restricts our ability to predict the future. The well known Lyapunov exponents (3; 22; 68) measures the predictability by calculating the average exponential uncertainty growth rates. Lorenz (62) discussed using finite time Lyapunov exponents to measure the predictability of high dimensional atmospheric model. The weakness of using Lyapunov exponents is revealed by Smith et al (82) by comparing q-pling times which reflects the time of error growth directly. The q-pling times are used to measure the predictability by directly quantifying the time at which initial uncertainty increases by a factor of q.

Outside PMS, there is not only uncertainty in the initial condition but also uncertainty in the dynamics. Measuring the predictability with the assumption that the model is perfect will simply overestimate the predictability. Without knowing the true state of the system, q-pling times can be used to estimate the uncertainty doubling (quadrupling, etc) time based on the sequence of observations. Knowing a particular q-pling time, however, from which the uncertainty growth rate can not be simply inferred, as discussed in Smith(1996), the relation $\tau_{q^2} \simeq 2\tau_q$ may not hold. We suggest that outside PMS one could define predictability being lost when the forecast adds no new information to the climatology (82). In practice, this is to say that the predictability is lost when the forecast skill score relative to climatology is arguably zero. Lyapunov Exponents

and q-pling time are discussed in Section 6.2.1 and 6.2.2. Applying forecast skill to measure the predictability is introduced and discussed in Section 6.2.3.

6.2.1 Lyapunov Exponents

Given an initial state on the attractor of the system x_0, The evolution of an infinitesimal uncertainty around x_0 over a finite time $\triangle t$ is determined by the linear propagator $M(x_0, \triangle t)$ (81), i.e.

$$\epsilon(t_0 + \triangle t) = M(x_0, \triangle t)\epsilon(t_0) \tag{6.1}$$

For a flow,

$$M(x_0, \triangle t) = exp(\int_{t_0}^{t_0 + \triangle t} J(x(t))dt)), \tag{6.2}$$

where $J(x(t))$ is the Jacobian along the trajectory. For discrete time maps, the linear propagator is simply the product of the Jacobians along the trajectory

$$M(x_0, k) = J(x_{k-1})J(x_{k-2})...J(x_1)J(x_0) \tag{6.3}$$

For a given x and $\triangle t$, the finite-time Lyapunov exponents (62) are defined by

$$\lambda_i(x, \triangle t) = \frac{1}{\triangle t}log_2\sigma_i, \tag{6.4}$$

where σ_i are the singular values (in rank order, i.e. with $\sigma_i > \sigma_j$ for $i < j$) of the linear propagator $M(x, \triangle t)$.

Since the singular values σ_i are positive, the Lyapunov exponents tells us, on

average, how fast the initial uncertainty grows exponentially over Δt. $\lambda_1(x, \Delta t)$, called the maximum average exponential growth rate, reflects the error growth in the fastest growing direction. In the limit $\Delta t \to \infty$, $\lambda_i(x, \Delta t)$ approaches the global Lyapunov exponents, which are the same for almost all x with respect to an ergodic measure (25).

It is proved (94) to be true that the largest finite time Lyapunov exponent(average over the invariant measure) is large or equal to the largest global Lyapunov exponent. A positive global Lyapunov exponent is therefore often said to destroy any hope of "long-term" predictability. Actually both finite time Lyapunov exponents and global Lyapunov exponents reflect average rates, not average times (81). Smith (94) gives several examples of common chaotic systems to show that even the system has positive global Lyapunov exponent, there are some states on the system attractor about which every infinitesimal uncertainty will shrink for certain finite time regardless of its orientation, which also indicates that the local dynamics of uncertainties about that initial condition are more relevant (62; 82).

6.2.2 q-pling time

In stead of averaging the error growth rate, the uncertainty q-pling time (82) measures the average of minimum time required for an uncertainty reaching a certain threshold. Given an uncertainty ϵ_0 at x_0, a q-pling time (82) $\tau_q(x_0, \epsilon_0)$ is defined by the smallest time for which the initial uncertainty ϵ_0 about x_0 has increased by a factor q

$$\tau_q(\tilde{x}_0, \epsilon_0) = min_{t>0}\{t \mid \|\ \tilde{F}_t(\tilde{x}_0 + \epsilon_0) - \tilde{F}_t(\tilde{x}_0)\ \| \geq q \parallel \epsilon_0 \parallel\} \qquad (6.5)$$

if single value is required, the average q-pling time, $\tau_q(\| \epsilon \|)$, is then defined by averaging the q-pling time over all points x on the attractor.

Although the q-pling time is often (81) defined based on $\| \epsilon \| \to 0$ in order to compare with Lyapunov exponents, the q-pling time can be calculated based on any initial uncertainty, which does not have to be infinitesimal. For Lyapunov exponents, the linearised dynamics, Equation 6.2, is based on the assumption that uncertainties remain effectively infinitesimal for the time scales of interest. Clearly, as long as an uncertainty is infinitesimal it can place no limit on predictability. Once the uncertainty becomes finite, the linearization, and hence Lyapunov exponents are, in general, irrelevant to error growth (82).

It is usually impossible to derive the Lyapunov exponents and q-pling times analytically for a nonlinear system. In practice, to estimate the global measure of them one sample initial conditions uniformly with respect to the invariant measure of the system. For each initial condition x, the Lyapunov exponents, i.e. the uncertainty growth rates, can be estimated by iterating the initial uncertainty about x for a fixed lead time; the q-pling times is obtained by iterating the initial uncertainty about x until the uncertainty has increased by a factor of q. Outside PMS, calculating the Lyapunov exponents which have to assume the model is perfect tells us nothing about the real predictability. Arguably, model error may be more responsible for poor predictions of real nonlinear systems than "chaos" (82). If the observational noise is free, one observes the projection [1] of the system states in the model state space precisely. In that case the q-pling is

---

[1] assume the projection operator is one-to-one identity

defined by

$$\tau_q(\mathbf{x}_0, \epsilon_0) = min_{t>0}\{t \; |\| \; F_t(\mathbf{x}_0 + \epsilon_0) - \mathbf{x}_t \; \|\geq q \; \| \; \epsilon_0 \; \|\} \qquad (6.6)$$

where x is the projection of system state in the model state space. One can calculate the q-pling times of uncertainty about such model states based on the imperfect model F [1]. When the observational noise is not free, it is reasonable to assume that the observational noise is relatively smaller than the growth of uncertainty. In that case the q-pling time can be defined based on the observations:

$$\tau_q(\mathbf{s}_0, \epsilon_0) = min_{t>0}\{t \; |\| \; F_t(\mathbf{s}_0 + \epsilon_0) - \mathbf{s}_t \; \|\geq q \; \| \; \epsilon_0 \; \|\}. \qquad (6.7)$$

Equation 6.7 uses random perturbation around the observation as the initial condition.

Figure 6.10 shows the doubling time in both noise free and low observational noise case. It appears that the doubling time estimated by assuming the model is perfect is much longer than the doubling time estimated based on the states generated system and the imperfect model, which indicates treating the model to be perfect will essentially over-interpret the predictability of the model.

6.2.3 Predictability measured by skill score

As we mentioned above, Lyapunov exponents measure the predictability through globally average error growth rates in the limits of large time and small un-

---

[1] As we discussed in the previous section, forecast with adjustment could improve the forecast performance, which indicates that it can also increase the q-pling time. Since adjusting the forecast is essentially turn the original deterministic model into a stochastic model, here the imperfect model F can represent any model including deterministic and stochastic models
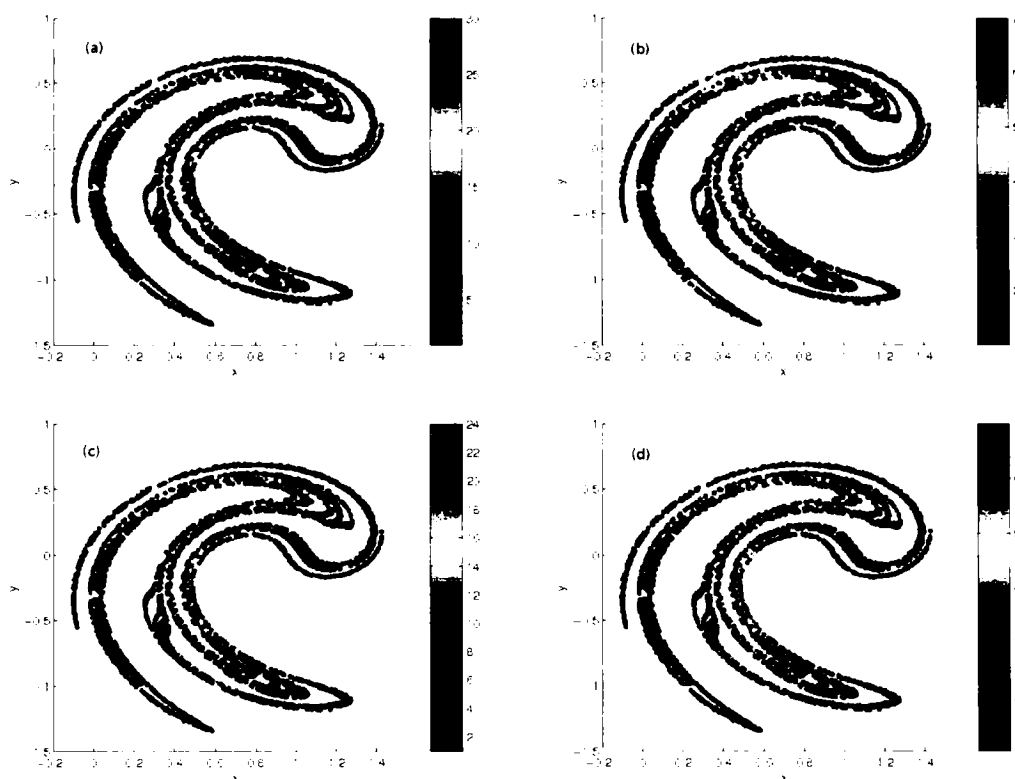
Figure 6.10: Doubling time of Ikeda system-model pair. Panels a) and c) estimate the doubling time by assuming the model is perfect. Panels b) and d) estimate the doubling time based on the states generated Ikeda Map and using the Truncated Ikeda Map as the model. a) and b) are noise free cases while c) and d) have observational noise $N(0, 0.0001)$. Note that the scale of the color bar is different in each panel.

certainty (94). they are of limited use in PMS and inapplicable outside PMS. q-pling time (82) measures the average of minimum time required for an uncertainty reaching a certain threshold. Such measurement is well defined and applicable for both perfect model and imperfect model scenarios. As measurement of the average minimum time that an uncertainty doubles can not be used to infer the average minimum time that an uncertainty reaches any other threshold.

predictability being lost has to be defined, in advance, upon a certain threshold. In this section we suggest another way to measure the predictability by comparing the model forecast performance with climatology, we call it forecast based measurement.

As the average forecast performance degenerates with forecast lead time, it will, for sure, happens at certain lead time that the model forecast does not do better than the climatology. We define predictability being lost when this happens, it indicates that the model forecast does no better than random drawn from the historical observations. Such measurement can be applied to both perfect model and imperfect model scenarios and places no restriction on the initial condition uncertainty. Comparing with the q-pling time, the predictability being lost is better defined. Although the measurement itself places no restriction on the initial uncertainties and the model, the model forecast performance depends on how good the initial conditions and the model are. Similar to q-pling time, the forecast based measurement measures the predictability given the initial conditions and the model, of course, better initial conditions or better model will have more predictability.

To evaluate the forecast performance, we use the Ignorance score (see section 4.3.3). Given an initial condition ensemble and the model (does not have to be perfect), the forecast ensemble at each lead can be produced by iterating the initial condition through the model [1]. To calculate the imperical ignorance score, a forecast ensemble is transformed into a forecast distribution by kernel

---

[1] we are aware that one may use different forecast scheme, e.g. direct forecast and forecast with adjustment defined in section 6.1. In this section we treat the model and forecast scheme as the forecast model, i.e. forecasting using a deterministic model with random adjustment is treated to be a stochastic model

dressing (details of kernel dressing can be found in section 4.3.2). To simplify the comparison between model forecast and climatology, the forecast distribution is blended with climatology (details can be found in section 4.3.2). After blending with climatology, we expect the forecast will do no worse than the climatology. By looking at the Ignorance score relative to climatology, one can measure when the predictability is lost. As the lead time goes larger, one may expect the relative Ignorance go to zero asymptotically. When the model is perfect, given the sample climatology based finite number of historical observations, we expect the relative ignorance goes to the values that relevant to proportion between the size of the ensemble and the size of the historical observations as the ensemble members will eventually become random draws from the invariant measure of the model. When the model is imperfect, we expect the relative ignorance goes to 0 eventually as the invariant measure of the model is different from that of the system.

We suggest using the forecast based measurement to measure the predictability as outside PMS the predictability should depend on not only the system and model but also the way initial condition ensemble is constructed and the size of ensemble. Figure 6.11 shows the ignorance score (relative to climatology) as a function of forecast lead time in the Ikeda system-model pair experiment, forecast based on two different initial condition ensembles with two different sizes are plotted separately. In all cases, the relative ignorance converges to 0 after certain lead time which indicates after that lead time the information in the initial conditions is lost. Using the same initial condition ensemble but with larger ensemble size provides more predictability and delay the convergence. As the results shown in section 5.5.2, the initial condition ensemble formed by $ISGD^c$ produces better estimate of the current states than the Inverse Noise ensemble, the information
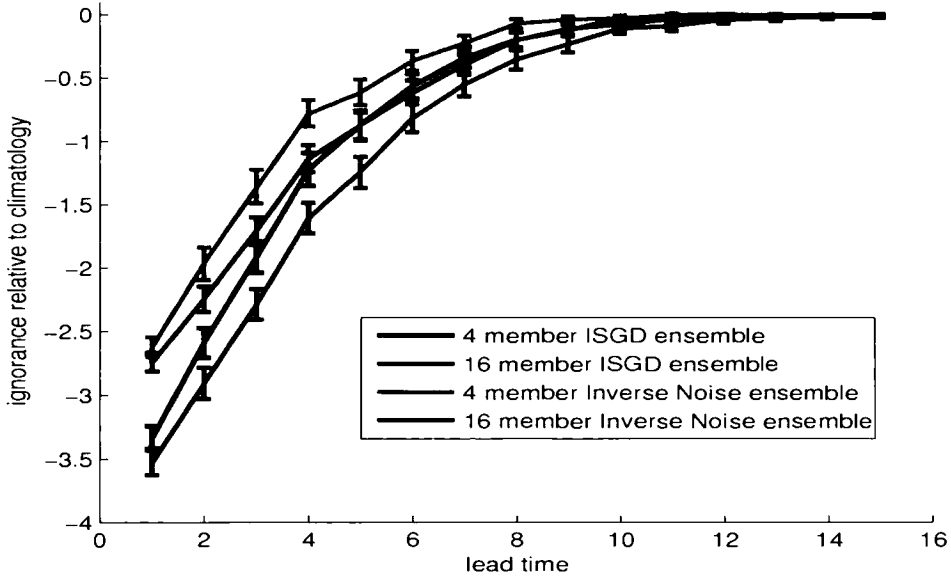
Figure 6.11: Ignorance as a function of forecast lead time in the Ikeda system-model pair experiment. The observations are generated by Ikeda Map with IID $N(0, 0.05)$ observational noise, initial condition ensemble is built by using Inverse Noise and $ISGD^c$ ensemble.

of the initial condition ensemble formed by $ISGD^c$ sustain longer than that of the Inverse Noise ensemble.

6.3 Conclusions

In this chapter, we firstly address the problem of estimating the future states of the model outside PMS. Directly iterating the initial condition ensemble forward is unable to provide good forecast ensemble as such method ignores the existence of model error. Two new methods, based on adjusting the forecast with imperfection error provided by $ISGD^c$ method, are introduced. The first method

adjust the forecast by adding random draws of the imperfection error onto the forecast. The other method selects the imperfection error using analogue models. Applying these methods to the Ikeda system-model pair, we demonstrate that forecast with random adjustment does not provide significantly better estimates than direct forecast as it discards the geometrical information of the imperfection error. Forecast with analogue adjustment is shown to outperforms both direct forecast and forecast with random adjustment.

Secondly we address the question of how to interpret predictability outside PMS. Traditional ways of evaluating the predictability, Lyapunov exponents and doubling time are discussed. Lyapunov exponents measure the predictability through globally average error growth rates in the limits of large time and small uncertainty, they are of limited use in PMS and inapplicable outside PMS. q-pling time (82), which measures the average of minimum time required for an uncertainty reaching a certain threshold, is applicable for both perfect model and imperfect model scenarios. A certain threshold is, however, required in advance in order to define when the predictability is lost. We suggest using the probabilistic forecast skill to interpret the predictability. In that case, the predictability being lost is well defined. In the IPMS, such forecast skill not only depends on the system, and model, and observation method but also depends on the way that initial conditions are formed and forecasts are determined from the ensemble.

Chapter 7

Conclusions

In this thesis, we addressed several nonlinear estimation problems by combining statistical methods with dynamical insight.

Methods based on Indistinguishable States theory are introduced to estimate the current state of the model in the PMS. By enhancing the balance between the information contained in the dynamic equation and the information in the observations, the IS method produces a good ensemble estimates of the current state. Our methods are applied in Ikeda Map and Lorenz96 flow, and shown to outperform the variational method, Four-dimensional Variational Assimilation, and the sequential method, Ensemble Kalman Filter.

To estimate the model parameter, we introduced two new approaches, Forecast Based estimates and Dynamical Coherent estimates. Forecast Based estimates method estimate the parameter values based on the probabilistic forecasting at a given lead time. Dynamical Coherent estimates method focuses on the geometric properties of trajectories and the property of the pseudo-orbits provided by the ISGD method. Both methods are tested on a variety of nonlinear models, the true parameter values are well identified.

Outside PMS, no model trajectories are consistent with infinite observations,

there are model pseudo-orbits that are consistent with the observations and their corresponding imperfection error reflects the model error. we find applying the ISGD method with a certain stopping criteria can produce such relevant pseudo-orbits. Our methods are applied in Ikeda Map and Lorenz96 flow, and shown to outperform the Weak Constrain Four-dimensional Variational Assimilation method.

Given the fact that the model is imperfect, to estimate the future states requires accounting the model inadequacy. We demonstrate that using the imperfection error produced by $ISGD^c$ method to adjust the forecast can improve the forecast performance. Forecast based measurement is suggested to measure the predictability outside PMS.

Main new results

- Chapter 3

    - A new ensemble filter approach within the context of indistinguishable states (48) is introduced to address the nowcasting problem in the perfect model scenario.

    - For the first time, IS method is compared with 4DVAR method when both applying to Ikeda Map and Lorenz96 system which demonstrates our method outperforms the 4DVAR method in state estimation.

    - For the first time, IS method is compared with Ensemble Kalman Filter method when both applying to Ikeda Map and Lorenz96 system which demonstrates our method outperforms the EnKF method in state estimation.

157

- A new probabilistic evaluation method, ϵ-ball, is introduced to evaluate the ensemble forecasts.

- Chapter 4

  - A new parameter estimation approach based on probabilistic forecast is introduced.

  - Another new parameter estimation approach, which focuses on the geometric properties of trajectories, is introduced.

  - For the first time, IS method, as part of the second parameter estimation approach, is successfully applied to partial observations.

- Chapter 5

  - A new methodology, i.e. applying the IS method with stopping criteria, is introduced to address the nowcasting problem in the imperfect model scenario.

  - For the first time, our methodology is compared with WC4DVAR method when both applying to Ikeda Map and Lorenz96 system which demonstrates our method outperforms the WC4DVAR method in terms of nowcasting.

  - For the first time, we demonstrate that applying WC4DVAR method will face the problem of increasing density of local minimums.

  - For the first time, IS method is applied to form ensemble of initial condition in the Imperfect Model Scenario.

- Chapter 6

- For the first time, we use the imperfection error obtained by applying IS method to adjust the forecast outside perfect model scenario. And by applying in the Ikeda system-model pair, we demonstrate that our method improves the forecast performance from direct forecast significantly.

- Forecast based measurement is suggested to measure the predictability outside PMS.

Appendix A

Gradient Descent Algorithm

In this appendix, we review the details of applying Gradient Descent (GD) Algorithm (48; 50) to find the minimum of the mismatch cost function 3.7 given a sequence of observations $s_{-N+1}, ..., s_0$.

The minimum of the mismatch cost function can be obtained by solving the ordinary differential equation

$$\frac{d\mathbf{u}}{d\tau} = -\nabla C(\mathbf{u}) \tag{A.1}$$

where $C(\mathbf{u})$ is the mismatch cost function. In practice, we initialise the minimisation with the observations, i.e. $\mathbf{u}^0 = \mathbf{s}$. After every iteration of the GD algorithm, the pseudo-orbit $\mathbf{u}$ will be updated (for instance, one obtain $\mathbf{u}^j$ after j iterations). To iterate the algorithm, one need to differentiate the mismatch cost

function given by

$$\frac{\partial C}{\partial \mathbf{u}} = \frac{2}{N+1} \times \begin{cases} -(\mathbf{u}_{t+1} - F(\mathbf{u}_t))d_t F(\mathbf{u}_t) & t = -N+1 \\ -(\mathbf{u}_t - F(\mathbf{u}_{t-1})) + (\mathbf{u}_{t+1} - F(\mathbf{u}_t))d_t F(\mathbf{u}_t) & -N+1 \le t \le 0 \\ -(\mathbf{u}_t - F(\mathbf{u}_{t-1})) & t = 0 \end{cases}$$

where $d_t F(\mathbf{u}_t)$ is the Jacobian of the model F at $\mathbf{u}_t$. We solve the ordinary differential equation A.1 using the Euler approximation.

Appendix B

Experiments Details

The tables below define the standard experiments which are used throughout the thesis.

System	Ikeda Map
Noise model	$N(0, 0.05)$
Number of assimilation	1024
Number of bootstrap samples	512
ISGD	no. of GD iterations	4096
	GD iteration step	0.2
4DVAR	Initial GD iteration step	0.2
	GD stops when iteration step $\leq$	5×10^{-6}

Table B.1: Details of Experiment A, note for 4DVAR method we shrink the iteration step by 2 when cost function not decrease.

System	Lorenz96 Model I
Dimension of the system	18
Noise model	$N(0, 0.5)$
Number of assimilation	1024
Number of bootstrap samples	512
ISGD — no. of GD iterations	4096
ISGD — GD iteration step	1
4DVAR — Initial GD iteration step	1
4DVAR — GD stops when iteration step $\leq$	10^{-6}

Table B.2: Details of Experiment B, note for 4DVAR method we shrink the iteration step by 2 when cost function not decrease.

System	Ikeda Map
Noise model	$N(0, 0.05)$
number of nowcast made	2048
ISIS — assimilation window length	12 steps
ISIS — no. of GD iterations	4096
ISIS — perturbation of the middle points by	$N(0, 0.025)$
ISIS — number of the perturbations	4096
ISIS — number of ensemble members	512
EnKF — number of ensemble members	512

Table B.3: Details of Experiment C

System	Lorenz96 Model I
Dimension of the system	18
Noise model	$N(0, 0.5)$
number of nowcast made	2048
ISIS — assimilation window length	1.2 time units
ISIS — no. of GD iterations	4096
ISIS — perturbation of the middle points by	$N(0, 0.25)$
ISIS — number of the perturbations	4096
ISIS — number of ensemble members	512
EnKF — number of ensemble members	512

Table B.4: Details of Experiment D

System	Ikeda Map
Noise model	$U(-0.025, 0.025)$
ISIS window length	12 steps
ISIS no. of GD iterations	4096
ISIS ·perturbation of the middle points by	$U(-0.01, 0.01)$
ISIS number of the perturbations	1024
ISIS number of ensemble members	64
DCEn number of ensemble members	64

Table B.5: Details of Experiment E

System	Ikeda Map	Lorenz96 Model II
Model	Truncated Ikeda Model	Lorenz96 Model I
Noise model	N(0,0.01)	N(0,0.4)
number of observations	2048	102.4 time unit
sample std of model error	0.018	0.0057

Table B.6: Details of Experiment F

System	Ikeda Map
Model	Truncated Ikeda Model
Noise model	$N(0, 0.05)$
Number of assimilation	1024
Number of bootstrap samples	512
$ISGD^c$ no. of GD iterations	75
$ISGD^c$ GD iteration step	0.2
WC4DVAR Initial GD iteration step	0.2
WC4DVAR GD stops when iteration step $\leq$	5×10^{-6}

Table B.7: Details of Experiment G, note for WC4DVAR method we shrink the iteration step by 2 when cost function not decrease.

System	Lorenz96 Model II
Model	Lorenz96 Model I
Dimension of the system	18×5
Noise model	$N(0, 0.1)$
Number of assimilation	1024
Number of bootstrap samples	512
$ISGD^c$	no. of GD iterations	4096
	GD iteration step	1
WC4DVAR	Initial GD iteration step	1
	GD stops when iteration step $\leq$	10^{-6}

Table B.8: Details of Experiment H, note for WC4DVAR method we shrink the iteration step by 2 when cost function not decrease.

Bibliography

[1] J.L. Anderson, An ensemble adjustment Kalman filter for data assimilation, *Mon. Weather Rev.*, 129, 2884-2903, (2001). 37, 41, 43

[2] J.L. Anderson, A local least squares framework for ensemble filtering, *Mon. Weather Rev.*, 131, 634-642, (2003). 37

[3] L. Arnold, Random Dynamical Systems, Springer, Berlin, (1998). 146

[4] A.F. Bennett, L.M. Leslie, C.R. Hagelberg and P.E. Powers, Tropical cyclone prediction using a barotropic model initialized by a generalized inverse method. *Mon. Wea. Rev.*, 121, 1714-1729, (1993). 111

[5] A.F. Bennett, B.S. Chua and L.M. Leslie, Generalized inversion of a global numerical weather prediction model. *Meteor. Atmos. Phys.*, **60**, 165-178, (1996). 111

[6] M.L. Berliner, Likelihood and Bayesian Prediction for Chaotic Systems, J. Am. Stat. Assoc. **86**, 938-952 (1991).

[7] C.H. Bishop, B.J.Etherton and S.J.Majumdar. Adaptive sampling with the Ensemble Transform Kalman Filter. Part I: Theoretical Aspects. *Mon. Wea. Rev.* **129**, 420C436, (2001). 41, 43

[8] A. Bjorck, Numerical Methods for Least Squares Problems, SIAM, (1996) 65

[9] E. Borel, *Probability and Certainty* Walker, New York, (1963). 80

[10] C.L.Bremer and D.T.Kaplan, Markov chain Monte Carlo estimation of non-linear dynamics from time series, Physica D **160** 116–126 (2001).

[11] G.W. Brier, Verification of forecasts expressed in terms of probabilities. *Mon. Wea. Rev.*, **78**, 1C3, (1950).

[12] J. Brocker and L.A. Smith, Scoring Probabilistic Forecasts: On the Importance of Being Proper, *Weather and Forecasting* 22(2), 382-388, (2007) 53, 73

[13] J. Brocker and L.A. Smith, From ensemble forecasts to predictive distribution functions, submitted to *Tellus*, (2007) 70, 71

[14] D. S. Broomhead and D. Lowe. Multivariable functional interpolation and adaptive networks. *J. Complex Systems*, 1:417-452, (1987). 17

[15] M. Casdagli. Nonlinear prediction of chaotic time series. *Physica D*, 35:335-356, (1989). 17

[16] M. Casdagli, S. Eubank, J. D. Farmer, and J. Gibson, State space reconstruction in the presence of noise, Physica D, **51**, 52 (1991);

[17] G. Casella and R.L. Berger, Statistical Inference, Wadsworth, Belmont, California, (1990). 66

[18] P. Courtier and O. Talagrand, Variational assimilation of meteorological observations with the adjoint vorticity equation. II: Numerical results, Q.J.R. *Meteorol Soc.*, 113, 1311-1328, (1987). 32

[19] P. Courtier, J.N. Thepaut and A. Hollingsworth, A strategy for operational implementation of 4DVAR, using an incremental approach, Q.J.R. *Meteorol Soc.*, 120, 1367-1387, (1994). 32

[20] M.C. Cuellar, Perspectives and Advances in Parameter Estimation of Nonlinear Models. PhD Thesis, London School of Economics, (2007). 66, 78, 82

[21] M.E.Davies, Noise reduction by gradient descent, Int. J. Bifurcation Chaos 3, 113-118, (1992).

[22] J.-P. Eckmann, D. Ruelle, Rev. Mod. Phys. 57 617, (1985). 146

[23] G. Evensen, Sequential data assimilation with a nonlinear quasi-geostrophic model using Monte Carlo methods to forecast error statistics, *J. Geophys. Res.*, 99, 10,143-10,162, (1994). 41

[24] G. Evensen, Sequential data assimilation with a nonlinear quasi-geostrophic model using Monte Carlo methods to forecast error statistics, *J. Geophys. Res.*, **127**, 2128-2142, (1994).

[25] J.P. Eckmann and D. Ruelle. Ergodic theory of chaos. *Rev. Mod. Phys.*, 45:617-656, 1985. 148

[26] J.D. Farmer and J.J. Sidorowich. Optimal shadowing and noise reduction. *Physica D*, 47:373-392, (1991). 79

[27] C. F. Gauss, Translated by G. W. Stewart. Theory of the Combination of Observations Least Subject to Errors: Part One, Part Two, Supplement. Philadelphia: Society for Industrial and Applied Mathematics, (1995). 65

[28] P. Gauthier, Chaos and quadri-dimensional data assimilation, A study based on the Lorenz model. *Tellus* 44A, 2-17, (1992).

[29] P. Gauthier, P. Courtier and P. Moll, Assimilation of simulated lidar data with a Kalman filter, *Mon. Weather Rev.*, **121**, 1803-20, (1993). 40

[30] M. Ghil and P. Malanotte-Rizzoli, Data assimilation in meteorology and oceanography, *Adv. Geophys.* **33**, 141-266, (1991). 40

[31] I. Gilmour, Nonlinear model evaluation: ι-shadowing, probabilistic prediction and weather forecasting, Ph.D. thesis, University of Oxford, (1998). 79

[32] P. Grassberger, T. Schreiber, and C. Schaffrath, Non–linear time sequence analysis, Int. J. Bif. and Chaos 1, 521 (1991).

[33] C. Grebogi, S.M. Hammel, J.A. Yorke, and T. Sauer. Shadowing of physical trajectories in chaotic dynamics: containment and refinement. *Phys. Rev. Letts.*, 65(13):1527-1530, (1990). 79

[34] J. Guckenheimer, J. Moser and S. Newhouse, Dynamical Systems, CIME Lectures, Birkhauser, 289pp., (1980).

[35] J. Guckenheimer and P. Holmes, *Nonlinear Oscillations, Dynamical Systems, and Bifurcations of Vector Fields*, Springer, New York, (1983). 7

[36] T.M. Hamill, Iterpretation of Rank Histograms for Verifying Ensemble Forecasts. *Monthly Weather Review:* Vol. 129, No. 3, 9-30, (2001)

[37] T.M. Hamill, Ensemble-based atmospheric data assimilation, Chapter 6 of *Predictability of Weather and Climate*, Cambridge Press, 124-156, (2006). 41, 42, 43, 44, 73

[38] J.A.Hansen, Adaptive observations in spatialy-extended nonlinear dynamical systems, Ph.D. thesis, University of Oxford, (1998).

[39] J.A. Hansen, L.A. Smith, Probabilistic noise reduction. *Tellus series A*, **53** (5), 585-598 (2001). 48

[40] M. Hénon, A two-dimensional mapping with a strange attractor, Commun. Math. Phys. **50** 69-77 (1976). 10

[41] P.L. Houtekamer and H.L. Mitchell. Data assimilation using an ensemble Kalman filter technique. *Mon. Weather Rev.*, **126**, 796-811, (1998). 41, 42

[42] P.L. Houtekamer and H.L. Mitchell. Reply to comment on "Data assimilation using an ensemble Kalman filter technique." *Mon. Weather Rev.*, **127**, 1378-9, (1999). 41, 42

[43] P.L. Houtekamer and H.L. Mitchell. A sequential ensemble Kalman filter for atmospheric data assimilation. *Mon. Weather Rev.*, **129**, 123-37, (2001). 41, 42

[44] G.E. Hutchinson, Circular casual systems in ecology, *Annals of the New York Academy of Sciences*, 50, 221-246, (1948). 8

[45] K. Ikeda, Multiple valued stationarity state and its instability of the transmitted light by a ring cavity system, Optical Communications, 30 257-261 (1979). 11

[46] L. Jaeger and H. Kantz, Unbiased reconstruction of the dynamics underlying a noisy chaotic time series, Chaos 6, 440 (1996).

[47] A.H. Jazwinski, *Stochastic Processes and Filtering Theory*. Academic Press, (1970). 40

[48] K. Judd and L.A. Smith, Indistinguishable States I: The Perfect Model Scenario, *Physica D* **151**: 125-141, (2001). 2, 19, 22, 25, 27, 28, 34, 65, 98, 157, 160

[49] K. Judd, Chaotic-time-series reconstruction by the Bayesian paradigm: Right results by wrong methods, Physics Review Letters, **67**, 026212,(2003).

[50] K. Judd and L.A. Smith, Indistinguishable States II: The Imperfect Model Scenario, *Physica D* **196**: 224-242, (2004). 3, 11, 93, 94, 95, 96, 98, 100, 108, 110, 126, 129, 160

[51] K. Judd and L.A. Smith and A. Weisheimer, Gradient free descent: shadowing and state estimation with limited derivative information, *Physica D*, 190, 153–166 (2004). 90

[52] K. Judd, Forecasting with imperfect models, dynamically constrained inverse problems, and gradient descent algorithms, *Physica D*, 237, 216-232, (2008). 34, 114

[53] K. Judd, C.A. Reynolds, T.E. Rosmond and L.A. Smith, The Geometry of Model error, *Journal of Atmospheric Science*, 65 (6), 1749–1772, 2008 29, 56, 62

[54] R. E. Kalman, A New Approach to Linear Filtering and Prediction Problems. *Trans AMSE Ser D J Basic Eng*, 82, 35-45, (1960). 37

[55] H. Kantz and L. Jaeger, Homoclinic tangencies and non-normal Jacobians - effects of noise in non-hyperbolic systems, Physica D 105, 79-96 (1997).

[56] T. Kariya, H. Kurata, Generalized Least Squares, Wiley, (2004). 65

[57] J.L. Kelly, Jr, A New Interpretation of Information Rate, *Bell System Technical Journal*, 35, 917-926, (1956) 74

[58] E.J. Kostelich and J.A. Yorke, Noise Reduction in Dynamical Systems, Phys Rev A 38, 1649, (1988). 79

[59] E.J. Kostelich, Problems in estimating dynamics from data, Physica D 58, 138 (1992).

[60] S.A. Levin and R.M. May, A note on difference-delay equations, *Theoretical Population Biology*, 9, 178-187, (1976). 8

[61] E.N. Lorenz, Deterministic nonperiodic flow. *J. Atmos. Sci.*, 20:130-141, (1963). 10, 34

[62] E.N. Lorenz. A study of the predictability of a 28-variable atmospheric model. *Tellus*, 17:321-333, (1965). 146, 147, 148

[63] E.N. Lorenz, Predictability A problem partly solved, in: ECMWF Seminar Proceedings on Predictability, Reading, United Kingdom, ECMWF, (1995). 12, 13, 96

[64] P.E. McSharry and L.A. Smith, Better nonlinear models from noisy data: Attractors with maximum likelihood, Phys. Rev. Lett 83, (21): 4285-4288, (1999). 3, 63, 65, 66, 86, 87, 103, 185

[65] R.N. Miller, M. Ghil and F. Gauthiez, Advanced data assimilation in strongly nonlinear dynamical systems. J.Atmos.Sci. 51, 1037-1056, (1994). 32, 33

[66] W. D.Moore and E. A.Spiegel, A thermally excited nonlinear oscillator. The Astrophysical Journal. Volume 143, pp. 871-887, (1966). 12

[67] D. Orrell, A shadow of a Doubt: Model Error, Uncertainty, and shadowing in Nonlinear Dynamical Systems. PhD Thesis, University of Oxford, (1999). 13

[68] V.I. Oseledec, Transactions of the Moscow Mathematical Society 19 197, (1968). 146

[69] E. Ott, *Chaos in Dynamical Systems*, Cambridge University Press, (1993). 9

[70] F. Paparella, A. Provenzale, L.Smith, C.Taricco, R.Vio, Local Random analogue prediction of nonlinear processes, *Phys. Lett. A* 235 233-240, (1997). 16, 132

[71] C. Pires, R. Vautard, and O. Talagrand, On extending the limits of variational assimilation in nonlinear chaotic systems. *Tellus*, 48A, 96-121, (1996). 32, 33, 34, 36

[72] V.F. Pisarenko and D. Sornette, Statistical methods of parameter estimation for deterministically chaotic time series, Phys Rev E, 69 (2004).

[73] W. H. Press, B. Flannery, S. Teukolsky, and W. Vetterling, *Numerical Recipes in C* (CUP, Cambridge, 1992).

[74] D. Ridout and K. Judd, Convergence properties of gradient descent noise reduction. *Physica D* 165 27-48, (2001).

[75] M.S. Roulston and L.A. Smith, Evaluating probabilistic forecasts using information theory, *Monthly Weather Review*, 130, 1653-1660, (2002) 70, 73

[76] Y. Sasaki, Some basic formalisms on numerical variational analysis. *Mon. Wea. Rev.*, 98, 875-883, (1970). 111

[77] T. Sauer, J.A. Yorke, M. Casdagli, Embedology, J. Stat. Phys. 65, 579, (1991). 79

[78] D.S. Sivia, Data analysis - a Bayesian tutorial, Clarendon Press, Oxford University Press, (1997).

[79] L. A. Smith. Identification and prediction of low-dimensional dynamics. *Physica D*, 58:50-76, (1992). 15, 17, 131

[80] L. A. Smith. Accountability and error in forecasts. In *Proceedings of the 1995 ECMWF Predictability Seminar*, (1996). 45, 46, 92

[81] L.A. Smith. The Maintenance of Uncertainty, Proc International School of Physics "Enrico Fermi", Course CXXXIII, pg 177–246, Societa Italiana di Fisica, Bologna, Italy (1997). 15, 147, 148, 149

[82] L. A. Smith, C. Ziehman, and K. Raedrich. Uncertainty in dymanamics and predictability in chaotic systems. *Q. J. R. Meteorol.* Soc., 125:2855C2886, (1999). 146, 148, 149, 151, 155

[83] L.A. Smith, Disentangling Uncertainty and Error: On the Predictability of Nonlinear Systems. Nonlinear Dynamics and Statistics, A.I.Mees, Ed., Birkhauser, 31-64 (2000). 13, 79

[84] L.A. Smith and M.S. Roulston, Evaluating Probabilistic Forecasts Using Information Theory. *Monthly Weather Review* 130, no. 6, pp. 1653-1660, (2001).

[85] L.A. Smith, M.C. Cuellar, H. Du, and K. Judd, Identifying dynamically coherent behaviours: A geometrical approach to parameter estimation in nonlinear models, *Physics Letter A*, under review (2009). 78

[86] H. Sorenson, Kalman Filtering: Theory and Application. IEEE Press, (1985). 37

[87] D.A.Stainforth, et al. Uncertainty in predictions of the climate response to rising levels of greenhouse gases, Nature, 433, 403C406, (2005). 89

[88] D.J. Stensrud and J.W. Bao, Behaviors of variational and nudging assimilation techniques with a chaotic low-order model. *Mon. Wea. Rev.* 120, 3016-3028, (1992).

[89] F. Takens. Detecting strange attractors in fluid turbulence. In D. Rand and L.-S. Young, editors, *Dynamical Systems and Turbulence*, pages 366-381, Berlin, Springer-Verlag, (1981). 15

[90] O. Talagrand and P. Courtier, Variational assimilation of meteorological observations with the adjoint vorticity equation. I: Theory, Q.J.R. *Meteorol Soc.*, 113, 1311-1328, (1987). 32, 111

[91] J. Timmer, Modeling noisy time series: physiological tremor, Int. J. Bif. Chaos 8, 1505C1516 (1998).

[92] J.S. Whitaker and T.M. Hamill, Ensemble data assimilation without perturbed observations. *Mon. Weather Rev.*, 130, 1913-24, (2002). 43

[93] D.S. Wilks, Comparison of ensemble-MOS methods in the Lorenz'96 setting. *Meteorological Applications*, 13, (2006). 71

[94] C. Ziehmann, L.A. Smith and J. Kurths, Localized Lyapunov Exponents and the Prediction of Predictability Phys. Lett. A, 271 (4): 237-251, (2000). 148, 151

Nomenclature

Roman Symbols

η observational noise or measurement error

δ implied noise

Γ covariance matrix of the observational noise

ω imperfection error

ζ forecast adjustment

$\mathbb{A}$ attractor or invariant measure

$\mathbb{H}(x)$ the set of indistinguishable states of x

$\mathbb{M}$ model space

$\mathbb{O}$ observation space

$\mathbb{S}$ state space

$\Phi(\mathbf{x})$ unconditional probability density function of $\mathbf{x}$

$\rho(\cdot)$ probability density function of the observation noise

a   model parameter

B   covariance matrix of x^b

e   mismatch error

u_i component of a pseudo-orbit

x   model state

x^a the posteriori estimate of system state

x^b first guess or background state of the model

y   pseudo-orbit obtained by ISGD method

z   reference trajectory

$\tilde{a}$ system parameter

$\tilde{x}$ system state

$\tilde{F}$ system dynamics

$\tilde{l}$ dimension of the system parameter space

$\tilde{m}$ dimension of the system space

F model dynamics

$h(\cdot)$ observation operator

K_t Kalman gain

l dimension of the model parameter space

m dimension of the model space

n number of observations

N^{cand} number of candidate trajectories

N^{ens} number of ensemble members

P^a analysis-error covariance

P^b background-error covariance

Q the density function measures the indistinguishability

Y verification

List of Figures